



## **DISCLAIMER**

This report was prepared as an account of work sponsored by an agency of the United States Government. Neither the United States Government nor any agency thereof, nor any of their employees, makes any warranty, expressed or implied, or assumes any legal liability or responsibility for the accuracy, completeness, or usefulness of any information, apparatus, product, or process disclosed, or represents that its use would not infringe privately owned rights. Reference herein to any specific commercial product, process, or service by trade name, trademark, manufacturer, or otherwise does not necessarily constitute or imply its endorsement, recommendation, or favoring by the United States Government or any agency thereof. The views and opinions of authors expressed herein do not necessarily state or reflect those of the United States Government.

## **ABSTRACT**

In the United States, more than 20 billion barrels of salt water are produced each year during oilfield operations. A tremendous economic incentive exists to reduce water production if that can be accomplished without significantly sacrificing hydrocarbon production. For each 1% reduction in water production, the cost savings to the oil industry could be between \$50,000,000 and \$100,000,000 per year. Reduced water production would result directly in improved oil recovery efficiency in addition to reduced oil-production costs. A substantial positive environmental impact could also be realized if significant reductions are achieved in the amount of water produced during oilfield operations.

This report describes work performed during the first year of the project, “Using Chemicals to Optimize Conformance Control in Fractured Reservoirs.” This research project has three objectives. The first objective is to develop a capability to predict and optimize the ability of gels to reduce permeability to water more than that to oil or gas. The second objective is to develop procedures for optimizing blocking agent placement in wells where hydraulic fractures cause channeling problems. The third objective is to develop procedures to optimize blocking agent placement in naturally fractured reservoirs. This research project consists of three tasks, each of which addresses one of the above objectives. Our work is directed at both injection wells and production wells and at vertical, horizontal, and highly deviated wells.

In Chapter 2, we report experimental results from studies of gel properties in fractures. In Chapter 3, we review updates to our software for sizing gelant treatments in hydraulically fractured production wells. Chapter 4 describes a study of the rheology of our gels. Chapter 5 reviews concepts directed at applying blocking agents in unfractured production wells where zones are not mechanically isolated during placement. Finally, in Chapter 6, we investigate the mechanism responsible for gels reducing the permeability to water more than that to oil.

The Executive Summary provides a brief description of our accomplishments in each of the above areas. This project was supported financially by the U.S. Department of Energy (National Petroleum Technology Office), and a consortium of 10 oil and service companies. Technology transfer activities are detailed in Appendix B.

## TABLE OF CONTENTS

DISCLAIMER.....	ii
ABSTRACT .....	iii
TABLE OF FIGURES .....	vi
LIST OF TABLES.....	viii
ACKNOWLEDGMENTS.....	ix
EXECUTIVE SUMMARY.....	x
Gel Properties in Fractures .....	x
Gelant Treatments in Hydraulically Fractured Production Wells.....	x
Rheological Properties of Gels Used for Conformance Control.....	xi
Water Shutoff in Unfractured Production Wells.....	xii
Disproportionate Permeability Reduction.....	xii
1. INTRODUCTION .....	1
Objectives .....	1
Report Content.....	1
2. GEL PROPAGATION THROUGH FRACTURES.....	2
Base Case: Extrusion Through a 48×1.5×0.04-in. Fracture in 650-mD Sandstone.....	3
Effect of Rock Permeability.....	13
Model for Gel Propagation and Dehydration.....	13
Effect of Fracture Width.....	18
Fractures with Varying Widths .....	19
Gel Permeability to Water Versus Gel Composition.....	20
Effect of Fracture Height.....	27
Effect of Injection Rate.....	31
Comparison of Model Predictions.....	42
Effect of Polymer Molecular Weight.....	43
Preliminary Predictions for Behavior in Long Fractures .....	48
Conclusions.....	50
Future Work.....	51
3. GELANT TREATMENTS IN HYDRAULICALLY FRACTURED WELLS.....	52
4. RHEOLOGICAL PROPERTIES OF GELS USED FOR CONFORMANCE CONTROL .....	53
Introductory Concepts.....	53
Gels Studied.....	55
Elastic and Viscous Moduli versus Strain.....	55
Strain versus Time.....	57
Elastic and Viscous Moduli versus Polymer and Crosslinker Concentration .....	58
Effect of Temperature .....	59
Effect of Gel Aging .....	60
Yield Stress and Stresses During Flow.....	62
Properties of Gel from a Fracture .....	64
Conclusions.....	65
Future Work.....	65

5. WATER SHUTOFF IN UNFRACTURED PRODUCTION WELLS .....	67
Polymers and Gels .....	67
Particulates .....	68
Foams .....	69
Reactive Water-Blocking Agents .....	70
Mobility-Matched Postflush .....	70
Thermally Triggered Diverting Agent .....	72
Dilution by Diffusion and Dispersion .....	74
Summary of Potentially Useful Ideas and Phenomena .....	74
6. DISPROPORTIONATE PERMEABILITY REDUCTION .....	76
Review of Previous Findings .....	76
Effect of Pressure Drawdown .....	76
Effect of Rock Permeability .....	77
Combined “Wall-Effect” and “Gel-Droplet” Model .....	78
Effect of Residual Oil Saturation .....	82
Imaging Experiments Using Synchrotron X-Ray Microtomography .....	83
Conclusions .....	84
NOMENCLATURE .....	85
REFERENCES .....	87
APPENDIX A: Data Supplement to Chapter 6 .....	90
APPENDIX B: Technology Transfer .....	99
Presentations .....	99
Internet Postings on the Project and Software to Download .....	99
Papers and Publications: .....	100

## TABLE OF FIGURES

Fig. 1—Pressure gradients required to extrude a gel through open fractures (no proppant).....	2
Fig. 2—Degree of gel dehydration versus fracture width. ....	3
Fig. 3—Illustration of the fractured core.....	4
Fig. 4—Core outlet configuration to separate fracture effluent from porous-rock effluent.....	4
Fig. 5—Pressure behavior in the fracture taps during gel injection (normal scale).....	5
Fig. 6—Pressure behavior in the fracture taps during gel injection (log scale). ....	5
Fig. 7—Pressure behavior in the matrix taps during gel injection.....	6
Fig. 8—Fractional flow measured at the core outlet (200 cm <sup>3</sup> /hr). ....	7
Fig. 9—Chromium and HPAM concentrations in the effluent: fracture versus matrix. ....	7
Fig. 10—Composition of gel in the fracture (relative to the injected gel).....	8
Fig. 11—Gel propagation rate in the fracture.....	9
Fig. 12—Brine flow in the porous rock during gel injection. ....	10
Fig. 13—Relative leakoff rates derived from Fig. 12. ....	11
Fig. 14—Predicted leakoff rates. ....	15
Fig. 15—Predicted versus measured leakoff rates for Section 1. ....	15
Fig. 16—Predicted versus measured leakoff rates for Section 2. ....	16
Fig. 17—Predicted versus measured leakoff rates for Section 3. ....	16
Fig. 18—Predicted versus measured leakoff rates for Section 4. ....	17
Fig. 19—Predicted versus measured leakoff rates for Section 5. ....	17
Fig. 20—Predicted versus actual fractional flow from the matrix at the core outlet. ....	18
Fig. 21—Predicted versus actual dehydration factors as a function of fracture width.....	19
Fig. 22—Pressure gradients in a fracture with varying widths. ....	19
Fig. 23—Gel composition along the fracture. ....	20
Fig. 24—Schematic of experiment to determine $k_{gel}$ versus gel composition. ....	21
Fig. 25—Pressure versus time during gel injection.....	22
Fig. 26—Calculated gel permeability versus composition for Case 1.....	22
Fig. 27—Calculated gel permeability versus composition for Case 2.....	24
Fig. 28—Filter-cake-growth calculations from Case 3. ....	25
Fig. 29—Schematic of experiment in 12×12×0.04-in. fracture. ....	27
Fig. 30—Effluent compositions from a 12×12×0.04-in. fracture (500 cm <sup>3</sup> /hr).....	28
Fig. 31—Effluent compositions from a 12×12×0.04-in. fracture (1,600 cm <sup>3</sup> /hr).....	28
Fig. 32—Fractional flow measured at the core outlet (12×12×0.04-in. fracture, 500 cm <sup>3</sup> /hr).....	29
Fig. 33—Fractional flow measured at the core outlet (12×12×0.04-in. fracture, 1,600 cm <sup>3</sup> /hr).....	29
Fig. 34—Illustration of a gel wormhole through concentrated gel.....	30
Fig. 35—Chromium/HPAM concentrations in a 12×12×0.04-in. fracture (500 cm <sup>3</sup> /hr). ....	31
Fig. 36—Chromium/HPAM concentrations in a 12×12×0.04-in. fracture (1,600 cm <sup>3</sup> /hr). ....	31
Fig. 37—Pressure behavior in the fracture taps during gel injection (500 cm <sup>3</sup> /hr). ....	33
Fig. 38—Pressure behavior in the fracture taps during gel injection (2,000 cm <sup>3</sup> /hr). ....	33
Fig. 39—Pressure behavior in the matrix taps during gel injection (500 cm <sup>3</sup> /hr). ....	34
Fig. 40—Pressure behavior in the matrix taps during gel injection (2,000 cm <sup>3</sup> /hr). ....	34
Fig. 41—Fraction of total flow in the matrix during gel injection (500 cm <sup>3</sup> /hr). ....	35
Fig. 42—Fraction of total flow in the matrix during gel injection (2,000 cm <sup>3</sup> /hr). ....	35
Fig. 43—Relative leakoff during gel injection (500 cm <sup>3</sup> /hr).....	36

Fig. 44—Relative leakoff during gel injection (2,000 cm <sup>3</sup> /hr).....	36
Fig. 45—Composition of gel in the fracture (relative to the injected gel) (500 cm <sup>3</sup> /hr).....	37
Fig. 46—Composition of gel in the fracture (relative to the injected gel) (2,000 cm <sup>3</sup> /hr).....	37
Fig. 47—Fractional flow measured at the core outlet (500 cm <sup>3</sup> /hr).....	38
Fig. 48—Fractional flow measured at the core outlet (2,000 cm <sup>3</sup> /hr).....	38
Fig. 49—Average leakoff rate from five experiments at different velocities.....	39
Fig. 50—Average permeability versus concentration based on Fig. 49.....	40
Fig. 51—Composition of gel in the fracture (500 cm <sup>3</sup> /hr).....	41
Fig. 52—Composition of gel in the fracture (2,000 cm <sup>3</sup> /hr).....	41
Fig. 53—Gel propagation in 48×1.5×0.04-in. fractures. Model: $k_{gel}=0.00011+1.0(C/C_o)^{-3}$ .....	42
Fig. 54—Gel propagation in 48×1.5×0.04-in. fractures. Model: $u_l = 0.374 t^{-0.557}$ .....	43
Fig. 55—Pressure behavior in the fracture taps during Percol 338 gel injection.....	45
Fig. 56—Chromium and HPAM concentrations in the effluent (0.2% Percol 338 gel).....	46
Fig. 57—Fraction of total flow measured at the core outlet (0.2% Percol 338 gel).....	46
Fig. 58—Composition of gel in the fracture (0.2% Percol 338 gel).....	47
Fig. 59—Minimum injection rates required in a two-wing fracture.....	50
Fig. 60—Oscillating shear strain produces a sinusoidal stress.....	54
Fig. 61—Elastic ( $G'$ ) and viscous ( $G''$ ) modulus versus strain.....	56
Fig. 62—Strain versus time for a Cr(III)-acetate-HPAM gel.....	57
Fig. 63— $G'$ and $G''$ versus polymer concentration for Cr(III)-acetate-HPAM gels.....	58
Fig. 64— $G'$ versus Cr(III)-acetate concentration.....	59
Fig. 65— $G'$ versus temperature for a Cr(III)-acetate-HPAM gel.....	60
Fig. 66— $G'$ versus HPAM concentration and storage time for Cr(III)-acetate-HPAM.....	61
Fig. 67— $G'$ versus strain and gel age for a Al(III)-sulfate-HPAM gel.....	61
Fig. 68—Yield stress determination.....	62
Fig. 69—Shear stress and complex viscosity versus shear rate.....	63
Fig. 70—Resistance factor versus velocity during gel extrusion.....	63
Fig. 71—Placement of a water-like gelant with crossflow.....	71
Fig. 72—Placement of a thermally triggered gelant with crossflow.....	73
Fig. 73—Gelant crossflow near the hot zone.....	73
Fig. 74—Wall-effect model proposed by Zaitoun <i>et al.</i> .....	79
Fig. 75—Gel-droplet model proposed by Nilsson <i>et al.</i> .....	80
Fig. 76—Gel-droplet model proposed by Nilsson <i>et al.</i> .....	80
Fig. 77—Modified wall-effect model.....	81
Fig. 78—Modified wall-effect model.....	81

## LIST OF TABLES

Table 1— Gel filter cake properties at the end of gel injection. ....	23
Table 2— Measured versus calculated $C/C_o$ values at the end of gel injection. ....	26
Table 3—Effect of injection rate on gel propagation. ....	32
Table 4—Regression data for curves in Fig. 50.....	40
Table 5—Experimental results versus predictions from Models 1 and 2. ....	44
Table 6—Properties of two gels during extrusion through a 48×1.5×0.04-in. fracture.....	47
Table 7—Effect of pressure drawdown on disproportionate permeability reduction .....	77
Table 8—Effect of rock permeability on disproportionate permeability reduction.....	78
Table 9—Effect of $S_{or}$ on disproportionate permeability reduction. ....	83
Table 10—Effect of $S_{or}$ on disproportionate permeability reduction.....	83

## **ACKNOWLEDGMENTS**

Financial support for this work is gratefully acknowledged from the United States Department of Energy (National Petroleum Technology Office), BP-Amoco, Chevron, Chinese Petroleum Corporation, Chinese National Petroleum Corporation, Halliburton Energy Services, Marathon, Saga, Schlumberger-Dowell, Shell, and Texaco. I greatly appreciate the efforts of those individuals who contributed to this project. Richard Schrader performed most of the experimental work described in Chapter 2, with considerable help from Kathryn Wavrik. The New Mexico Bureau of Mines Chemistry Laboratory determined the chromium concentrations. Jin Liu performed the work in Chapter 4 as part of her studies toward an MS degree in Petroleum Engineering. Dr. Jenn-Tai Liang played the major role in conducting the work described in Chapters 5 and 6 and the programming associated with Chapter 3. John Hagstrom performed the experiments described in Chapter 6. I especially appreciate the thorough reviews of this manuscript by Julie Ruff and Liz Bustamante.

## EXECUTIVE SUMMARY

This report describes work performed during the first year of the project, “Using Chemicals to Optimize Conformance Control In Fractured Reservoirs.” This research project has three objectives. The first objective is to develop a capability to predict and optimize the ability of gels to reduce permeability to water more than that to oil or gas. The second objective is to develop procedures for optimizing blocking agent placement in wells where hydraulic fractures cause channeling problems. The third objective is to develop procedures to optimize blocking agent placement in naturally fractured reservoirs. This research project consists of three tasks, each of which addresses one of the above objectives. Our work is directed at both injection wells and production wells and at vertical, horizontal, and highly deviated wells.

### *Gel Properties in Fractures*

Many conformance control treatments rely on the ability of gels to extrude through fractures during the placement process. Chapter 2 describes an experimental investigation of the mechanism for propagation of a Cr(III)-acetate-HPAM gel through fractures. When large volumes of this gel were extruded through a fracture, progressive plugging (i.e., continuously increasing pressure gradients) was not observed. Effluent from the fracture had the same appearance and a similar composition as the injected gel, even though a concentrated, immobile gel formed in the fracture. The concentrated gel formed when water leaked off from the gel along the length of the fracture. The driving force for gel dehydration (and water leakoff) was the pressure difference between the fracture and the adjacent porous rock. During gel extrusion through a fracture of a given width, the pressure gradients along the fracture and the dehydration factors were the same for fractures in 650-mD sandstone as in 50-mD sandstone and 1.5-mD limestone. A simple model was developed that accounted for many of the experimental results. However, refinements are needed in the model, especially to account for behavior as a function of injection rate and fracture height and width. For Cr(III)-acetate-HPAM gels, experiments revealed that gel permeability varied with polymer concentration raised to a power between  $-2.5$  and  $-3.0$ . The initial permeability of our 1X Cr(III)-acetate-HPAM gel was around 1 mD. We also examined the properties of a gel made from an HPAM (Percol 338) with roughly twice the molecular weight of our standard HPAM (Alcoflood 935). Extrusion, propagation, and dehydration behaviors of the Percol 338 gel were similar to, or better than, those for an Alcoflood 935 gel. Since the Percol 338 gel required 2.5 times less polymer and chromium than the Alcoflood 935 gel, a significant economic advantage may be realized by preparing gels with polymers having the highest available molecular weight. Preliminary analyses indicated that dehydration will limit the distance of gel penetration into a fracture and that the maximum distance of gel penetration should increase with the square root of injection rate.

### *Gelant Treatments in Hydraulically Fractured Production Wells*

One-third of all newly drilled wells are intentionally fractured. Often, when hydraulic fracturing stimulates production wells, the fracture unintentionally extends through shale or calcite barriers into water zones, causing substantially increased water production. Gelant treatments have frequently been applied in an attempt to correct this problem. However, the design of the gelant volumes for these applications has been strictly empirical, and consequently, the success rates for these treatments have been erratic. We developed a sound engineering basis and a simple 11-step

procedure for sizing gelant treatments in hydraulically fractured production wells. This procedure was incorporated in user-friendly graphical-user-interface software. Details can be found in SPE paper 38835 and in our report, DOE/PC/91008-4. The software can be downloaded from our web site at <http://baervan.nmt.edu/ResSweepEffic/reservoir.htm>. We hope that our method will increase confidence in and applications of gel technology for reducing water production in hydraulically fractured production wells.

For recent field applications of the software, we noted several cases where engineers overestimated the static reservoir pressure (used as input for the program). This situation occurred because the engineers either used the original reservoir pressure or an outdated or inappropriate estimate of the reservoir pressure (e.g., a pre-fracture measurement or a measurement from a different part of the field). Consequently, the pressure drawdown used as input for our software was too high, and the program identified the wells (possibly incorrectly) as bad candidates for a gelant treatment. This experience emphasizes the need for recent, accurate pressure data for the target well, if our program is to be used.

We updated the software to Version 1.07. After a candidate well was determined to be inappropriate for a gel treatment, the previous version (1.05) required the user to return to the beginning of the program if the user wished to examine a new case. In contrast, Version 1.07 allows the user to continue and modify previous data entries without re-entering all reservoir and fluid properties.

In Version 1.07, improvements also were made in the routines to back-calculate in-situ water and oil residual resistance factors from previous field applications of gelant treatments.

### ***Rheological Properties of Gels Used for Conformance Control***

Because extrusion experiments in fractures are expensive and time consuming, we implemented a study of gel rheology, in hopes of correlating the results to our measurements during gel extrusion through fractures. Our study focused on a one-day-old Cr(III)-acetate-HPAM gel, although Al(III)-sulfate-HPAM gels were also examined. We measured elastic modulus ( $G'$ ) and viscous modulus ( $G''$ ), as a function of strain (0 to 10,000%), polymer concentration (0.3% to 1.7%), crosslinker concentration (0.01% to 0.06%), and gel aging time (0 to 12 days). For 24-hr-old Cr(III)-acetate-HPAM and Al(III)-sulfate-HPAM gels, the elastic modulus was fairly constant for strain values up to 200%. The elastic nature of these gels was evident even at strain values over 1,000%. This finding is consistent with observations concerning the ease with which these gels extrude through fractures. For 24-hr-old Cr(III)-acetate-HPAM gels, as the polymer concentration in the gel increased from 0.3% to 1.7%, the elastic modulus increased from 4 to 115 Pa. In contrast, the viscous modulus remained near 1 Pa. Thus, as expected, the elastic component became increasingly dominant (over the viscous component) as the polymer concentration increased.

For 24-hr-old Cr(III)-acetate-HPAM gels that contained 0.5% HPAM,  $G'$  exhibited a broad maximum at ~7-8 Pa for Cr(III)-acetate concentrations between 0.02% and 0.05%. For Cr(III)-acetate-HPAM gels with various compositions,  $G'$  increased with increased aging time at 41°C (up to 9 days). We speculate that this increase may have been caused by “curing” or more

complete inter-molecular crosslinking reactions with increased time. In contrast, for Al(III)-sulfate-HPAM gels,  $G'$  increased with increased aging time at 41°C up to 7 days, and then declined between 7 and twelve days. We speculate that  $G'$  may have decreased because of “syneresis” or a shift from inter-polymer crosslinks to intra-polymer crosslinks. More work is needed to test these hypotheses.

For a Cr(III)-acetate-HPAM gel, shear stress was fairly insensitive to shear rate. When shear rate was increased by a factor of 100,000, shear stress only increased by a factor of 10. This result was consistent with our earlier observations that the pressure gradient required to extrude a gel through a fracture was fairly insensitive to injection velocity. A log-log plot of complex viscosity versus shear rate gave a slope of  $-0.8$ . This value was very similar to that for a log-log plot of resistance factor versus injection velocity that was noted earlier during gel extrusion through fractures. Considerable additional work is needed to establish a correlation between gel behavior in fractures versus in a viscometer.

### ***Water Shutoff in Unfractured Production Wells***

A review of the literature identified some ideas and phenomena that might be useful in future development of blocking agents that reduce water production from wells without damaging oil productivity. First, polymers and gels that reduce  $k_w$  much more than  $k_o$  could be extremely valuable if the property could be predicted reliably and if the reduction of  $k_o$  is no more than a factor of 2. Second, the limiting capillary pressure effect could allow a low-mobility foam to form in high-permeability zones while preventing foam formation in low-permeability zones. Third, oil-free water zones may be restricted by oil-soluble particles, oil-collapsible foams, or reactive chemicals that form a blocking agent upon contact with water. Fourth, gelled foams could conceivably provide a more reliable disproportionate permeability reduction. Finally, under limited circumstances in reservoirs where free fluid crossflow can occur, thermally triggered diverting agents or mobility-matched postflushes could allow a desirable gel placement. A substantial amount of additional development is required before these ideas will receive widespread application.

### ***Disproportionate Permeability Reduction***

The purpose of water shutoff treatments in production wells is to reduce water production without damaging the oil productivity. Many polymers and gels can reduce the permeability to water more than that to oil or gas. This property is critical to the success of water shutoff treatments in production wells if hydrocarbon-productive zones cannot be protected during placement. However, the mechanism of this disproportionate permeability reduction is not fully understood.

In Chapter 6, we continue our study of the most promising mechanism—a combined “wall-effect” and “gel-droplet” model. Our analyses suggest that if a gelant is the wetting phase, a modified wall-effect model could explain why the disproportionate permeability reduction occurs. In contrast, when the gelant is the non-wetting phase, a gel-droplet model could explain the disproportionate permeability reduction. The combined model predicts that the disproportionate permeability reduction should increase with increasing residual non-wetting-phase saturation. In support of this prediction, our oil/water experiments showed that in strongly water-wet Berea

cores, the disproportionate permeability reduction increased with increased residual oil saturation. Also, results from our oil/water experiments suggest that maintaining a higher residual oil saturation in the treated region of an oil zone could significantly reduce the damage to oil productivity after treatment.

We also studied the effect of pressure drawdown on the disproportionate permeability reduction. Results from our oil/water experiments indicated that the disproportionate permeability reduction increased with increased pressure drawdown (between 45 psi/ft to 180 psi/ft). This finding suggests that to a certain extent, an increase in pressure drawdown after treatment might reduce the productivity damage to oil without affecting the ability of the gel to reduce water production.

## 1. INTRODUCTION

In the United States, more than 20 billion barrels of water are produced each year during oilfield operations. Today, the cost of water disposal is typically between \$0.25 and \$0.50 per bbl for pipeline transport and \$1.50 per bbl for trucked water. Therefore, a tremendous economic incentive exists to reduce water production if that can be accomplished without significantly sacrificing hydrocarbon production. For each 1% reduction in water production, the cost savings to the oil industry could be between \$50,000,000 and \$100,000,000 per year. Reduced water production would result directly in improved oil recovery (IOR) efficiency in addition to reduced oil-production costs. A substantial positive environmental impact could also be realized if significant reductions are achieved in the amount of water produced during oilfield operations.

In an earlier project,<sup>1</sup> we identified fractures (either naturally or artificially induced) as a major factor that causes excess water production and reduced oil recovery efficiency, especially during waterfloods and IOR projects. We found fractures to be a channeling and water production problem that has a high potential for successful treatment by gels and certain other chemical blocking agents. We also determined that the ability of blocking agents to reduce permeability to water much more than that to oil is critical to the success of these blocking treatments in production wells if zones are not isolated during placement of the blocking agent.

### *Objectives*

This research project has three objectives. The first objective is to develop a capability to predict and optimize the ability of gels to reduce permeability to water more than that to oil or gas. The second objective is to develop procedures for optimizing blocking agent placement in wells where hydraulic fractures cause channeling problems. The third objective is to develop procedures to optimize blocking agent placement in naturally fractured reservoirs. This research project consists of three tasks, each of which addresses one of the above objectives. Our work is directed at both injection wells and production wells and at vertical, horizontal, and highly deviated wells.

### *Report Content*

This report describes work performed during the first year of the project. In Chapter 2, we report experimental results from studies of gel properties in fractures. In Chapter 3, we review updates to our software for sizing gelant treatments in hydraulically fractured production wells. Chapter 4 describes a study of the rheology of our gels. Chapter 5 reviews concepts directed at applying blocking agents in unfractured production wells where zones are not mechanically isolated during placement. Finally, in Chapter 6, we investigate the mechanism responsible for gels reducing the permeability to water more than that to oil.

## 2. GEL PROPAGATION THROUGH FRACTURES

Some of the most successful treatments to reduce water and gas channeling in reservoirs used large volumes of gel that extruded through fractures during the placement process.<sup>2-5</sup> A need exists to determine how much gel should be injected in a given application and where that gel distributes in a fractured reservoir. These parameters depend critically on the properties of gels in fractures. Therefore, we have a research program to determine these properties. In previous work,<sup>6-9</sup> we demonstrated that a minimum pressure gradient was required to extrude a given gel through a fracture. Once this minimum pressure gradient was exceeded, the pressure gradient during gel extrusion was insensitive to the flow rate. This behavior was attributed to a strong “slip” effect exhibited by the gel.<sup>6,8</sup> In particular, when an element of gel extruded through a fracture, it moved as a plug, with a flow discontinuity occurring between the gel plug and the fracture faces. In other words, little or no viscous dissipation of energy occurred within the moving gel plug.

The pressure gradient required for gel extrusion varied inversely with the square of fracture width (Eq. 1 and Fig.1). We also found that gels can concentrate (dehydrate) during extrusion through fractures. Depending on fracture width (see Fig. 2), this dehydration effect can significantly retard gel propagation (e.g., by factors up to 50). Figures 1 and 2 apply to a one-day-old Cr(III)-acetate-HPAM gel [0.5% Alcoflood 935 HPAM, 0.0417% Cr(III) acetate] at 41°C. (Ref. 1 provides details of the experiments.)

$$dp/dl = 0.02/w_f^2 \dots\dots\dots (1)$$

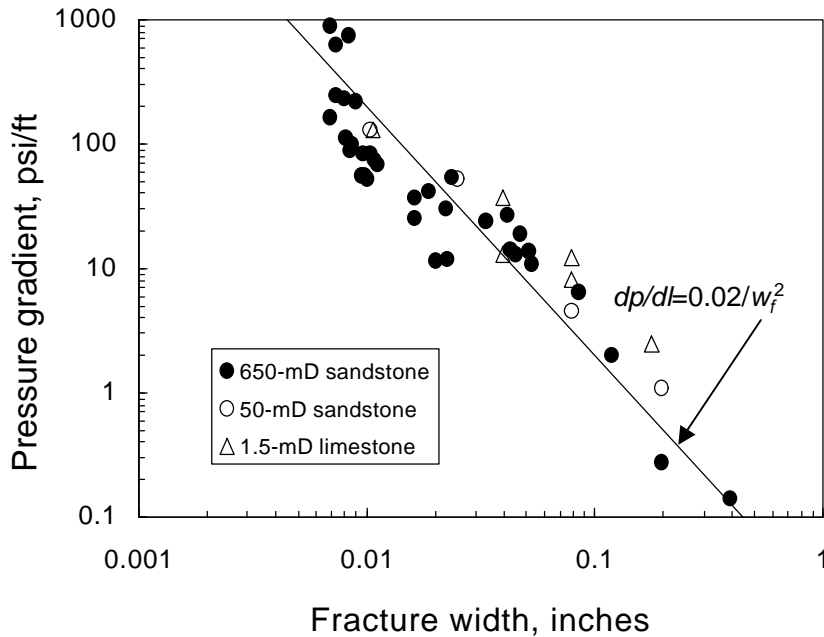


Fig. 1—Pressure gradients required to extrude a gel through open fractures (no proppant).

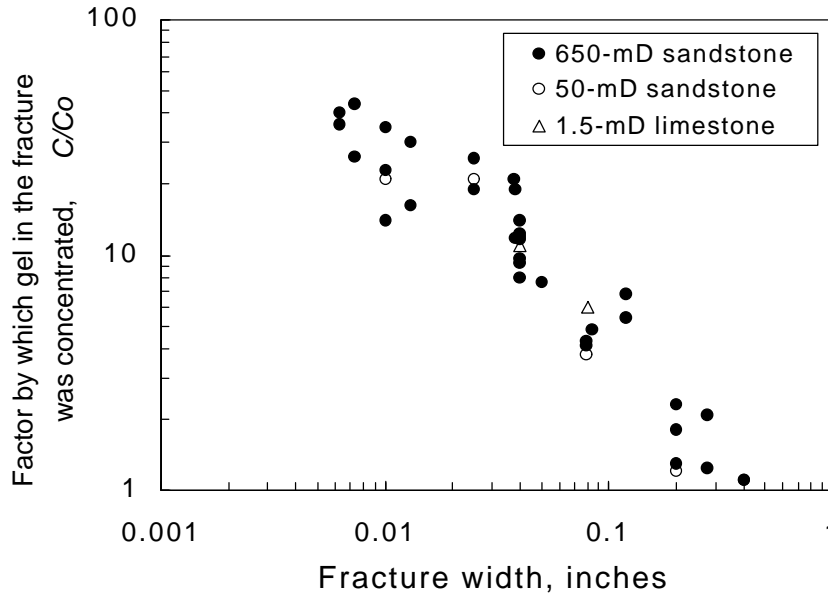


Fig. 2—Degree of gel dehydration versus fracture width.

The objective of our current work is to understand the mechanism for gel extrusion and dehydration in fractures. With this understanding, we ultimately hope to predict conditions, gel compositions, and gel volumes that provide the optimum gel placement in fractured reservoirs. The specific questions addressed in this chapter are:

1. If a large volume of gel is injected into a fracture, will pressure gradients stabilize or continuously increase?
2. During gel extrusion, how do pressure gradients in the porous rock compare to those in the fracture?
3. What is the composition of fluids that flow in the fracture versus the porous rock?
4. Where and how does gel dehydrate during extrusion through a fracture?
5. During extrusion, does the performance of the gel depend on the permeability of the porous rock?
6. How does gel permeability to water vary with gel composition?
7. How does gel dehydration and extrusion depend on fracture height?
8. How does gel dehydration and extrusion depend on injection rate?
9. What are the extrusion and dehydration properties of gel made with a polymer of higher molecular weight?

***Base Case: Extrusion Through a 48×1.5×0.04-in. Fracture in 650-mD Sandstone***

To probe the mechanism for gel propagation and dehydration, an experiment was performed where a Cr(III)-acetate-HPAM gel was extruded through a four-ft-long fractured core. The core (see Fig. 3) was prepared from 650-mD Berea sandstone, fractured lengthwise, and cast in epoxy using our standard method.<sup>6-9</sup> The core height and width were both 1.5 in. (3.81 cm). The fracture height was also 1.5 in., and the fracture was oriented vertically during the experiments. The

effective average fracture width was 0.04 in. (0.1 cm), and the average fracture conductivity was 277 darcy-ft. The fracture volume was 2.84 in.<sup>3</sup> (46.5 cm<sup>3</sup>), and the core pore volume was 24.1 in.<sup>3</sup> (395 cm<sup>3</sup>). Four equally spaced internal taps were positioned to measure pressures along the length of the fracture. Four equally spaced internal taps also were placed to measure pressures along the length of the porous rock. These sets of taps divided the core into five sections of equal length. One additional internal pressure tap was placed to measure pressure in the matrix just after the inlet sand face. A special fitting (Fig. 4) was epoxied to the core outlet to segregate the effluent from the fracture and that from the porous rock. Before gel injection, the fractured core was saturated with brine and characterized using tracer studies and flow measurements.<sup>6-9</sup>

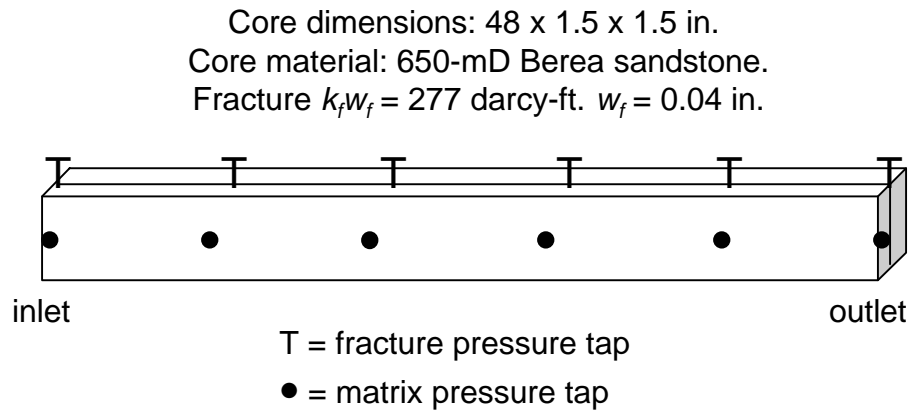


Fig. 3—Illustration of the fractured core.

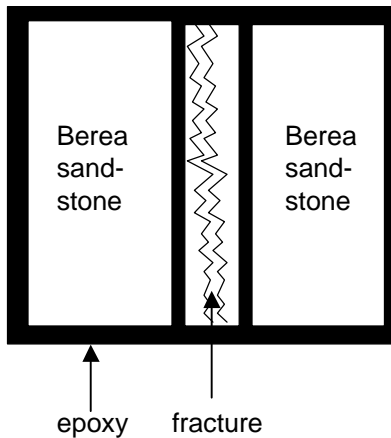


Fig. 4—Core outlet configuration to separate fracture effluent from porous-rock effluent.

Our experiments used an aqueous gel that contained 0.5% Allied Colloids Alcoflood 935 HPAM (molecular weight  $\approx 5 \times 10^6$  daltons; degree of hydrolysis 5% to 10%), 0.0417% Cr(III) acetate, 1% NaCl, and 0.1% CaCl<sub>2</sub> at pH=6. All experiments were performed at 41°C (105°F). The gelant formulations were aged at 41°C for 24 hours (five times the gelation time) before injection into a fractured core.

**Pressure Gradients in the Fracture.** We extruded 80 fracture volumes (226 in.<sup>3</sup> or 3,700 cm<sup>3</sup>) of one-day-old Cr(III)-acetate-HPAM gel through the 4-ft-long fractured core using an injection rate of 12.2 in.<sup>3</sup>/hr (200 cm<sup>3</sup>/hr). Figures 5 and 6 show the pressure gradients in the fracture for the five fracture sections during gel injection. At the end of gel injection, the average pressure gradient in the fracture was 28 psi/ft for the first three fracture sections and 50 psi/ft in the last two fracture sections. This result suggests that the last two fracture sections were slightly narrower and less conductive than the first three fracture sections. In all sections, the pressure gradients were reasonably stable during the last 60 fracture volumes of gel injection. Thus, gel injection did not exhibit progressive plugging (i.e., continuously increasing pressure gradients) in any part of the fracture.

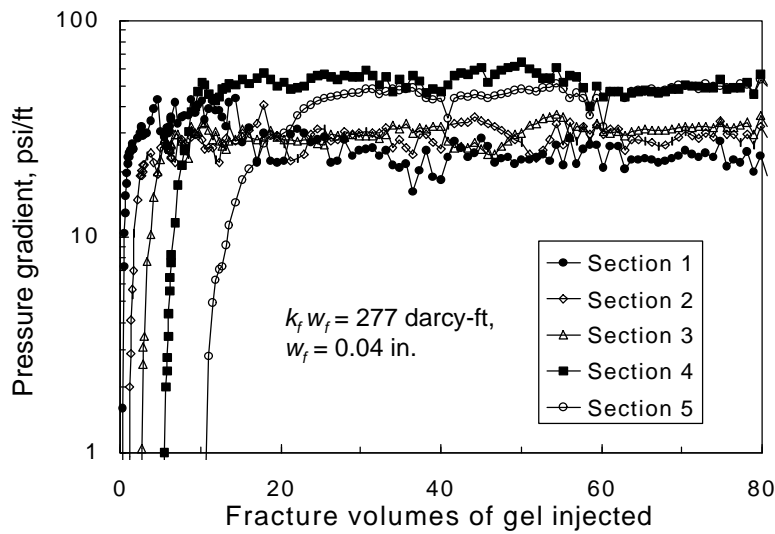


Fig. 5—Pressure behavior in the fracture taps during gel injection (normal scale).

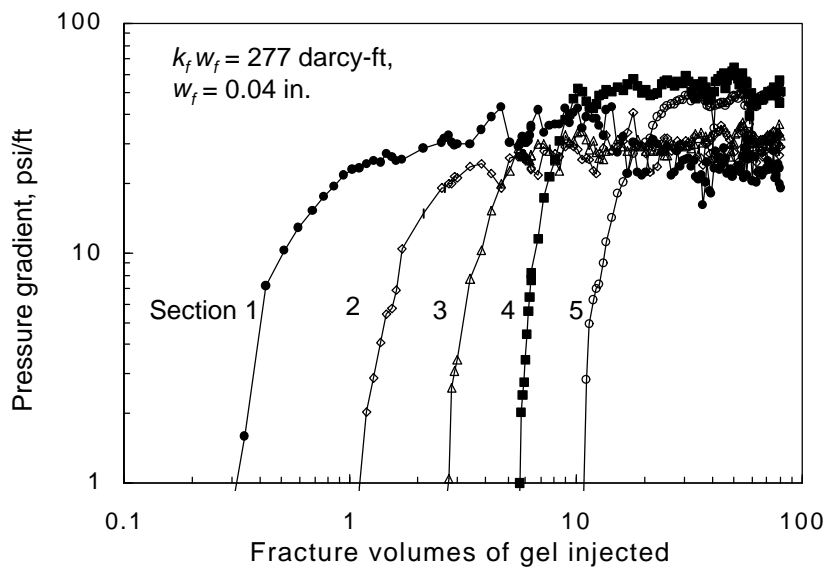


Fig. 6—Pressure behavior in the fracture taps during gel injection (log scale).

**Pressure Gradients in the Porous Rock.** During gel injection, pressure gradients in the porous rock are shown in Fig. 7 for the five sections of the core. These pressure gradients were typically between 0.2 and 1.0 psi/ft—much lower than the values observed in the fracture. For a given section, the onset of a pressure response occurred at the same injection volume for both the fracture pressure gradients and the matrix pressure gradients (compare Figs. 6 and 7).

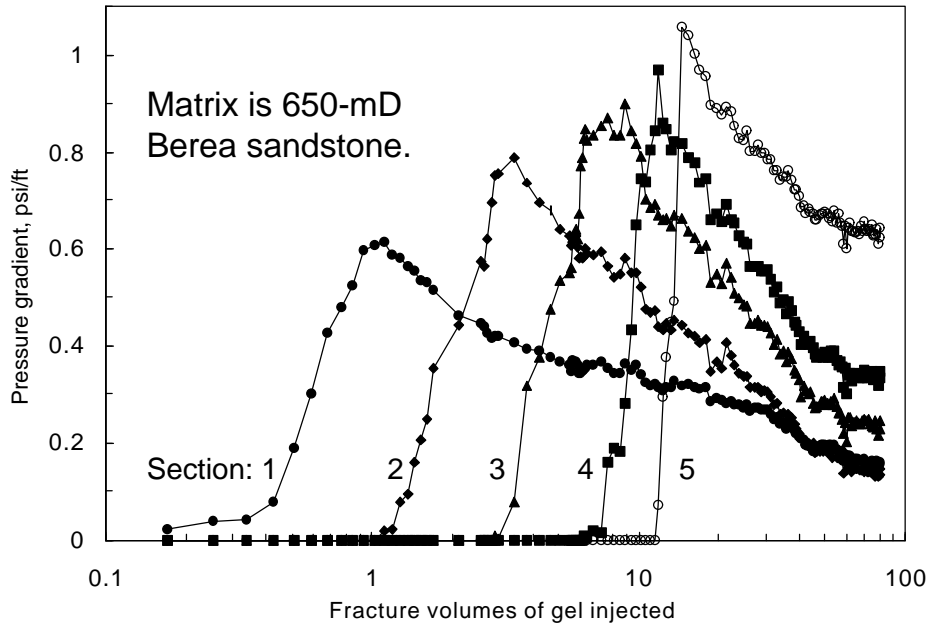


Fig. 7—Pressure behavior in the matrix taps during gel injection.

**Produced Fluids.** As mentioned earlier, a special outlet fitting segregated the effluent from the fracture and that from the porous rock. Figure 8 plots the fraction of the effluent that was produced from the fracture versus from the porous rock. During the first 15 fracture volumes of gel injection, virtually 100% of the flow was produced from the fracture. This result was expected. Before gel injection, the calculated flow capacity of the fracture was 3,400 times greater than the flow capacity of the porous rock. Gel arrived at the fracture outlet after injecting 15 fracture volumes of gel. Coincident with gel arrival, flow from the fracture abruptly stopped for a period of about two fracture volumes of gel injection. (So, 100% of the effluent was produced from the matrix during this time.) Subsequently, the fraction of flow from the fracture increased, while flow from the porous rock decreased. After injecting 80 fracture volumes of gel, flow from the fracture accounted for 65% of the total flow, while flow from the matrix accounted for 35% of the total flow.

The physical appearance of the gel from the fracture outlet was the same as that of the injected gel. Also, the composition of the gel from the fracture outlet was similar to that of the injected gel. Chromium concentrations were measured using atomic absorption spectroscopy (by the New Mexico BMMR Chemistry Laboratory), and HPAM concentrations were determined using total organic carbon analysis (Shimadzu TOC-5050A). The chromium and HPAM concentrations are

plotted in Fig. 9 for effluent samples from the fracture and the matrix. This figure confirms that the fracture provided the only conduit for the gel. After gel breakthrough, the chromium concentration averaged 1.17 times that of the injected gel, while the polymer concentration averaged 1.35 times that of the injected gel. Chromium and polymer concentrations in the matrix effluent were negligible.

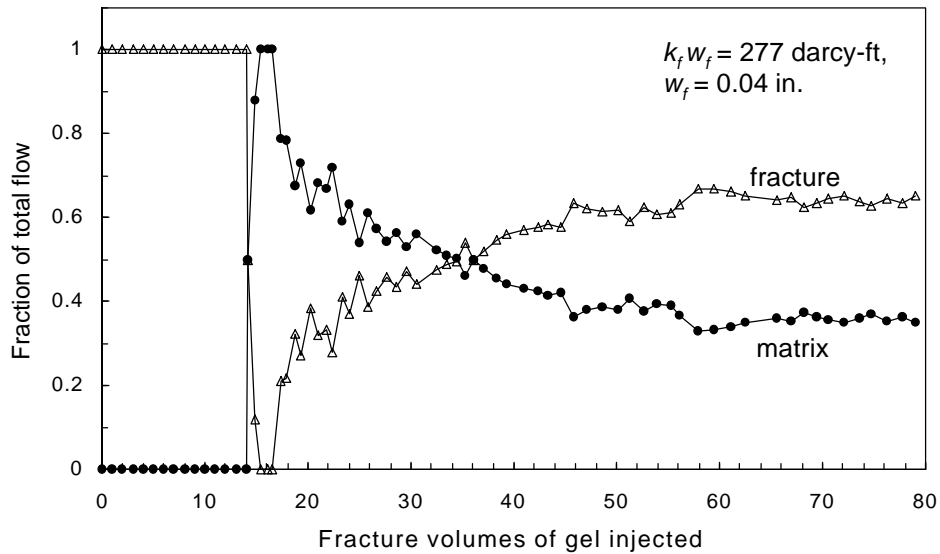


Fig. 8—Fractional flow measured at the core outlet (200 cm<sup>3</sup>/hr).

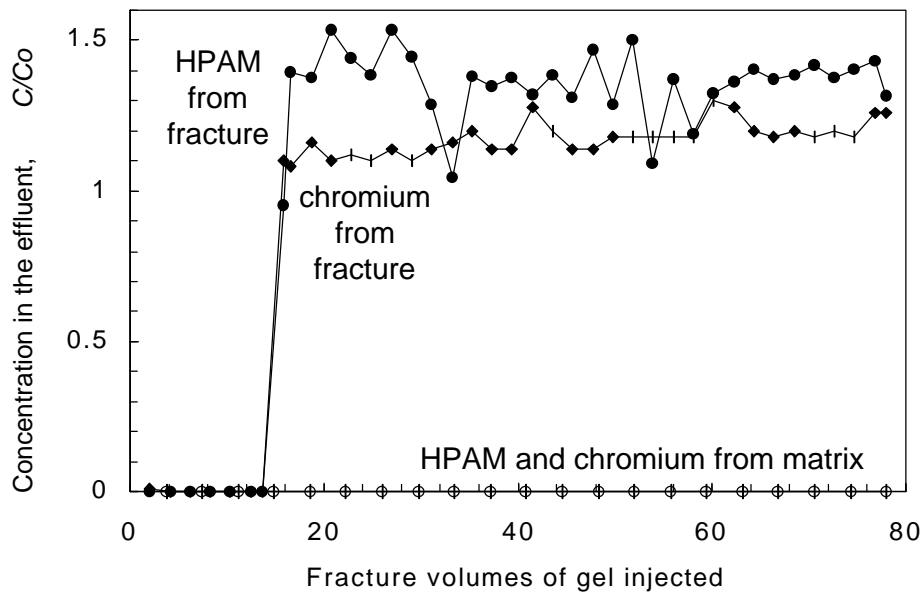


Fig. 9—Chromium and HPAM concentrations in the effluent: fracture versus matrix.

**Gel Composition in the Fracture.** After gel injection, the fracture was opened to reveal a rubbery gel that completely filled the fracture. This gel (after 80 fracture volumes of gel injection) was analyzed for chromium and HPAM as a function of length along the fracture (solid symbols in Fig. 10). The chromium and HPAM concentrations in the fracture averaged 28.7 and 26.0 times those for the injected gel, respectively. The gel became somewhat less concentrated with increased distance along the fracture. In the first 25% of the fracture, the gel was about 50% more concentrated than in the final 25% of the fracture.

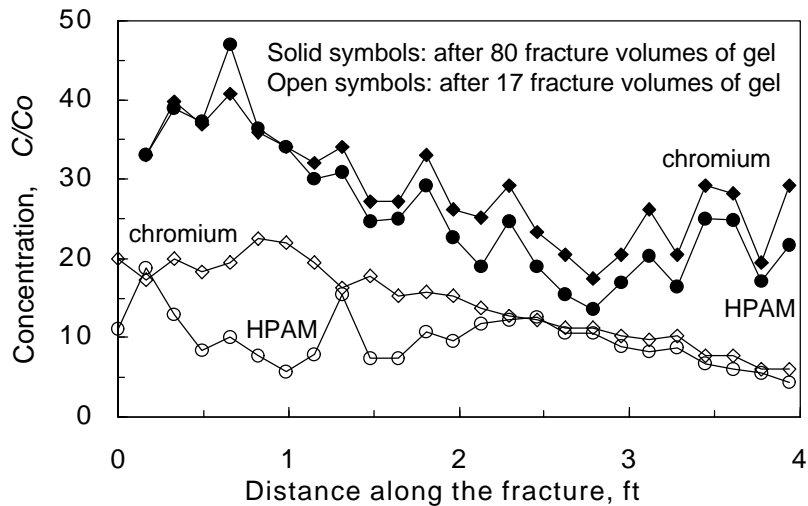


Fig. 10—Composition of gel in the fracture (relative to the injected gel).

The open symbols in Fig. 10 show chromium and HPAM content for gel from a separate, identical experiment, except that only 17 fracture volumes of Cr(III)-acetate-HPAM gel were injected. (Details of this experiment can be found in Ref. 1.) At the end of this experiment, the chromium and HPAM concentrations in the fracture averaged 14.3 and 9.5 times those for the injected gel, respectively. Again, the gel became somewhat less concentrated with increased distance along the fracture. Figure 10 suggests that gel in the fracture became more concentrated with increased throughput and time of gel injection.

**Gel Injection Did Not Cause Progressive Plugging.** In previous work using 4-ft-long fractured cores, less than 20 fracture volumes of gel were typically injected.<sup>6-8</sup> During these experiments, pressure gradients appeared to stabilize along the fracture during gel injection at a fixed flow rate. However, we wondered whether pressure gradients might continuously increase during injection of larger gel volumes. The results from our new experiment (Fig. 5) diminish this concern.

The pressure behavior in Fig. 6 shows the rate of gel propagation through the fracture. In particular, gel first entered Fracture Sections 2, 3, 4, and 5 after injecting 1.1, 2.7, 5.6, and 11 fracture volumes of gel, respectively. (Figure 6 also suggests that 0.3 fracture volumes of gel were required before entering Section 1. This result simply reveals the experimental error associated with timing at the start of the coreflood.) Gel was first detected in the effluent from the fracture

after injecting 15 fracture volumes of gel. Figure 11 indicates the rate of gel propagation in the five fracture sections relative to that expected for a displacement with no retardation or dispersion of the gel front in the fracture. In the first fracture section, the rate of gel propagation was 18% that for an unimpeded displacement, while in the fourth and fifth fracture sections, gel propagated at about 4%-5% of the rate for an unimpeded displacement.

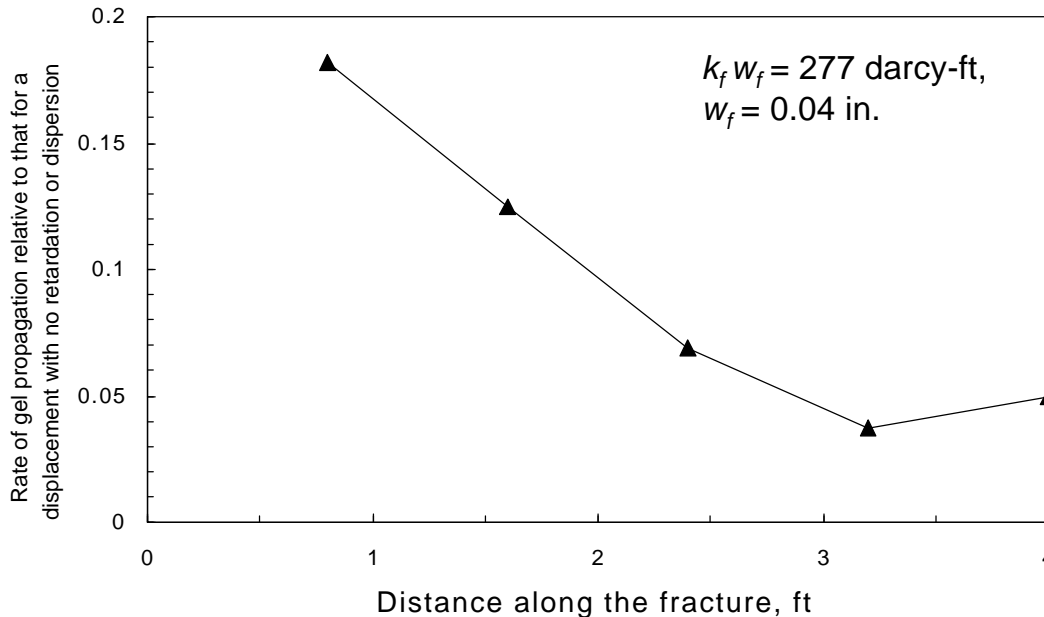


Fig. 11—Gel propagation rate in the fracture.

**Gel That Concentrated Became Immobile.** Although gel that remained in the fracture at the end of the experiment was concentrated by factors up to 40 (Fig. 10), the gel that actually propagated through the fracture had a composition similar to that of the injected gel (Fig. 9). This result implies that for the most part, gel that dehydrated in the fracture ceased to propagate. In the next three sections, dehydrated gel will be shown to form as a filter cake on the fracture faces.

**Brine Flow in Porous Rock Was Substantial.** The pressure gradients shown in Fig. 7 indicate fluid flow in the porous rock during gel injection. That fluid was exclusively brine—based on Figs. 8 and 9 and previous proof that the Cr(III)-acetate-HPAM gel does not flow through porous rock.<sup>7</sup> Of course, the source of this flow was water that left the gel in the fracture—i.e., water from the gel dehydration process.

The Darcy equation was used to convert the pressure gradients in Fig. 7 to flow rates. (Rock permeability was 650 mD, and brine viscosity was 0.67 cp at 41°C.) Since the total injection rate was fixed (at 200 cm<sup>3</sup>/hr), the matrix flow rates, in turn, were converted to the fraction of total flow that occurred through the rock matrix at any given time. Figure 12 plots the results of this conversion. For a given position along the core, flow through porous rock did not become significant until the gel front reached that position in the fracture. Shortly after arrival of the gel

front in the adjacent fracture, flow in the porous rock rose to a maximum between 35% and 60% of the total flow (i.e., a minimum between 40% and 65% of the total flow occurred in the fracture). Then, the fraction of total fluid flow gradually declined. After injecting 80 fracture volumes of gel, the fraction of flow in the matrix ranged from 0.1 to 0.35.

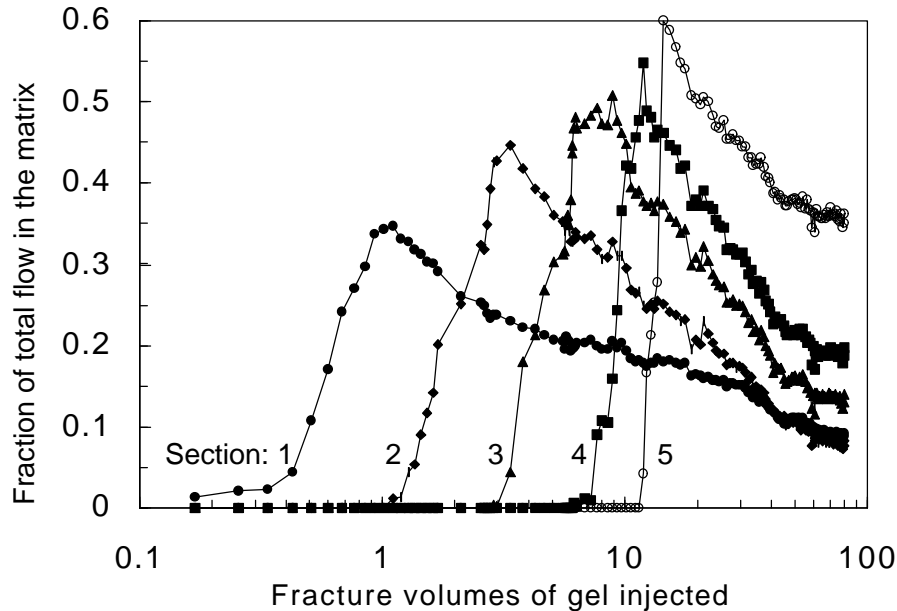


Fig. 12—Brine flow in the porous rock during gel injection.

At any given time, Fig. 12 plots the average fraction of the total flow that occurred in the porous rock in each of the five core sections. For comparison, Fig. 8 plots the measured fraction of total flow (in the matrix versus in the fracture) at a single position—at the outlet of the fractured core. The two data sets were consistent in that at the end of gel injection, the final fractional flow from the matrix (35%) was the same in Fig. 8 as that in Fig. 12 for the fifth section of the core.

**Brine Leakoff Peaked after the Gel Front Passed.** Utilizing a mass balance, the data in Fig. 12 was used to determine the leakoff rate through the fracture faces for the different sections of the core. In particular, the flow rate in the matrix of a given core section was the sum of the leakoff from the fracture faces plus the flow rate from the matrix of the previous (upstream) core section. Figure 13 plots the leakoff rate per unit of fracture face versus the fracture volumes of gel injected for the various sections of the core. Again, the source of the leakoff was water that left the gel in the fracture. The leakoff rates were normalized relative to the largest leakoff rate observed during the experiment (i.e.,  $1.89 \times 10^{-4}$  ft<sup>3</sup>/ft<sup>2</sup>/min or  $9.63 \times 10^{-5}$  cm<sup>3</sup>/cm<sup>2</sup>/s).

For any given section, Fig. 13 demonstrates that the leakoff rate rapidly rose to a maximum and then gradually diminished. A comparison of Figs. 6 and 13 suggests that in all but the first section, the onset of leakoff lagged significantly behind the arrival of the gel front in the fracture. In particular, in each section, the onset of leakoff corresponded very closely to the arrival of the gel

front at the beginning of the next (downstream) fracture section. Since each core section was about 10 in. long, the onset of leakoff lagged about 10 in. behind the gel front.

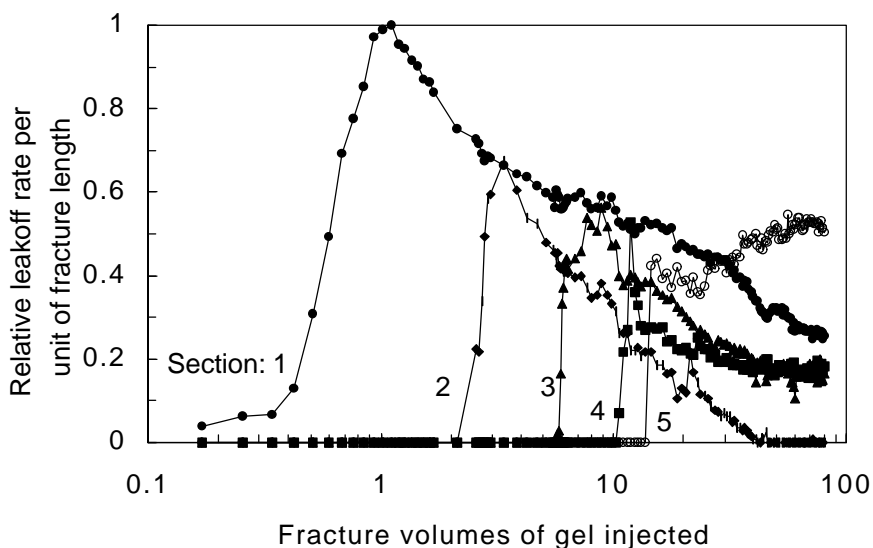


Fig. 13—Relative leakoff rates derived from Fig. 12.

The greatest leakoff rate was observed in the first core section after injecting about one fracture volume of gel. In Fig. 13, this maximum rate was arbitrarily assigned a value of unity. The peak leakoff rates in Sections 2, 3, 4, and 5 were 67%, 56%, 53%, and 54% of this value, respectively. After injecting 80 fracture volumes of gel, the relative leakoff rates varied from 0 (in Section 2) to 0.5 (in Section 5).

**Concentrated Gel Formed as a Filter Cake.** How does concentrated gel form in the fracture? Figure 13 provides some insight into this issue. As mentioned earlier, at a given point along the fracture, the onset of leakoff may lag behind the gel front by about 10 in. Of course, gel in the fracture near the front inhibits flow for gel farther upstream. Also, the pressure differences between the fracture and the matrix are greater in the early parts of the fracture than near the gel front. Thus, the upstream gel has a greater tendency to form a filter cake of concentrated gel against the fracture face.

Behind the gel front, Fig. 13 reveals that leakoff occurred and the gel lost water along most of the gel-contacted portion of the fracture. In other words, gel dehydration did not occur all at once when the gel first entered the fracture, nor did it occur exclusively at the gel front. Our results suggest that a filter cake of concentrated gel formed gradually along the length of the fracture. We envision that the gel filter cake formed on the fracture face because of the high-pressure gradient between the fracture and the adjacent matrix.

At a given point in the fracture, Fig. 13 reveals that the leakoff rate gradually decreased after the gel front passed. This result indicates that thicker or more concentrated gel filter cakes

accumulated on the fracture faces in the upstream sections. This suggestion is supported by Fig. 10. Furthermore, in our experience to date,<sup>6-9</sup> the concentrated gel completely filled the width of the fracture, no matter how much (or how little) gel was injected. We saw no direct evidence that the filter cake increased in thickness with increased gel throughput. In other words, for most of the gel placement process, the filter cake “grew” (or increasingly inhibited water leakoff) by becoming more concentrated, rather than by increasing in thickness. This suggestion is supported by a comparison of the solid and open data points in Fig. 10. Interestingly, even though the gel became increasingly concentrated with increased throughput, the pressure gradient required for extrusion did not increase during the last 60 fracture volumes of gel injection (Fig. 5).

The leakoff data was used to estimate the average permeability to water for the concentrated gel. Near the end of gel injection, the average permeability of the gel filter cake was 0.2  $\mu\text{D}$ .

Given that gel does not flow into the porous rock,<sup>7</sup> a mass balance was applied to the data in Fig. 13 to estimate the total weight of chromium and HPAM that remained in the fracture after 80 fracture volumes of gel injection. This calculation was performed for the entire fracture and for each of the five fracture sections. The results were compared with the actual final mass of chromium and HPAM in the fracture, based on the solid symbols in Fig. 10. This comparison revealed that the final chromium mass in the fracture accounted for 92% of the value expected from the leakoff calculation. The final HPAM mass in the fracture accounted for 76% of the value expected from the leakoff calculation. These values apply to the entire core. Individual results for the first, third, and fourth sections of the core were very similar to those for the entire core. For the second core section, the actual chromium and HPAM masses in the fracture were two to three times those expected from the leakoff calculation. For the fifth core section, the actual chromium and HPAM masses in the fracture were 30-45% of those expected from the leakoff calculation. The discrepancies for the second and fifth sections may have been caused by pressure errors during the flow measurements.

The above results indicate that when an element of gel experiences dehydration, most of the chromium and HPAM remain in the fracture. However, a fraction of free chromium and uncrosslinked HPAM may leak off into the porous rock along with the water from the dehydration process. This suggestion was confirmed during a sandpack experiment that was described in Ref. 9. Presumably, in Berea sandstone, the free chromium and uncrosslinked HPAM were retained by the rock, so they were never produced through the matrix. During the experiment, the total amount of brine produced from the matrix was 4.1 core pore volumes (PV). If 76% to 92% of the original HPAM and chromium, respectively, were removed from the brine before entering the rock (as indicated above), the remaining HPAM and chromium in 4.1 PV of brine could easily be removed by retention in the Berea sandstone. Thus, the absence of chromium and HPAM in the effluent from the matrix was not surprising (Fig. 9).

**Flowing Gel May Be Concentrated Slightly.** Figure 8 suggests that after 80 fracture volumes, each new element of injected gel should be concentrated by 35% (because water produced from the matrix stabilized at 35% of the total flow). Figures 5, 8, and 9 indicate that near the end of the experiment, a steady state was attained. Therefore, some concentrated (dehydrated) gel appeared to propagate through the fracture. Three possibilities are evident. First, the propagating gel may

be homogeneous (i.e., with a uniform concentration that was roughly 35% greater than the injected gel). Alternatively, the propagating gel may be a mixture of two components. The injected gel may comprise the dominant component, while a minor component may be very concentrated gel with the composition of the material found in the fracture at the end of the experiment (i.e., gel that was ~27 times more concentrated than the injected gel). In other words, at steady state, we suggest that pressure gradients may be great enough to mobilize a small amount of the dehydrated gel. The third possibility is that experimental errors cause the produced HPAM and chromium concentrations to appear higher than the actual values. While we believe the concentration measurements were correct, we cannot completely rule out this possibility. More work is needed to distinguish between these possibilities.

### ***Effect of Rock Permeability***

Of course, the extrusion properties of a gel depend on the fracture width (see Figs. 1 and 2). However, does the performance of the gel depend on the permeability of the rock that is adjacent to the fracture? Most of our previous work used fractured 650-mD Berea sandstone. Therefore, several extrusion experiments were conducted using fractured 50-mD Berea sandstone and 1.5-mD Indiana limestone. Details of the experimental procedures can be found in Ref. 1. The pressure gradients required for extrusion are shown by the open symbols in Fig. 1, while the degrees of dehydration experienced by the gel are shown by the open symbols in Fig. 2. These figures demonstrate that the performance of the gel was not sensitive to rock permeability.

To understand this finding, note that gel permeability (typically in the  $\mu\text{D}$  range) was always much less than the rock permeability (1.5 mD or greater). Therefore, the gel permeability determined the rate at which water (from the dehydration process) entered the rock. The degree of dehydration was affected by the pressure difference between the fracture and the porous rock next to the fracture. In most of our experiments, the flow capacity of the rock was sufficient to rapidly drain any water of dehydration from the gel. (This condition also occurs in virtually all field applications.<sup>1</sup>) Therefore, the pressure in the rock was always quite low, and the pressure difference was fairly high between the fracture and the adjacent porous rock. For a given position along the fracture, this pressure difference was insensitive to rock permeability, since the pressure gradient in the fracture was determined primarily by fracture width (Fig. 1). Consequently, the degree of gel dehydration was also insensitive to rock permeability. (Incidentally, when performing experiments with 1.5-mD limestone, the core must be designed or sized with sufficient flow capacity to adequately drain the water that dehydrated from the gel. Otherwise, gel dehydration may be underestimated.)

### ***Model for Gel Propagation and Dehydration***

The experimental results suggest that gel dehydration occurred because the pressure in the fracture was much greater than that in the porous rock next to the fracture. Since the gel had a finite permeability to water<sup>10</sup> and since the crosslinked polymer did not penetrate into the porous rock,<sup>7</sup> water flowed from the gel (in the fracture) into the porous rock. This action increased the average gel concentration in the fracture. For the most part, the concentrated gel was immobile.

At a given point along the fracture, the leakoff rate per unit area of fracture face,  $u_1$ , was estimated from the Darcy equation.

$$u_1 = 2k_{\text{gel}} \Delta p / (w_f \mathbf{m}) \dots\dots\dots (2)$$

In Eq. 2,  $k_{\text{gel}}$  was gel permeability to water,  $\mathbf{m}$  was water viscosity,  $w_f$  was fracture width, and  $\Delta p$  was pressure drop between the fracture and the porous rock. Equation 2 assumed that the average distance that water traveled to reach the porous rock was  $w_f / 2$ —i.e., from the center of the fracture to the fracture face. Consistent with our experimental observations, the gel composition at a given time and point along the fracture was assumed to be uniform across the width of the fracture. In our experiments, the pressure in the porous rock was small (Fig. 7), so  $\Delta p$  in Eq. 2 was close to the actual pressure in the fracture.

As mentioned earlier, after the gel dehydrated, it generally became immobile in the fracture. The mobile gel basically had the same composition as the injected gel. Therefore, at any given time,  $t$ , and gel-contacted point along the fracture, the relative gel composition,  $C/C_o$ , was estimated using Eq. 3.

$$C/C_o = 1 + \int (2 u_1 / w_f) dt \dots\dots\dots (3)$$

A relation was not available between gel composition and gel permeability to water,  $k_{\text{gel}}$ . Therefore, a simple empirical equation was developed.

$$k_{\text{gel}} = 0.00011 + 1.0 (C/C_o)^{-3} \dots\dots\dots (4)$$

In Eq. 4,  $k_{\text{gel}}$  had units of mD when the gel composition,  $C/C_o$ , was expressed relative to the composition of our standard Cr(III)-acetate-HPAM gel. Of course, the validity of this empirical equation can be questioned. Equation 4 was used simply because it allows a reasonable fit for the experimental results. The actual relation between gel permeability and composition will be discussed later.

Equations 2, 3, and 4 were combined with a mass balance to form a simple model of gel propagation and dehydration in fractures. Based on Figs. 5 and 6, pressure gradients in the gel-contacted portions of the fracture were fixed at 28 psi/ft in the first three fracture sections and 50 psi/ft for the last two fracture sections. In other modeling work with fractures of different widths (to be described shortly), Eq. 1 was also incorporated into the model to account for the dependence of extrusion pressure gradient and fracture width.

**Predictions Versus Experimental Results.** Leakoff rates predicted by the model are shown in Figs. 14-19. The model accurately accounted for several experimental observations. First, the model predicted gel arrival at the ends of the first through fifth fracture sections after injecting 0.9, 2.8, 5.7, 10.7, and 16 fracture volumes, respectively. Experimentally, gel actually arrived after 1.1, 2.7, 5.6, 11, and 15 fracture volumes, respectively.

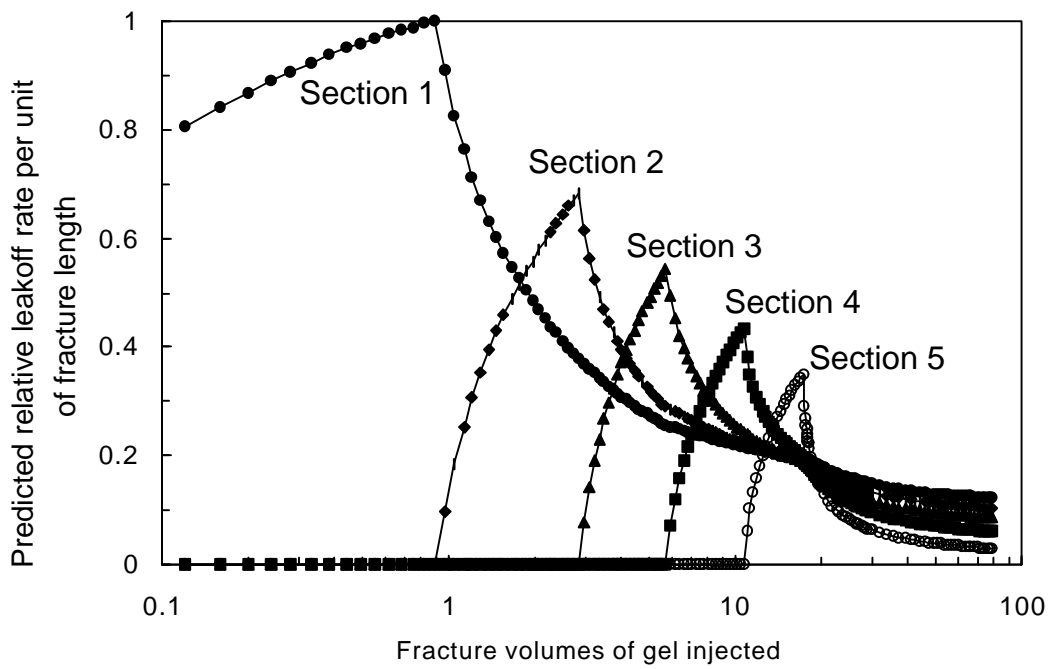


Fig. 14—Predicted leakoff rates.

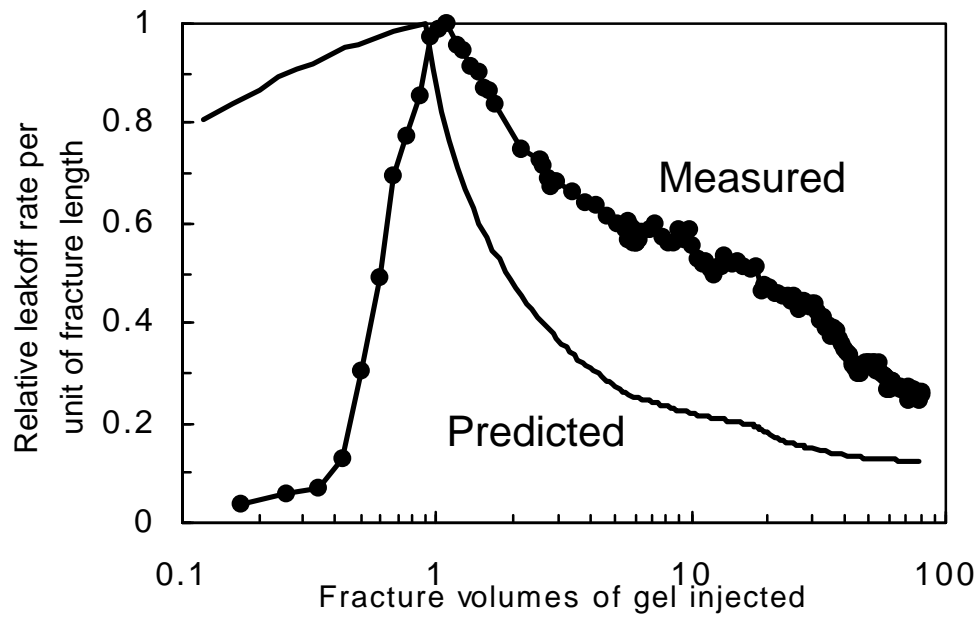


Fig. 15—Predicted versus measured leakoff rates for Section 1.

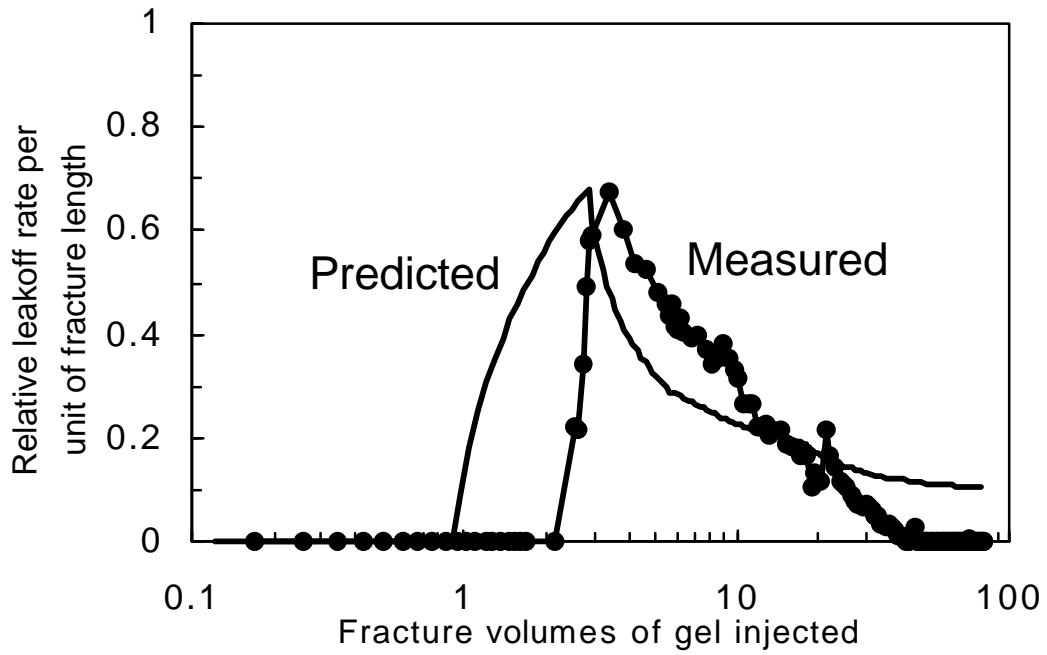


Fig. 16—Predicted versus measured leakoff rates for Section 2.

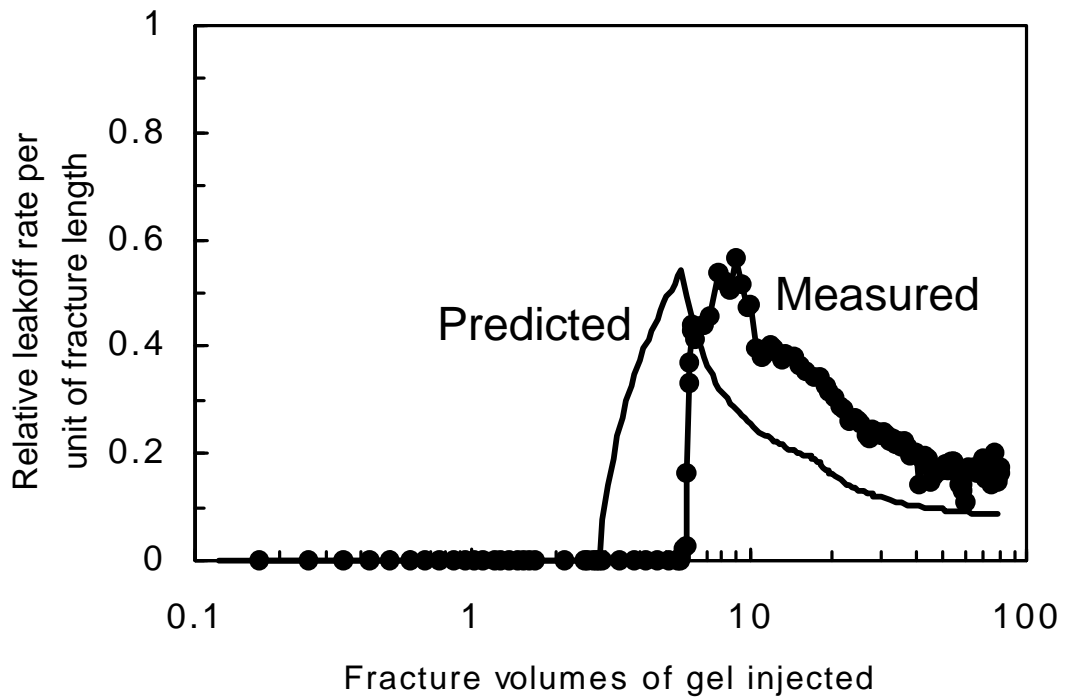


Fig. 17—Predicted versus measured leakoff rates for Section 3.

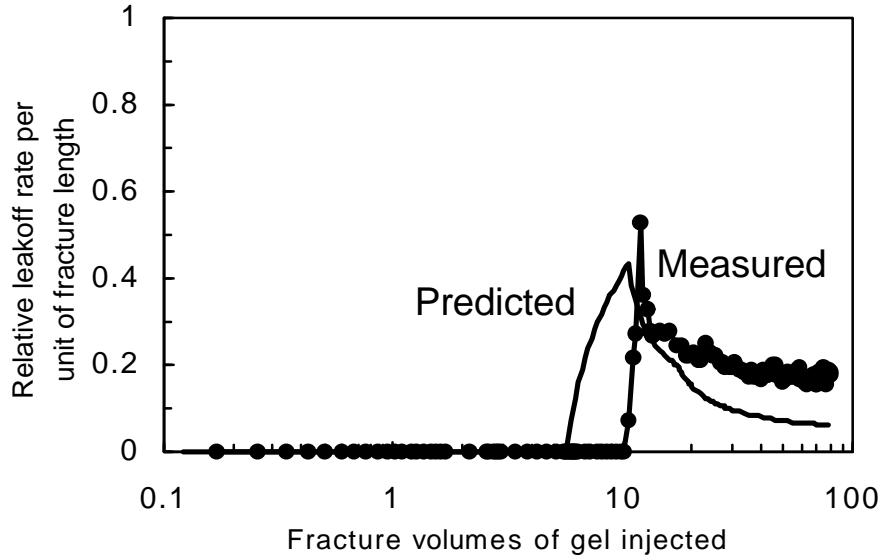


Fig. 18—Predicted versus measured leakoff rates for Section 4.

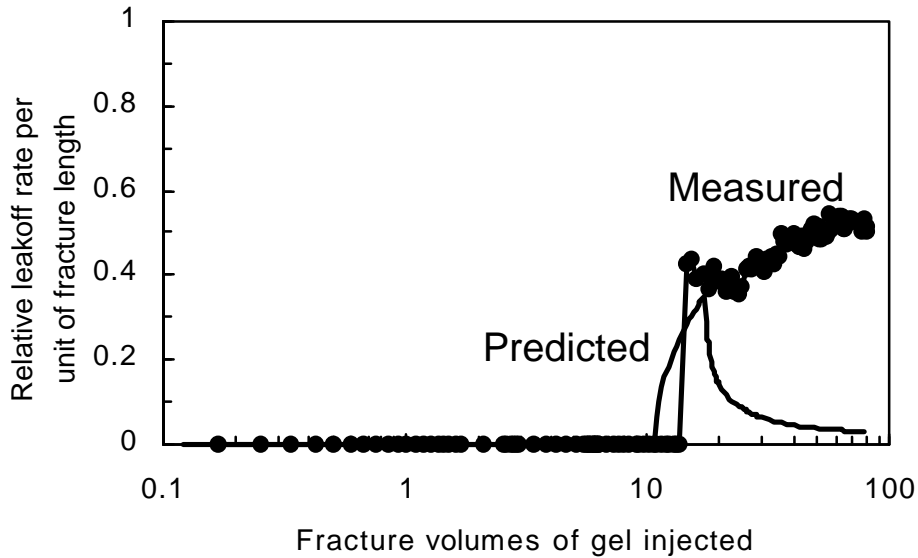


Fig. 19—Predicted versus measured leakoff rates for Section 5.

Second, the general shapes of the predicted water leakoff curves (Fig. 14) matched the experimental curves (Fig. 13) reasonably well. (Detailed comparisons are shown in Figs. 15-19.) The predicted maximum leakoff rate occurred in the first section after injecting 0.9 fracture volumes of gel. For comparison, the experimental maximum in Section 1 was reached after injecting 1.1 fracture volumes. The predicted peak leakoff rates in Sections 2, 3, 4, and 5 were 68%, 54%, 43%, and 35%, respectively, of the predicted peak value in Section 1. The experimental peak leakoff rates in Sections 2, 3, 4, and 5 were 67%, 56%, 53%, and 54%, respectively, of the actual peak leakoff rate.

Third, the model predictions matched the experimental results quite well with regard to the fraction of water flow from the matrix at the core outlet (see Fig. 20).

Fourth, the predicted profiles of final concentrations in the fracture matched the experimental values reasonably well. After 17 fracture volumes of gel injection, the predicted  $C/C_0$  values for gel in the fracture ranged from 25 near the fracture inlet to 12 in the fourth fracture section. The experimental values were 20 and 9, respectively (Fig. 10). After 80 fracture volumes of gel injection, the predicted  $C/C_0$  values for gel in the fracture ranged from 64 near the fracture inlet to 30 in the fourth fracture section. The experimental values were 36 and 25, respectively (Fig. 10). The model did not account for any entry of free chromium or uncrosslinked polymer into the porous rock. Therefore, the predicted concentrations in the fracture were expected to be somewhat higher than the experimental values.

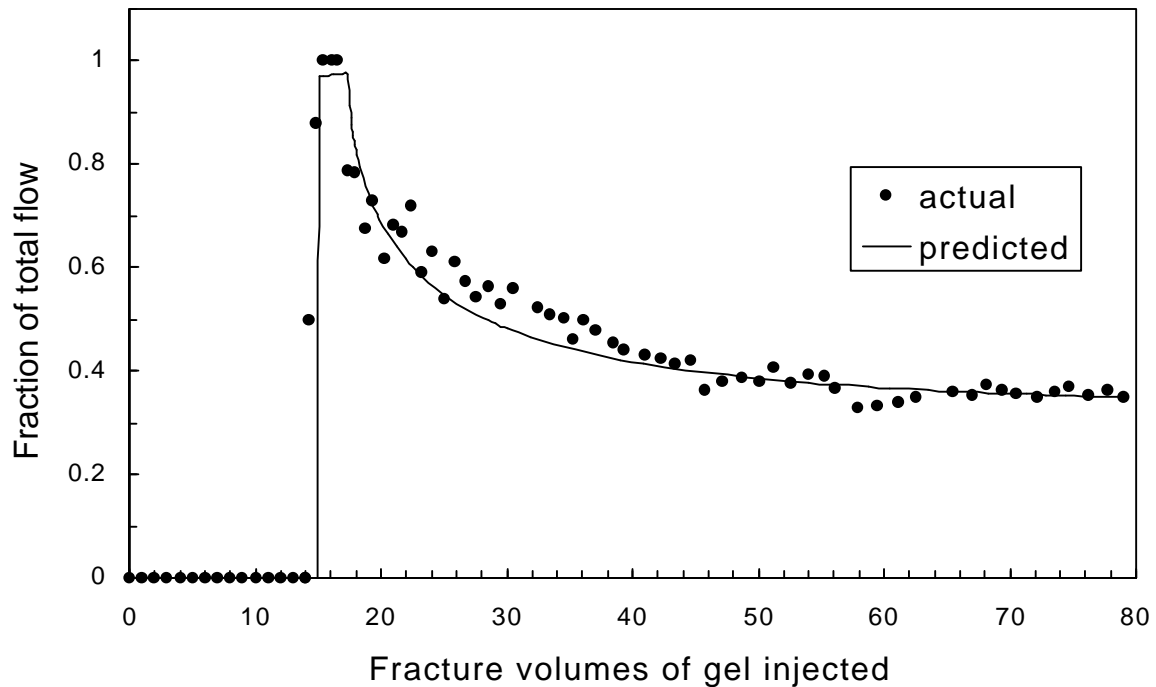


Fig. 20—Predicted versus actual fractional flow from the matrix at the core outlet.

### ***Effect of Fracture Width***

The data points in Fig. 21 show dehydration factors as a function of fracture width in 4-ft-long fractures. This figure shows the results from over 40 separate experiments. Most of these data points were obtained shortly after gel arrival at the end of the fracture. The solid curve shows the predicted values based on our model and an experimentally determined relation between fracture width and the pressure gradient required to extrude gel through the fracture. The predictions matched the experimental values fairly well for fracture widths greater than 0.02 in. For more narrow fractures, our predictions were significantly greater than the actual values.

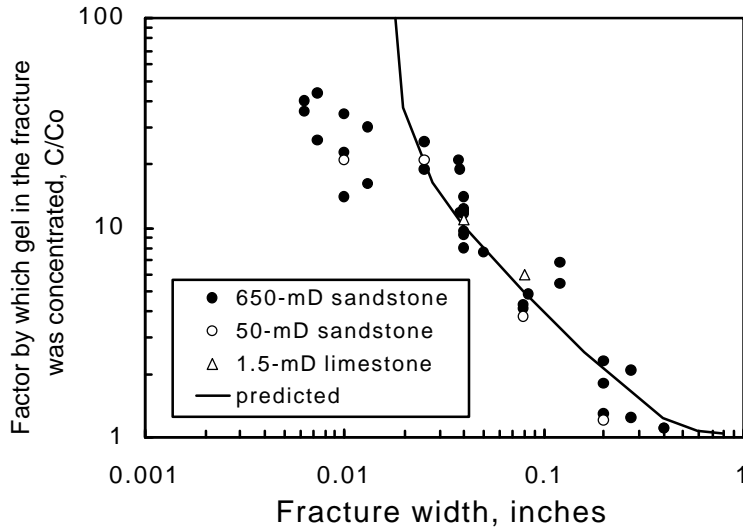


Fig. 21—Predicted versus actual dehydration factors as a function of fracture width.

### Fractures with Varying Widths

To further test our model, an experiment was performed where our 1-day-old Cr(III)-acetate-HPAM gel was extruded through a 4-ft-long fracture with varying widths. The fracture width was 0.02 in. (0.05 cm) for the middle third of the fracture, while the remainder of the fracture was 0.08 in. (0.2 cm) wide. Internal fracture pressure taps were located at 1/6, 1/3, 2/3, and 5/6 of the total fracture length. Figure 22 shows the pressure behavior during gel injection. Typical stabilized pressure gradients were 15 psi/ft in the first and second fracture sections, 76 psi/ft in the third section, and 7.5 psi/ft in the fourth and fifth sections. From pressure and gel breakthrough data, gel arrival occurred at 0.55, 1.3, 8, 10.5, and 11.2 fracture volumes, respectively, for the ends of the first through fifth fracture sections.

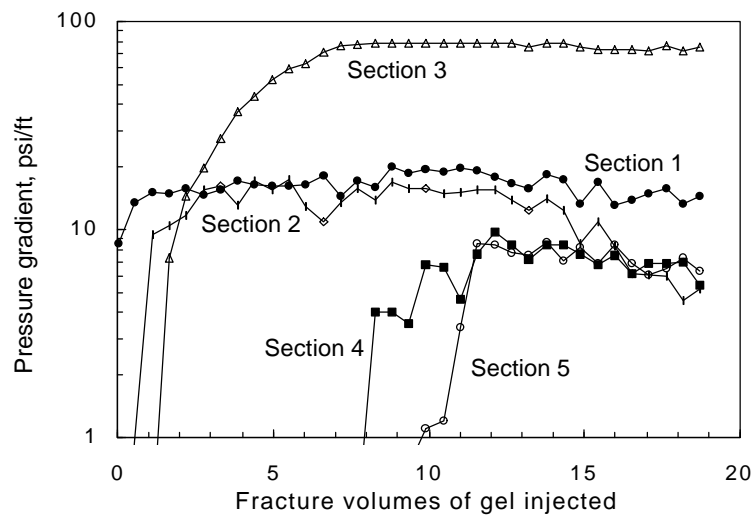


Fig. 22—Pressure gradients in a fracture with varying widths.

After injecting 18.7 fracture volumes of gel (1,300 cm<sup>3</sup>), the fracture was opened to determine the composition of gel in the fracture. Figure 23 shows chromium and HPAM concentrations for gel in the fracture relative to the values for the original gel. We are uncertain why the HPAM concentrations were so much lower than the chromium concentrations in the first two-thirds of the fracture. This result was unexpected and will be re-examined in our future work.

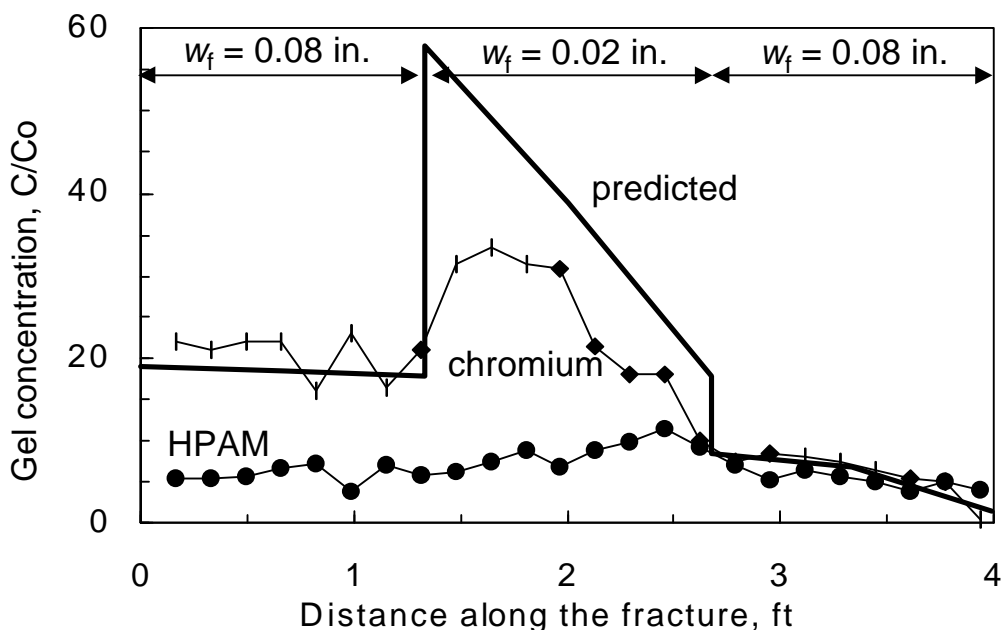


Fig. 23—Gel composition along the fracture.

Our predictive model was applied using the observed pressure gradients for the experiment and the new fracture widths and tap spacings. No other parameters were changed from the previous modeling effort. Our model predicted gel arrival at the ends of the first through fifth fracture sections at 0.59, 1.9, 7, 9.1, and 11.7 fracture volumes, respectively. These values were reasonably close to the experimental values of 0.55, 1.3, 8, 10.5, and 11.2, respectively.

The solid curve in Fig. 23 compares the predicted gel compositions along the fracture with the actual compositions. The model correctly predicted the chromium concentrations in the first and last third of the fracture. It also predicted increased chromium concentrations in the middle third of the fracture, although the model over-predicted the magnitude of the increase.

### ***Gel Permeability to Water Versus Gel Composition***

Since our model of gel propagation and dehydration obviously requires improvement, we reconsidered the various elements of the model. As a reminder, our model of gel propagation and dehydration used five equations: (1) the Darcy equation for water flow through a gel, (2) a mass balance for water flow through the fracture faces (i.e., leakoff), (3) a mass balance for gel (i.e., crosslinked polymer) flow within the fracture, (4) an experimentally determined relation between fracture width and the pressure gradient required to extrude gel through the fracture, and (5) a

relationship between gel composition and gel permeability to water. Four of these equations had a sound theoretical or experimental basis. However, the relation between gel composition and gel permeability was strictly an empirical three-parameter fit that allowed our model to predict the rate of gel propagation through a fracture. This relation was given by Eq. 4.

$$k_{gel} = 0.00011 + 1.0 (C/C_o)^{-3} \dots\dots\dots (4)$$

In Eq. 4,  $k_{gel}$  had units of mD when the gel composition,  $C/C_o$ , was expressed relative to the composition of our original Cr(III)-acetate-HPAM gel.

Experiments were performed to establish the actual relation between gel permeability and composition. Our base-case (1X) gel contained 0.5% Allied Colloids Alcoflood 935 HPAM, 0.0417% Cr(III) acetate, 1% NaCl, and 0.1% CaCl<sub>2</sub> at pH=6. The experiments were performed at 41°C (105°F). The gelant formulations were aged at 41°C for 24 hours (five times the gelation time) before use.

The gel was forced into a 6-in.-long, 650-mD Berea sandstone core at a constant rate. Because crosslinked polymer did not enter the porous rock, pressure continuously built up at the inlet sandface. The inlet end cap was positioned 0.081 cm from the inlet sand face (see Fig. 24). Pressures were allowed to build to a maximum value of 1,000 psi. Of course, during injection, the crosslinked polymer formed a filter cake on the inlet face, while some water left the gel and flowed through the Berea core—effectively as a filtrate. We monitored the inlet pressure as a function of the equivalent parameters: injection time, injection volume, and filtrate volume. Using the base-case (1X) gel, experiments were performed (using separate cores for each experiment) with injection rates of 2, 5, 10, and 20 cm<sup>3</sup>/hr. Experiments were also performed injecting (at 2 cm<sup>3</sup>/hr) 2X and 4X gels—i.e., gels with twice and four times, respectively, the HPAM and Cr(III)-acetate concentrations in the 1X gel. Pressure/time data are shown in Fig. 25.

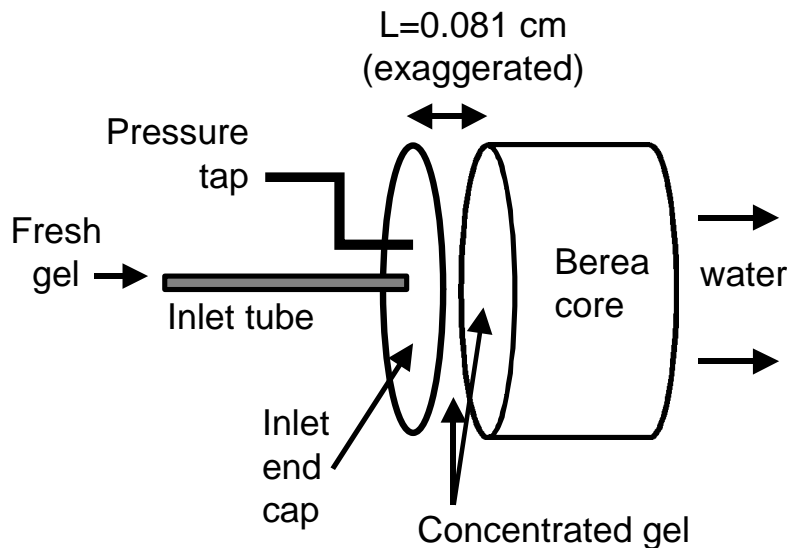


Fig. 24—Schematic of experiment to determine  $k_{gel}$  versus gel composition.

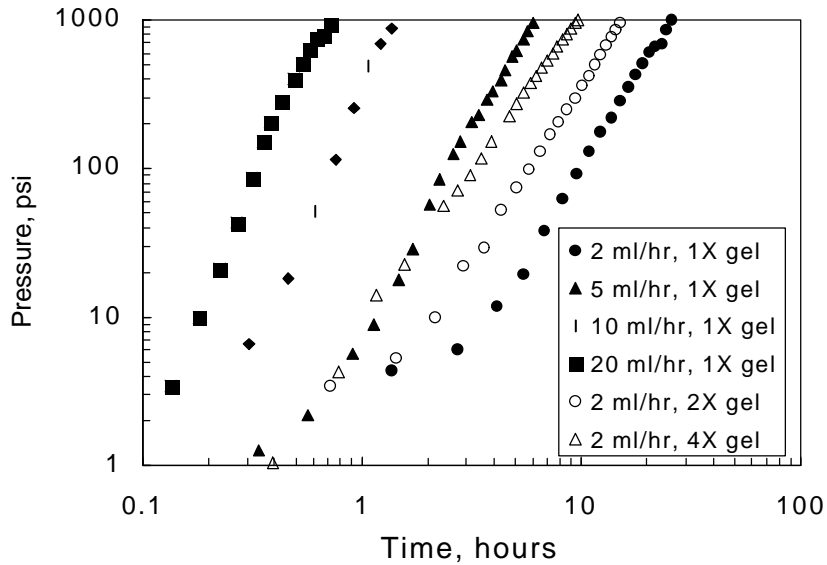


Fig. 25—Pressure versus time during gel injection.

**Case 1.** For a first-case analysis, assume that (1) no polymer or crosslinker entered the porous rock, (2) the system, fluids, and gel were incompressible, (3) the concentrating gel only formed and collected between the inlet end cap and the inlet sandface, (4) the concentrating gel distributed homogeneously between the inlet end cap and the inlet sandface, and (5) the pressure drop across the short brine-filled Berea core was negligible compared to the pressure drop across the gel filter cake. In this case, the Darcy equation and a mass balance was used to find how  $k_{gel}$  varied with gel composition. In these calculations, water viscosity at 41°C was 0.67 cp, and the core cross-section was 10 cm<sup>2</sup>. Figure 26 shows the results of applying these calculations to the data from Fig. 25.

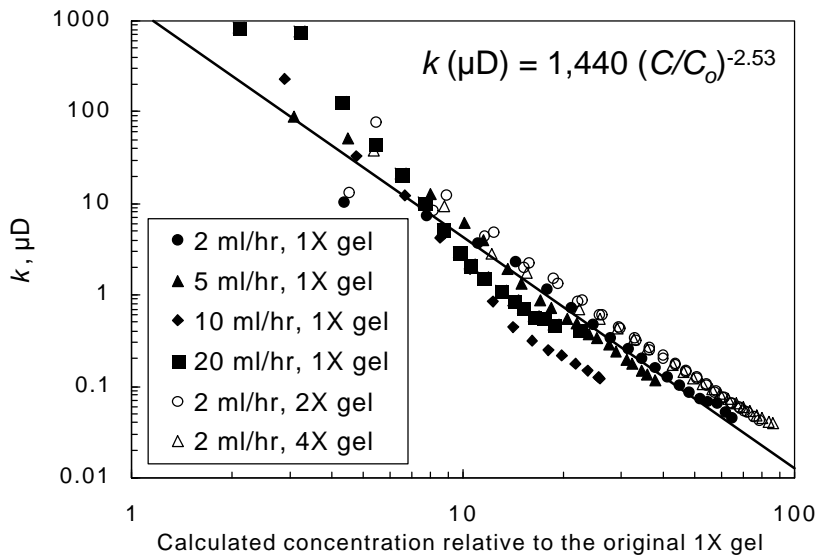


Fig. 26—Calculated gel permeability versus composition for Case 1.

The solid line in Fig. 26 represents a least-squares fit of the data. The correlation coefficient ( $r^2$ ) was 0.918. The equation in Fig. 26 expresses the relation between gel permeability to water, in  $\mu\text{D}$ , and relative gel concentration. Equation 5 shows this same equation, where permeability is expressed in mD.

$$k_{\text{gel}} = 1.44 (C/C_o)^{-2.53} \dots\dots\dots (5)$$

A comparison of Eqs. 4 and 5 reveals the similarity between the coefficients and exponents of the  $C/C_o$  terms.

**Case 2.** In Case 1, we assumed that the concentrated gel only formed and accumulated between the inlet end cap and the inlet sand face. In other words, we assumed that the thickness of the concentrated gel filter cake became no greater than 0.081 cm during the experiment. Was this assumption reasonable? To answer this question, we measured the polymer concentration in the concentrated gel on the inlet sand face at the end of each experiment. These values are listed in Table 1. Assuming that the filter cake had a uniform composition, these values were used to recalculate the thickness of the filter cake. The recalculated cake thickness values are listed in the last column of Table 1. These calculated values were typically two to three times the value of 0.081 cm that was assumed in Case 1.

Table 1—Gel filter cake properties at the end of gel injection.

Injection rate, $\text{cm}^3/\text{hr}$	Injected gel concentration	HPAM in filter cake*, $C/C_o$	Calculated cake thickness, cm
2	1X	33.2	0.161
2	2X	24.5	0.279
2	4X	27.2	0.292
5	1X	19.6	0.161
10	1X	15.7	0.137
20	1X	10.0	0.193

\* Relative to the concentration in a fresh 1X gel.

The calculated thickness values from Table 1 were used to revise Fig. 26. In particular, in the calculations, we simply substituted the appropriate cake thickness from Table 1 in place of the original value of 0.081 cm. The results of these revisions are shown in Fig. 27.

The solid line in Fig. 27 represents a least-squares fit of the data. Equation 6 describes this relationship between gel permeability and concentration when permeability is expressed in mD.

$$k_{\text{gel}} = 1.03 (C/C_o)^{-2.82} \dots\dots\dots (6)$$

The coefficients and exponents of the  $C/C_o$  terms from Eqs. 4 and 6 are very similar.

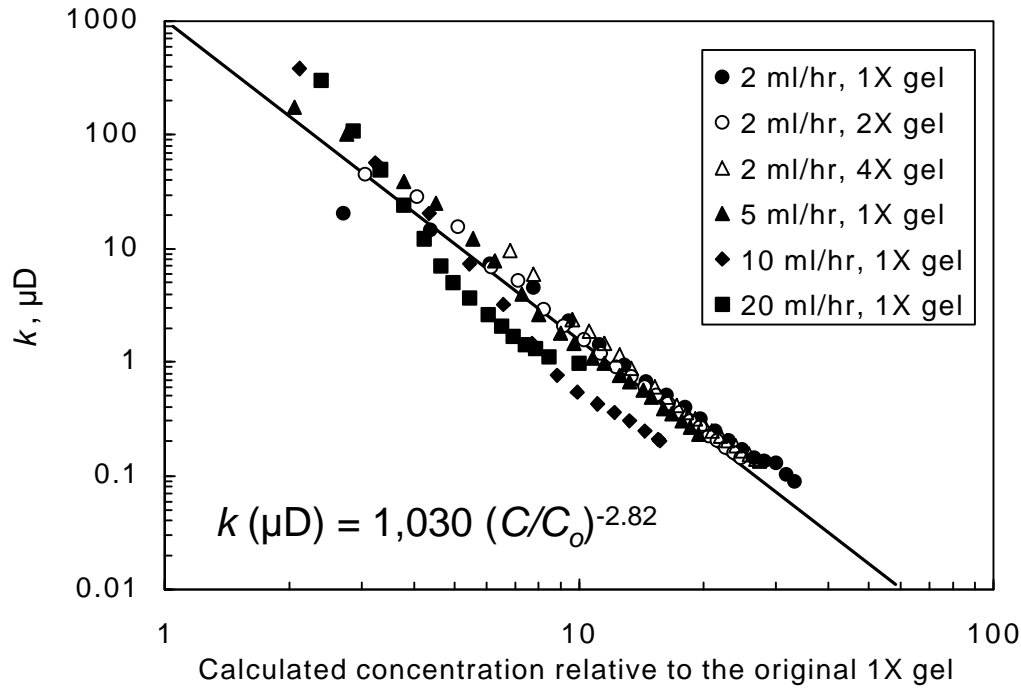


Fig. 27—Calculated gel permeability versus composition for Case 2.

In Fig. 26, the greatest data scatter occurred for concentrations that were less than four times the original 1X gel concentration (i.e., the left part of the plot). Several factors could account for this scatter. First, permeabilities for the lower concentrations were obtained early in the experiment (at relatively low pressures), when fluids exhibited their greatest compressibility. Compressibility effects made permeability appear greater than expected in this experiment. Second, the experimental system (pump, flow lines, pressure transducers etc.) had a finite response time that may be seen early in an experiment. These effects could also make permeability appear high, especially at high injection rates. Third, early in an experiment, the filter cake was thinnest, so it may have extended only a fraction of the distance from the sand face to the inlet end cap. Since our calculations assumed the cake thickness was at least 0.081 cm, gel permeability would be overestimated until the cake grew to a sufficient thickness.

Equations 5 and 6 indicate that gel permeability varied with polymer concentration raised to a power between  $-2.5$  and  $-3.0$ . They also suggest that the initial permeability of our 1X Cr(III)-acetate-HPAM gel was around 1 mD. These findings were consistent with the empirical permeability-concentration relation (Eq. 4) that was assumed in our model of gel propagation and dehydration in fractures.

**Case 3.** In Case 3, we assumed that Eq. 7 correctly described the relation between gel permeability to water and gel composition.

$$k_{\text{gel}} = 1.0 (C/C_0)^{-3} \dots\dots\dots (7)$$

Assuming that all concentrating gel accumulated within the filter cake, Eq. 8 describes the average filter cake composition versus time. In Eq. 8,  $q$  is flow rate,  $t$  is time, and  $A$  is area.

$$C/C_o = 1 + (q t) / (A L) \dots\dots\dots (8)$$

Except near the start of an experiment, the constant, 1, in Eq. 8 can be often be neglected. Then, Eqs. 7 and 8 can be combined with the Darcy equation to estimate the growth of the filter cake thickness,  $L$ .

$$L = t^{3/2} (q/A)^2 (\mu/\Delta p)^{1/2} \dots\dots\dots (9)$$

In Eq. 9, the pressure drop,  $\Delta p$ , was assumed to occur dominantly across the filter cake.

Figure 28 plots the calculated filter cake thickness versus time for different experiments. At a given time, these plots suggest that the filter cake thickness for a 1X gel should be nearly independent of injection rate. They also suggest that the filter cake thickness for a 1X gel should be about twice that for a 2X and four times that for a 4X gel. The latter suggestion is contrary to the results listed in Table 1. For gel of a given initial composition in Fig. 28, a regression revealed that the slope of the plots was about 0.4—indicating that the filter cake grew with the 0.4 power of time.

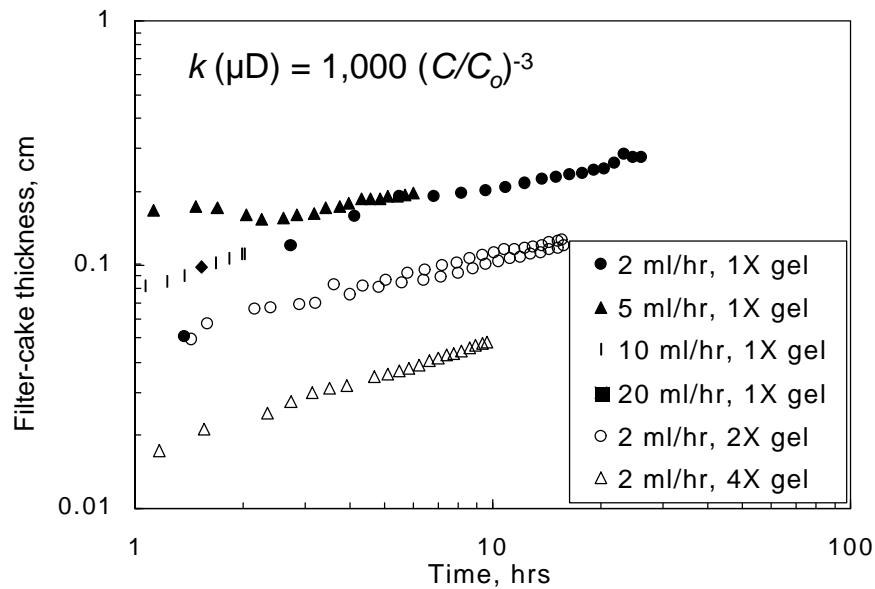


Fig. 28—Filter-cake-growth calculations from Case 3.

For Case 3, Eq. 8 can be used to estimate the final concentration of the filter cakes. Table 2 compares the results of these predictions with measured values. With two exceptions (the first and third entries), the predictions match the measured values reasonably well.

Table 2—Measured versus calculated  $C/C_o$  values at the end of gel injection.

Injection rate, cm <sup>3</sup> /hr	Injected gel concentration	Measured cake concentration, $C/C_o$	Predicted cake concentration, $C/C_o$
2	1X	33.2	19.8
2	2X	24.5	25.3
2	4X	27.2	39.0
5	1X	19.6	16.2
10	1X	15.7	19.2
20	1X	10.0	11.6

\* Relative to the concentration in a fresh 1X gel.

**Comparison with Previous Gel Permeability Measurements.** In Ref. 10, the permeability to water for several gels was determined by a different method. We wondered whether our current permeability/gel-composition relation was consistent with our earlier findings. In the earlier work,<sup>10</sup> two-dimensional glass micromodels were fabricated and filled with gel. The internal dimensions for these rectangular micromodels were 10.3 cm x 0.2 cm x 0.02 cm. Before placing gelant in the models, the “permeability” to water was found to be about 900 darcys. The direction of flow was perpendicular to the 0.2-cm x 0.02-cm face.

The gelants were prepared, placed in a micromodel, and allowed to gel at 41°C. After gelation, brine was injected using a fixed pressure drop. Pressure drops between 5 psi and 25 psi were applied. The brine had the same composition as that used to prepare the gel. The flow rate was determined by timing the movement of the brine/air interface in a capillary tube (0.019-cm inner radius) that was connected to the outlet of the micromodel. Because of the low permeabilities that were observed, days or weeks were usually required to perform an experiment. Experiments were conducted to confirm that water evaporation at the brine/air interface did not influence the results.

Permeability to water was calculated using the Darcy equation. The permeability to water was 42 μD for a gel that contained 1.39% HPAM, 0.116% Cr(III)-acetate, and 1% NaCl. This HPAM was supplied by Marathon and reportedly had a molecular weight of  $2 \times 10^6$  daltons.

Recall that the molecular weight of the Alcoflood 935 gel used in our recent work had a molecular weight of  $5 \times 10^6$  daltons. Some uncertainty exists whether permeability measurements should be comparable for gels made with polymers of different molecular weight. On the other hand, one could argue that polymer molecular weight should be of minor importance after the gel has formed. Instead, the average distance between crosslinks or overlap points on polymer chains should be of greater significance. Above a certain polymer concentration, the latter property should vary primarily with polymer concentration, and not depend on polymer molecular weight.

At any rate, using Eq 7 to estimate permeability for the gel that contained 1.39% HPAM, the calculated value was 46.5 μD—very similar to the value of 42 μD reported in Ref. 10.

$$k_{gel} = 1.0 (C/C_o)^{-3} = 1.0 (1.39/0.5)^{-3} = 0.0465 \text{ mD} = 46.5 \text{ } \mu\text{D} \dots\dots\dots (7)$$

Note that Eqs. 5 and 6 do not contain the constant, 0.00011, that was included in Eq. 4. We suspect that this constant reflects leakoff from flowing gel (that has not been concentrated) that has worm-holed through the concentrated gel. This hypothesis will be discussed later.

### ***Effect of Fracture Height***

To this point, the height of our fractures was 1.5 in. (3.8 cm). Will gel extrusion and dehydration be affected by fracture height? To address this question, two experiments were performed with fracture heights of 12 in. Figure 29 illustrates the fractured cores that were used. The cores were formed by stacking two 12×12×3-in. 650-mD Berea sandstone slabs. Spacers were used to separate the two slabs by 0.04 in. (0.1 cm) to form a 12×12×0.04-in. fracture. Because of the method of construction, the faces of the fracture were fairly smooth. The total fracture volume was 92.9 cm<sup>3</sup> and the total pore volume of the system was 2,831 cm<sup>3</sup>. The fractures were actually oriented horizontally, but for consistency, we identify the fracture “height” as the dimension perpendicular to the fracture length and fracture width dimensions.

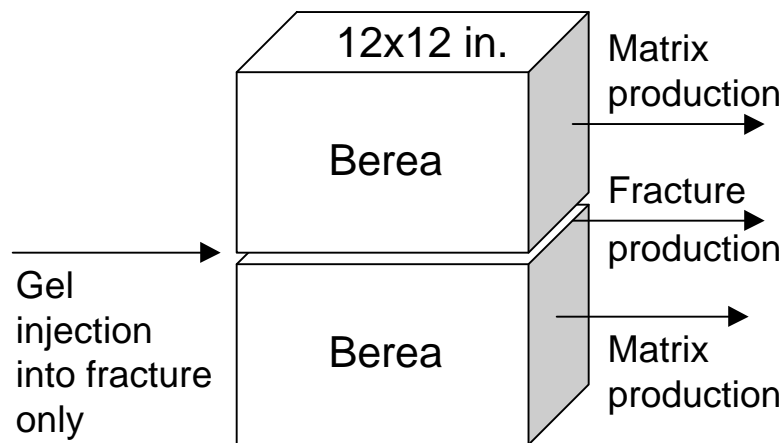


Fig. 29—Schematic of experiment in 12×12×0.04-in. fracture.

A manifold distributed the injected gel evenly over the 12-in. height of the fracture. A similar manifold collected the effluent from the fracture. Two production ports also allowed collection of effluent from each of the matrix slabs.

In the first experiment, 30 fracture volumes (~2,800 cm<sup>3</sup>) of our standard 1X 24-hr-old Cr(III)-acetate-HPAM gel were injected at a fixed rate of 500 cm<sup>3</sup>/hr. Considering the cross-sectional flow area of the fracture (12×0.04 in.), the injection flux or velocity was 164 cm/hr. This value compares with a flux of 525 cm/hr when injecting gel at a rate of 200 cm<sup>3</sup>/hr into our earlier 48×1.5×0.04-in. fractured cores.

In the second experiment, 61 fracture volumes (~5,700 cm<sup>3</sup>) of our standard 1X 24-hr-old Cr(III)-acetate-HPAM gel were injected at a fixed rate of 1,600 cm<sup>3</sup>/hr. The injection flux in this experiment was 525 cm/hr.

During both experiments, the pressure gradient during gel injection averaged 29 psi/ft. This value was very similar to those observed earlier during extrusion through fractures of the same width, but with heights of 1.5 in. (Fig. 5). The insensitivity of pressure gradient to injection rate was consistent with our earlier findings.

The concentrations of HPAM and chromium in the fracture and matrix effluents are shown in Figs. 30 and 31. Consistent with Fig. 9, no significant HPAM or chromium was produced from the matrix during these experiments. For the 500- and 1,600- $\text{cm}^3/\text{hr}$  experiments, gel breakthrough was noted after injecting 6 and 2.6 fracture volumes of gel, respectively.

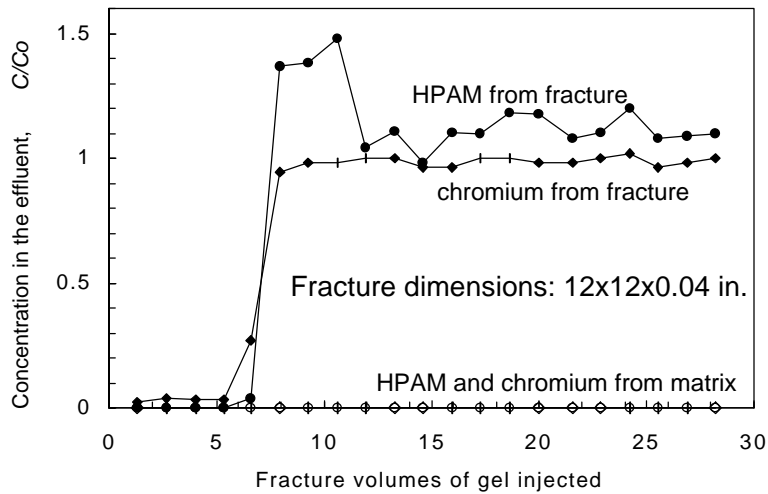


Fig. 30—Effluent compositions from a 12×12×0.04-in. fracture (500  $\text{cm}^3/\text{hr}$ ).

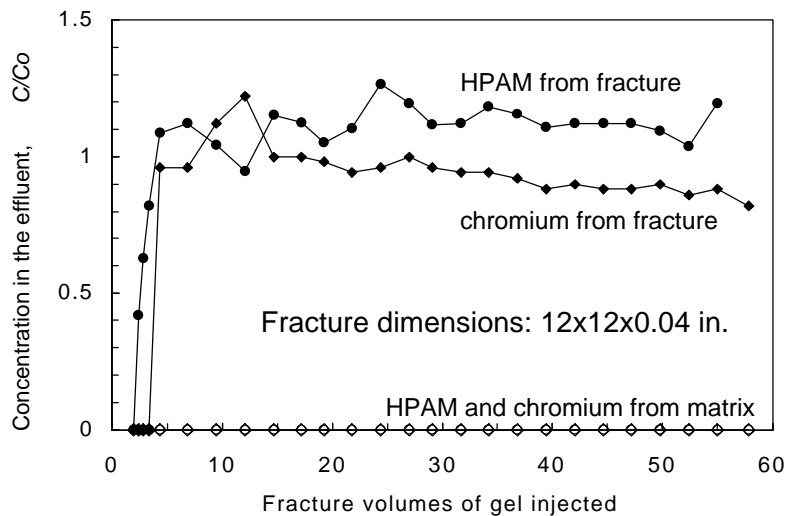


Fig. 31—Effluent compositions from a 12×12×0.04-in. fracture (1,600  $\text{cm}^3/\text{hr}$ ).

After gel breakthrough, the gel produced from the fractures was similar in composition to that for the injected gel (Figs. 30 and 31). This observation was consistent with the findings from Fig. 9.

The fraction of fluid produced from the fracture versus the matrix is shown in Figs. 32 and 33. Consistent with the findings of Fig. 8, no significant fluid was produced from the matrix until gel breakthrough. At gel breakthrough, the fraction of fluid from the matrix jumped to 97% of the total flow for the 500-cm<sup>3</sup>/hr experiment and to 91% of the total flow for the 1,600-cm<sup>3</sup>/hr experiment. With further gel injection in the 500-cm<sup>3</sup>/hr experiment, this fraction gradually declined to 55% of the total after injection of 30 fracture volumes. During the 1,600-cm<sup>3</sup>/hr experiment, the matrix fractional flow declined to 33% after 30 fracture volumes and 17% after 61 fracture volumes. (The data jumps in Fig. 33 occurred when switching injection pumps.)

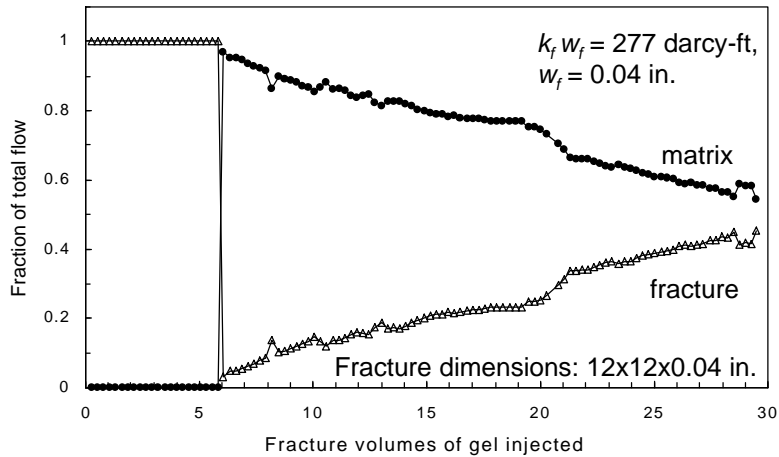


Fig. 32—Fractional flow measured at the core outlet (12×12×0.04-in. fracture, 500 cm<sup>3</sup>/hr).

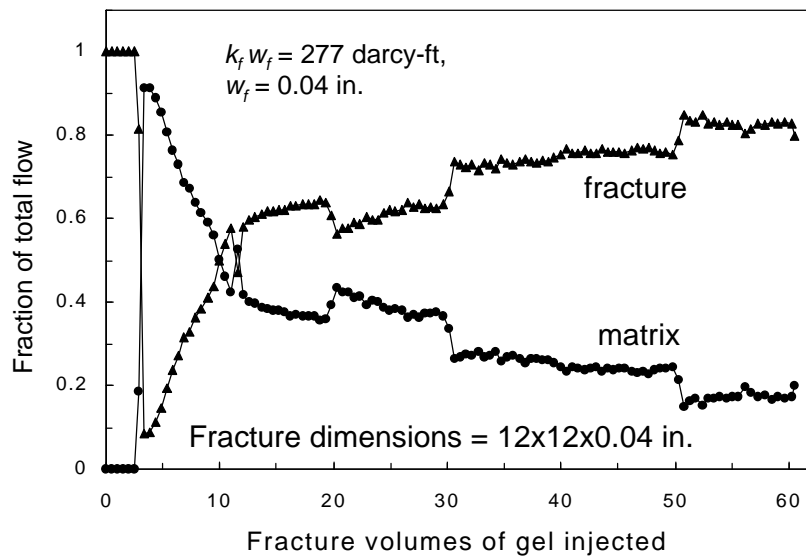


Fig. 33—Fractional flow measured at the core outlet (12×12×0.04-in. fracture, 1,600 cm<sup>3</sup>/hr). For both experiments, near the end of gel injection, dyed gel of the same composition was injected. For the 500- and 1,600-cm<sup>3</sup>/hr experiments, dye breakthrough was noted after injecting 9 cm<sup>3</sup> (0.097 fracture volumes) and 8 cm<sup>3</sup> (0.086 fracture volumes), respectively. At the time of dyed-gel breakthrough, the average gel dehydration factors for newly injected gel were 55% and

17%, respectively (because these were the fractions of total flow produced as water from the end of the matrix). Thus, the estimated volume of the pathways for the dyed gel were  $4 \text{ cm}^3$  [i.e.,  $9 \times (1 - 0.55)$ ] or 0.044 fracture volumes for the  $500\text{-cm}^3/\text{hr}$  experiment and  $6.6 \text{ cm}^3$  [i.e.,  $8 \times (1 - 0.17)$ ] or 0.071 fracture volumes for the  $1,600\text{-cm}^3/\text{hr}$  experiment. These results suggest that the injected gel formed small-volume wormholes through concentrated gel in the fracture.

Consistent with this suggestion, wormhole pathways were noted (highlighted by the dye) through the concentrated gel in the fracture after opening the fracture at the end of the experiments. Typically, these wormholes were 0.1 to 0.2 in. in height, compared to the total fracture height of 12 in. In the  $500\text{-cm}^3/\text{hr}$  experiment, one wormhole in the center of the pattern appeared dominant, while six other significant wormholes were present in various locations. A limited amount of branching was noted on these wormholes. In contrast, for the  $1,600\text{-cm}^3/\text{hr}$  experiment, highly branched wormhole patterns were found after dye injection. For both experiments, after removing the gel from the fractures, streaks of dyed rock were noted under the wormholes—revealing the leakoff pathways for water that dehydrated from the gel.

Thus, Fig. 34 presents a possible picture of gel propagation through a fracture. The wormhole(s) provided a conduit for gel that had basically the same composition as the injected gel. Since these wormholes were filled with gel of a nearly fixed composition, they may be responsible for a source of leakoff that was fairly constant (i.e., the constant term in Eq. 4). On the other hand, other gel in the fracture was concentrated and immobile. Under pressure, this gel continually lost water, so it became increasingly concentrated. However, because gel permeability decreased with increased gel concentration, the leakoff contribution from this source gradually declined—thus suggesting the source of the  $(C/C_o)^{-3}$  term in Eq. 4.

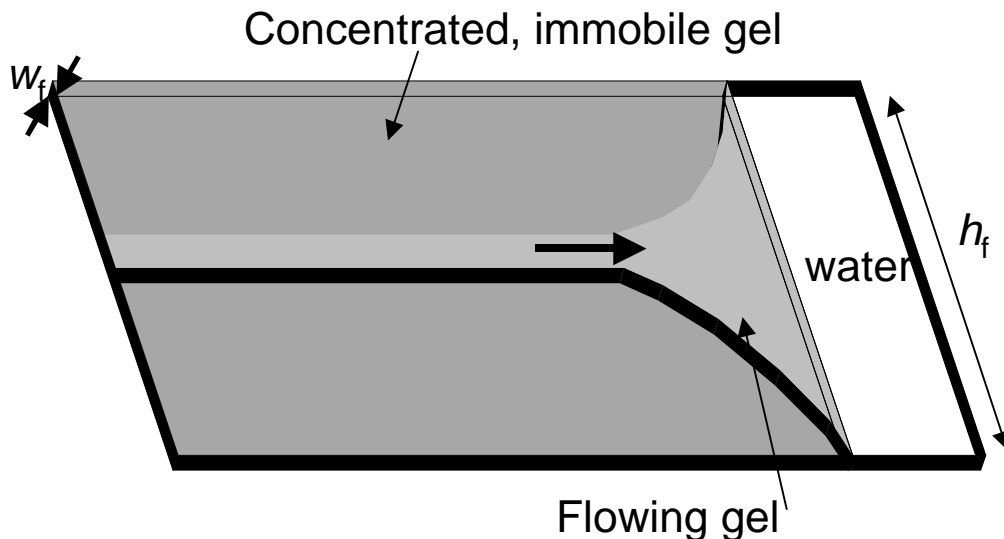


Fig. 34—Illustration of a gel wormhole through concentrated gel.

The gel from the fractures was divided into  $2 \times 2$ -in. squares and analyzed for chromium and HPAM. Figures 35 and 36 show these concentrations relative to those of the injected gel. In any given square, the first number gives the chromium concentration relative to the chromium concentration in the original gel. The second number gives the HPAM concentration relative to

the HPAM concentration in the original gel. For the 500-cm<sup>3</sup>/hr experiment, the average relative chromium and HPAM concentrations were 11.3 and 12.8, respectively. Thus, on average, the gel in the fracture was about 12 times more concentrated than the injected gel. Gel concentrations were distributed fairly uniformly through the fracture. For the 1,600-cm<sup>3</sup>/hr experiment, the average relative chromium and HPAM concentrations were 14.4 and 4.6, respectively. At present, we have no explanation for the difference between these chromium and HPAM values.

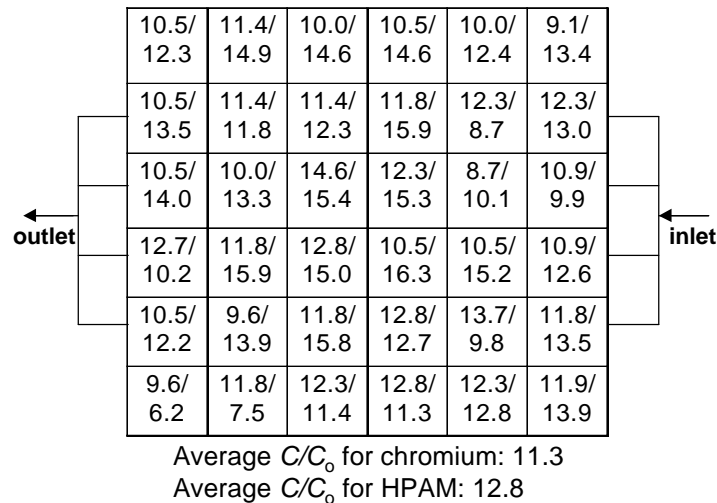


Fig. 35—Chromium/HPAM concentrations in a 12×12×0.04-in. fracture (500 cm<sup>3</sup>/hr).

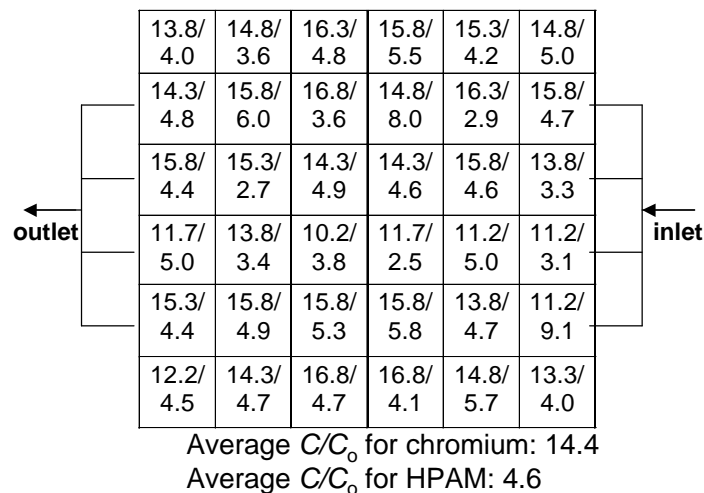


Fig. 36—Chromium/HPAM concentrations in a 12×12×0.04-in. fracture (1,600 cm<sup>3</sup>/hr).

In summary, the extrusion and dehydration properties of gel in 12-in.-high fractures were similar to those found in a 1.5-in.-high fracture.

#### ***Effect of Injection Rate***

Two additional experiments were performed to examine the effects of injection rate on gel extrusion and dehydration. Except for the injection rate, these tests were identical to that described in the first part of this chapter. Specifically, in each test, we extruded 80 fracture

volumes (~3.7 liters) of our standard 1X 24-hr-old Cr(III)-acetate-HPAM gel through a 0.04-in.-wide fracture in a 4-ft-long, 650-mD Berea sandstone core. The cross-sectional area of the core was 14.5 cm<sup>2</sup> (3.8 x 3.8 cm), so the fracture height was 3.8 cm (1.5 in.). The core had five sections of equal length that were delineated by sets of fracture and matrix pressure taps. A fitting at the core outlet separated the effluent from the fracture and matrix. (Of course, a new core was used for each test.) To complement the 200-cm<sup>3</sup>/hr test that was described in the first part of this chapter, the two new tests were performed using gel injection rates of 500 and 2,000 cm<sup>3</sup>/hr, respectively. Table 3 summarizes the results from these tests. Table 3 also includes results from the 12×12×0.04-in. fracture experiments described in the previous section.

Table 3—Effect of injection rate on gel propagation.

Fracture dimensions ( $L_f \times h_f \times w_f$ )	48×1.5×0.04-in.			12×12×0.04-in.	
Injection rate, cm <sup>3</sup> /hr	200	500	2,000	500	1,600
Estimated velocity in the fracture, cm/hr	525	1,312	5,250	164	525
Total fracture volumes of gel injected	80	80	80	30	61
Average pressure gradient, psi/ft	28	29	40	29	29
Gel front arrival at core end, fracture volumes	15	6.0	4.0	6.0	2.6
Peak fraction of matrix flow, %	100	93	75	97	91
Final fraction of flow produced from matrix, %	35	26	16	55	17
Average $C/C_o$ in fracture at end of experiment	27	17	11	12	4.6-14
Wormhole volume, fracture volumes		0.10	0.14	0.044	0.071

Consistent with our earlier findings,<sup>6-9</sup> pressure gradients along the fracture were insensitive to injection rate. Table 3 shows that the average pressure gradients ranged from 28 to 40 psi/ft for estimated gel velocities ranging from 164 to 5,250 cm/hr. (For comparison, the velocity in a 100-ft-high, 0.04-in.-wide, two-wing fracture would be 15,600 cm/hr using an injection rate of 1 barrel per minute.) For the 500-cm<sup>3</sup>/hr experiment in a 48×1.5×0.04-in. fracture, pressure measurements along the fracture failed after 22 fracture volumes of gel injection (Fig. 37). Up to that point, the pressure gradients stabilized at values ranging from 40 psi/ft in the first fracture section to 20 psi/ft in the last two fracture sections. The average pressure gradient (at 22 fracture volumes) was 29 psi/ft.

For the 2,000-cm<sup>3</sup>/hr experiment in a 48×1.5-in. fracture, pressure gradients were quite high (110 psi/ft) in the first fracture section (Fig. 38). In the other four fracture sections, the pressure gradients appeared to stabilize at values ranging from 28 to 59 psi/ft—averaging 40 psi/ft after 80 fracture volumes. During brine flow before gel injection, flow was more constricted in the first and fourth sections of the fracture than in the other three sections. This observation accounts for the high-pressure gradients observed in the first and fourth sections during gel injection.

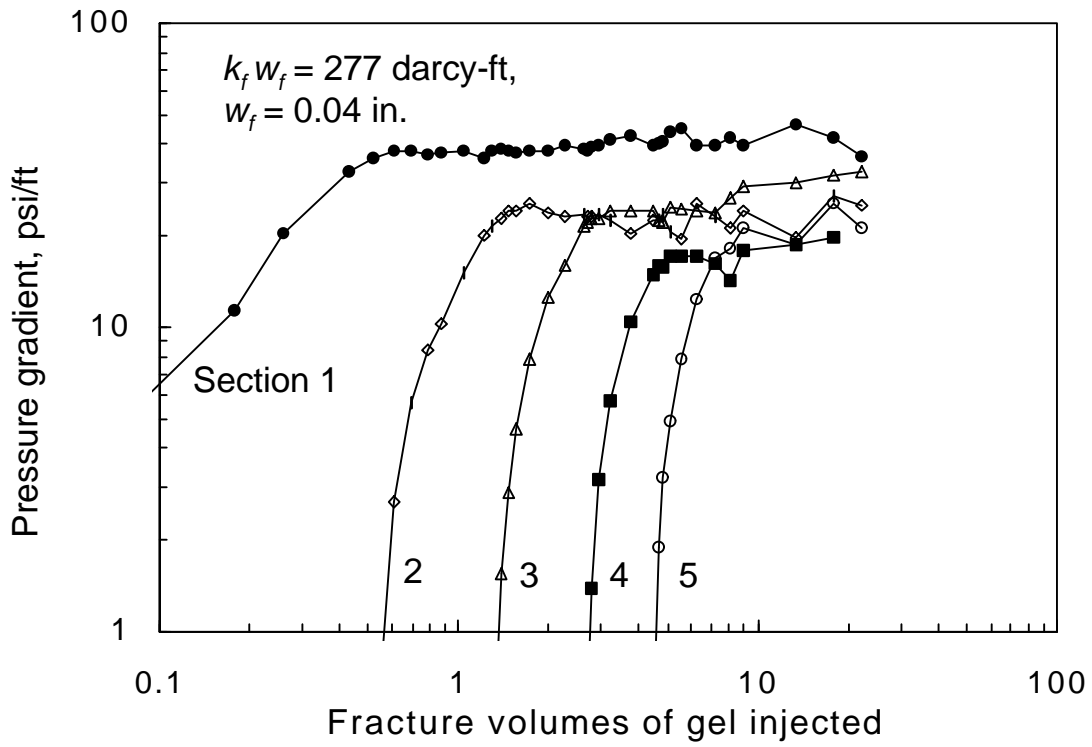


Fig. 37—Pressure behavior in the fracture taps during gel injection (500 cm<sup>3</sup>/hr).

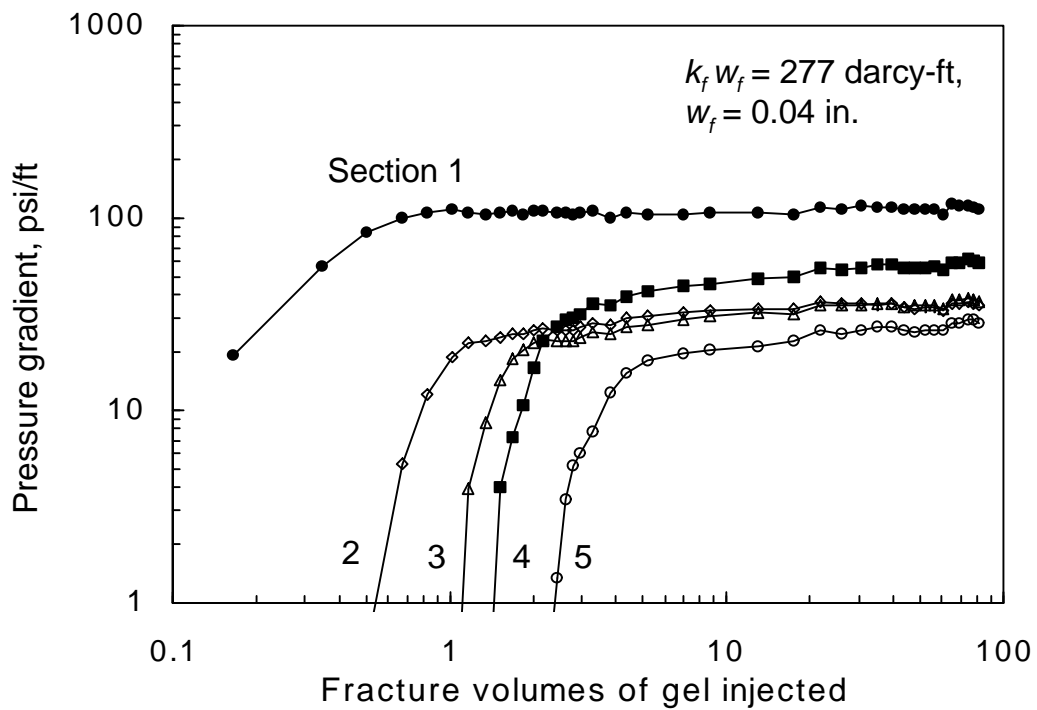


Fig. 38—Pressure behavior in the fracture taps during gel injection (2,000 cm<sup>3</sup>/hr).

The rapid increases in pressure gradient in Figs. 37 and 38 indicate the arrival of the gel front at the beginning of the specified fracture section. These arrival volumes are listed in Table 3 along with similar data from the 200-cm<sup>3</sup>/hr experiment. Comparison reveals that the rate of gel-front propagation increased significantly with increased injection rate. This result was expected since the gel had less time to dehydrate as the injection rate increased. A lower level of gel dehydration (concentration) allowed the gel propagate a greater distance for a given total volume of gel injection.

The pressure gradients observed along the matrix during gel injection are shown in Figs. 39 and 40 for the 500- and 2,000-cm<sup>3</sup>/hr experiments, respectively. Both figures are qualitatively similar to Fig. 7. (In Fig. 39, an anomaly in Sections 1-3 occurred between 3 and 4 fracture volumes because a transducer valve was opened.) However, the maximum pressure gradient increased with increased injection rate. For example, the maximum pressure gradients in Section 5 were 1, 5, and 16 psi/ft for injection rates of 200, 500, and 2,000 cm<sup>3</sup>/hr, respectively.

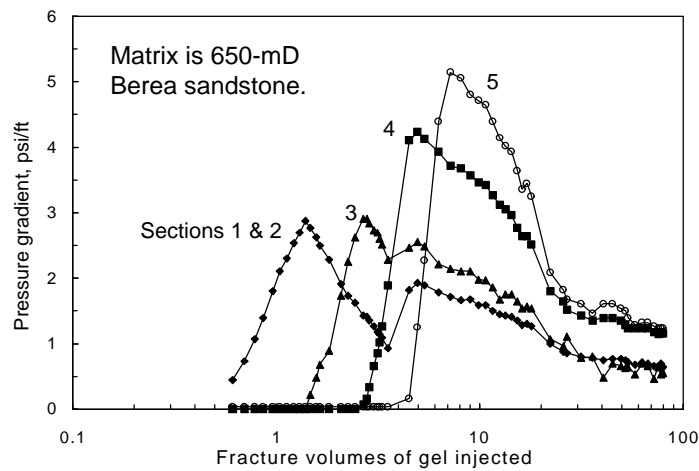


Fig. 39—Pressure behavior in the matrix taps during gel injection (500 cm<sup>3</sup>/hr).

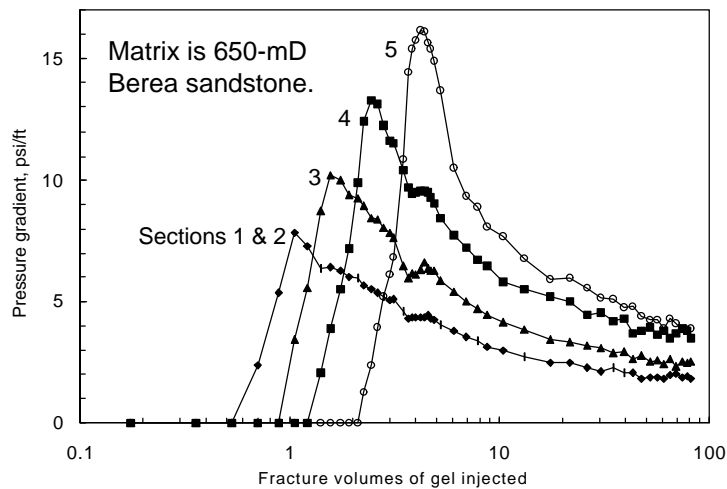


Fig. 40—Pressure behavior in the matrix taps during gel injection (2,000 cm<sup>3</sup>/hr).

The Darcy equation was applied to convert the pressure gradients in Figs. 39 and 40 to water flow rates in the matrix. These rates are expressed as fractions of the total injection rate (i.e., either 500 or 2,000 cm<sup>3</sup>/hr) in Figs. 41 and 42. Consistent with Fig. 12, the peak water flow rates increased from section to section through the core. The maximum water flow rate in Section 5 was near 1 (the maximum possible real flow rate) for both the 500- and 2,000-cm<sup>3</sup>/hr cases. (In Fig. 41, experimental uncertainty was responsible for the maximum rate in Section 5 slightly exceeding a value of 1.)

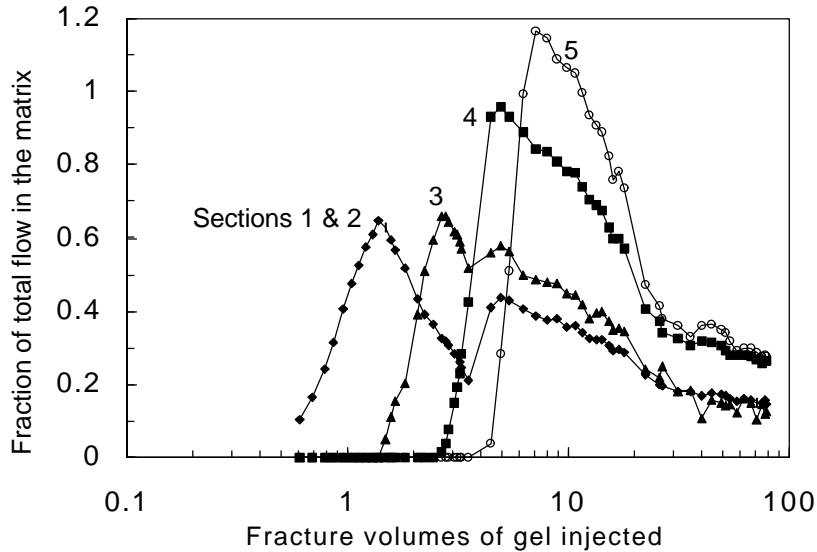


Fig. 41—Fraction of total flow in the matrix during gel injection (500 cm<sup>3</sup>/hr).

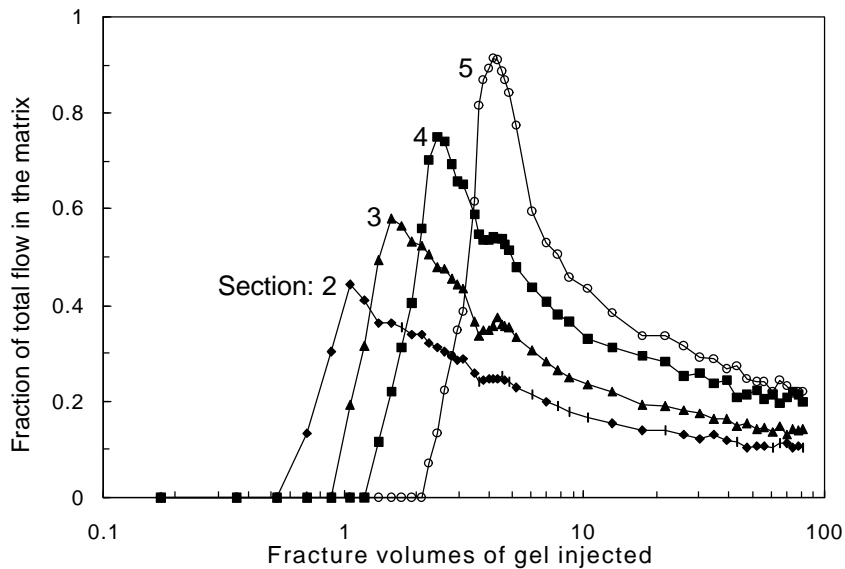


Fig. 42—Fraction of total flow in the matrix during gel injection (2,000 cm<sup>3</sup>/hr).

A mass balance can convert the flow data from Figs. 41 and 42 into leakoff data. As mentioned in the discussion of Fig. 13, the flow rate in the matrix of a given core section was the sum of the leakoff from the fracture faces plus the flow rate from the matrix of the previous (upstream) core section. Figures 43 and 44 plot the leakoff rate per unit of fracture face versus the fracture volumes of gel injected for the various sections of the core. Of course, the source of the leakoff was water that left the gel in the fracture. The leakoff rates were normalized relative to the largest leakoff rate observed in the first two sections of the core. These leakoff rates were  $9.25 \times 10^{-4}$  and  $2.54 \times 10^{-3} \text{ cm}^3/\text{cm}^2/\text{s}$  for injection rates of  $500 \text{ cm}^3/\text{hr}$  and  $2,000 \text{ cm}^3/\text{hr}$ , respectively. For comparison, the peak leakoff rate in the first section for the  $200\text{-cm}^3/\text{hr}$  experiment was  $9.63 \times 10^{-5} \text{ cm}^3/\text{cm}^2/\text{s}$ . Thus, the peak leakoff rate in the first section increased significantly with increased injection rate. A comparison of Figs. 13, 43, and 44 suggests that the leakoff peaks can increase, decrease, or remain roughly the same as one progresses from section to section in a given core.

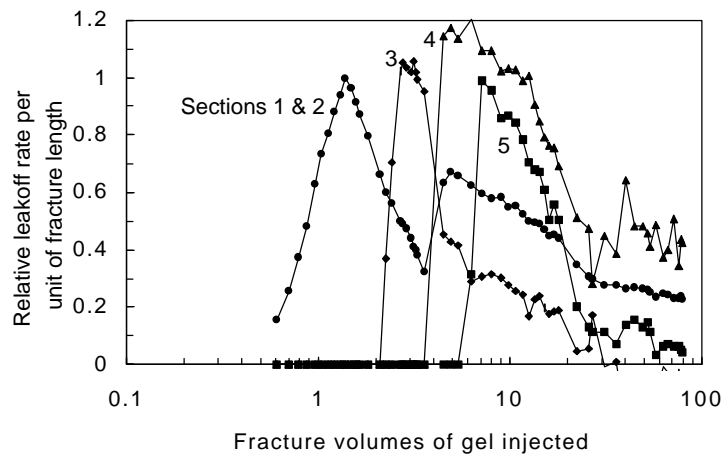
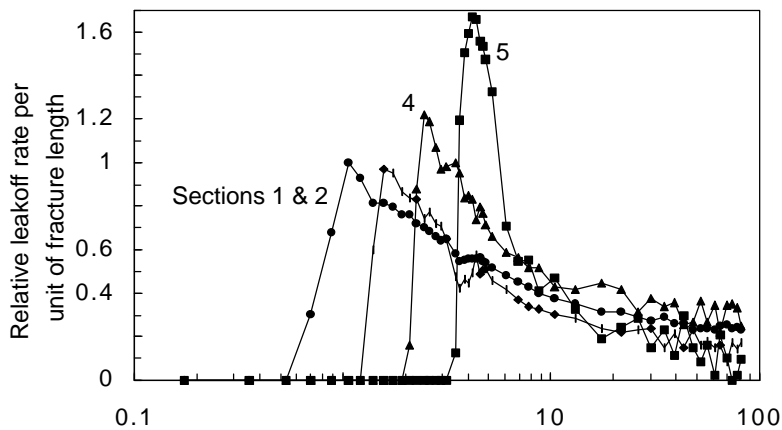


Fig. 43—Relative leakoff during gel injection ( $500 \text{ cm}^3/\text{hr}$ ).



—Relative leakoff during gel injection ( $2,000 \text{ cm}^3/\text{hr}$ ).

The concentrations of chromium and HPAM (relative to those in the original gel) in the effluent from the fracture and matrix are shown in Figs. 45 and 46 for the 500- and 2,000-cm<sup>3</sup>/hr experiments, respectively. Consistent with earlier observations (Figs. 9, 30, and 31), no significant chromium or HPAM were produced from the matrix, and the gel produced from the fracture had basically the same composition as the injected gel. Gel breakthrough was noted at 6.0 and 4.0 fracture volumes for the 500- and 2,000-cm<sup>3</sup>/hr experiments, respectively. As shown in Table 3 (Row 6), gel breakthrough decreased significantly with increased injection rate.

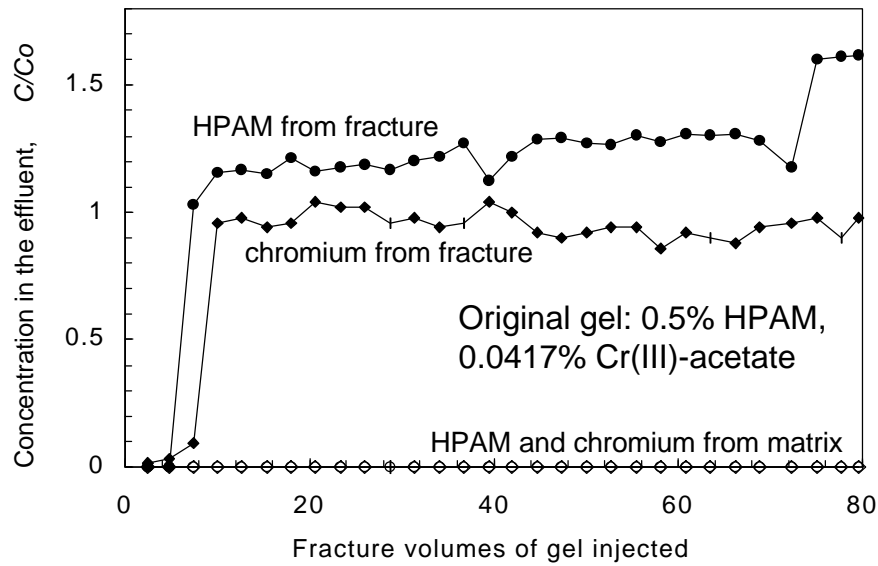


Fig. 45—Composition of gel in the fracture (relative to the injected gel) (500 cm<sup>3</sup>/hr).

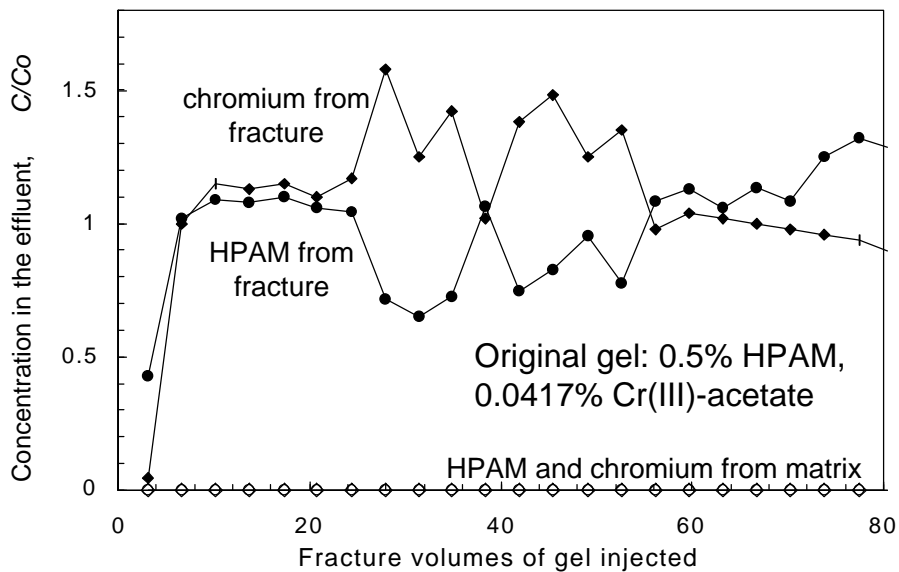


Fig. 46—Composition of gel in the fracture (relative to the injected gel) (2,000 cm<sup>3</sup>/hr).

The fraction of the total flow produced from the fracture versus the matrix is illustrated in Figs. 47 and 48 for the 500 and 2,000-<sup>3</sup>/hr experiments, respectively. In both cases, the peak in the reaktthrough of gel at the end of the fracture. This observation is consistent with earlier results (Figs. 8, 32, and 33).

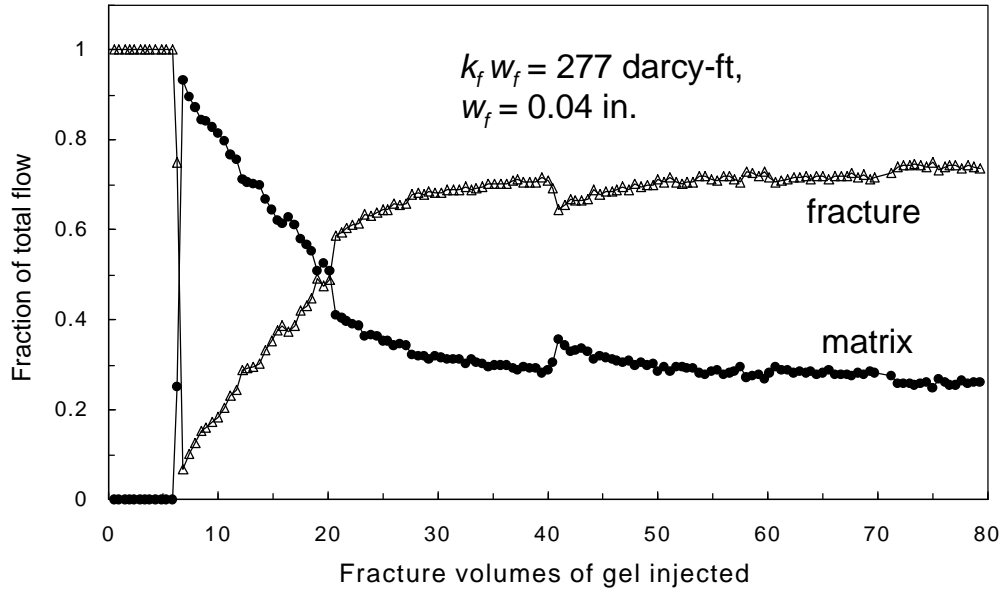


Fig. 47—Fractional flow measured at the core outlet (500 cm<sup>3</sup>/hr).

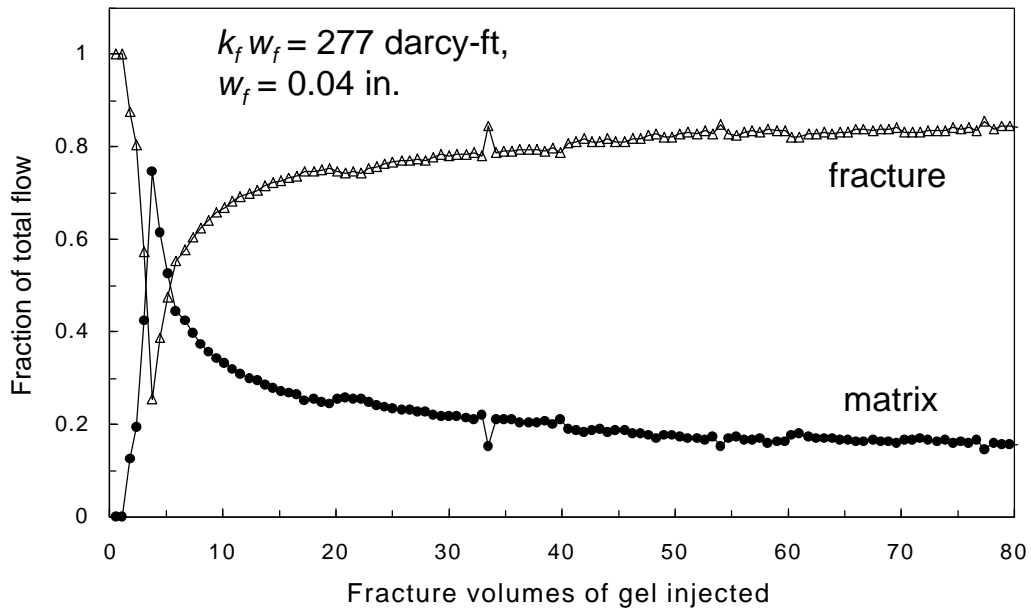


Fig. 48—Fractional flow measured at the core outlet (2,000 cm<sup>3</sup>/hr).

After 80 fracture volumes of gel injection, the fractions of total flow from the matrix were 35%, 26%, and 16%, for injection rates of 200, 500, and 2,000 cm /hr, respectively (see Figs. 8, 47, and 48 and Table 3). Thus, for a given throughput, total flow from the matrix decreased significantly with increased injection rate. This result was expected since for a given throughput, the time under pressure for the gel decreased in direct proportion to the injection rate. The time available for the gel to have water squeezed out decreased with increased injection rate.

To amplify this point, Fig. 49 plots the average leakoff rate ( $u_l$ , in cm/hr) versus time ( $t$ , in hrs) for the five experiments listed in Table 3. The velocities shown in the injection rate by the fracture width (0.04 in.) and height (either 1.5 or 12 in.). For the 48x12-in. fractures, the velocities were 525, 1,312, and 5,250 cm/hr for injection rates of 200, 500, and 2,000 cm<sup>3</sup>/hr, respectively. The average leakoff rate from the matrix (at the end of the core) divided by the total fracture area in the core. For a given experiment, Fig. 49 includes only the data after the peak in matrix flow. The data from the five experiments fall nicely on a single trend that can be described by Eq. 10.

$$u_l = 0.374 t^{-0.557} \quad \text{.....(10)}$$

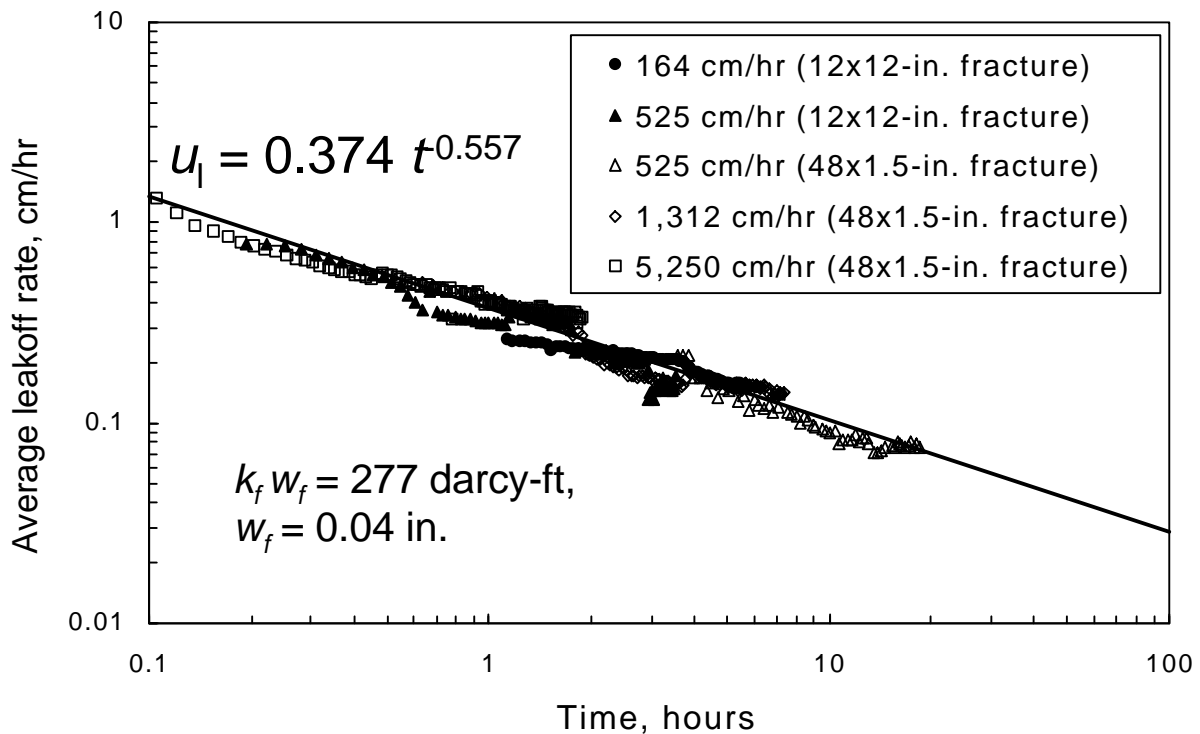


Fig. 49—Average leakoff rate from five experiments at different velocities.

The Darcy equation can convert the leakoff values from Fig. 49 into gel permeabilities. These permeabilities were averaged over the entire length of the fracture. Using Eq. 3 and the leakoff and time data from Fig. 49, gel concentrations were calculated. These concentrations were also averaged over the entire length (and volume) of the fracture. A plot of average gel permeability versus average gel concentration is shown in Fig. 50. In contrast to Fig. 27, the permeability-concentration data did not follow a single trend. Instead, a separate trend was noted for each of the five experiments. Table 4 summarizes regression data for the five experiments after fitting the data to Eq. 11.

$$k_{gel} = intercept (C/C_o)^{slope} \dots\dots\dots(11)$$

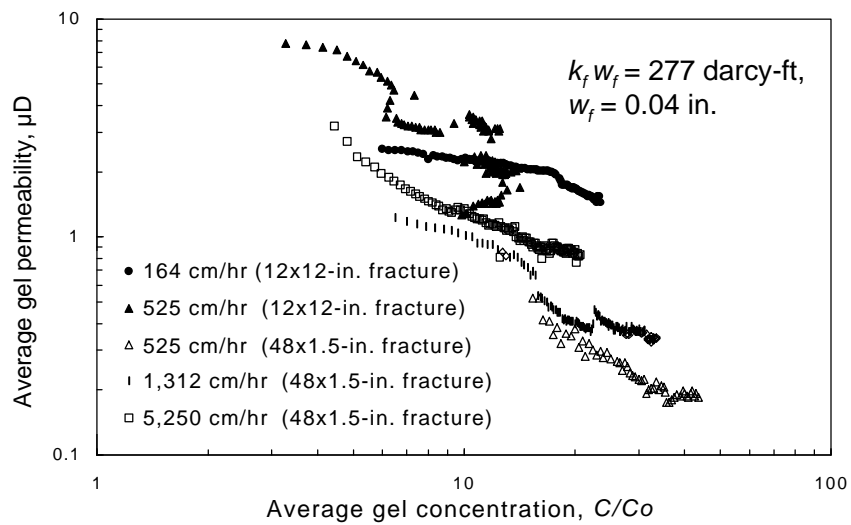


Fig. 50—Average permeability versus concentration based on Fig. 49.

Table 4—Regression data for curves in Fig. 50.

Injection velocity, cm/hr	Intercept (initial gel $k$ ), $\mu\text{D}$	Slope (power in Eq. 11)	Correlation coefficient, $r^2$
164*	5.8	-0.407	0.88
525*	33.7	-1.119	0.67
525**	5.6	-0.934	0.93
1,312**	6.7	-0.877	0.90
5,250**	7.0	-0.729	0.95

\*(12×12-in. fracture) \*\* (48×1.5-in. fracture)

In contrast to Eqs. 6 and 7, Table 4 suggests that  $k_{gel}$  was proportional to gel concentration raised to a power between  $-0.4$  and  $-1.2$ . Table 4 also suggests that the initial permeability (the *intercept* in Eq. 11) for our 1X Cr(III)-acetate-HPAM gel was about  $6 \mu\text{D}$  rather than  $1,000 \mu\text{D}$ , as indicated by Eqs. 6 and 7. (This observation ignores the  $33.7 \mu\text{D}$  value.)

Why did these differences occur? For two reasons, we suspect that Fig. 27 provides a more credible permeability-concentration relation than Fig. 50. First, for all five experiments shown in Fig. 50, the calculated final gel concentrations (at the end of the experiment) were typically twice the measured values (listed in Table 3). Second, for Fig. 50 the analysis assumed that leakoff was uniform throughout the fracture. However, our work has shown that leakoff was not uniform throughout the fracture. In particular, wormholes provided a conduit for low-concentration gel (Fig. 34). As mentioned earlier, injection of dyed gel revealed that leakoff was substantially greater near the wormholes than elsewhere in the gel-filled fracture.

At the end of the experiments, gels in the fractures were analyzed. For the 500- and 2,000-cm<sup>3</sup>/hr experiments in 48×1.5×0.04-in. fractures, Figs. 51 and 52 show the chromium and HPAM compositions of these gels as a function of fracture length. For the 500-cm<sup>3</sup>/hr experiment, the average chromium and HPAM concentrations were 17.0 and 24.3 times more concentrated, respectively, than in the originally injected gel. For the 2,000-cm<sup>3</sup>/hr experiment, the average chromium and HPAM concentrations were 10.5 and 13.6 times more concentrated, respectively, than in the originally injected gel. As shown in the second to last row of Table 3, for a given gel throughput, gel dehydration decreased significantly with increased injection rate.

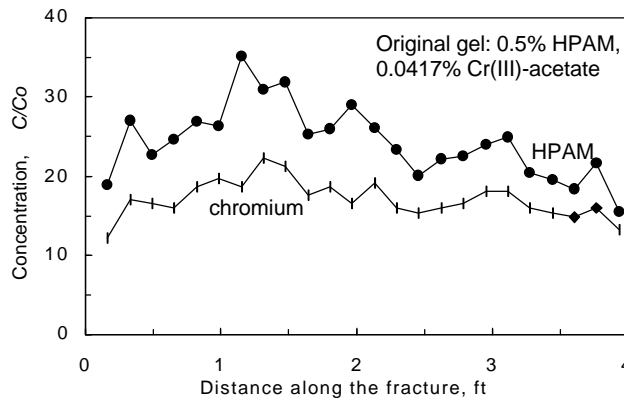


Fig. 51—Composition of gel in the fracture (500 cm<sup>3</sup>/hr).

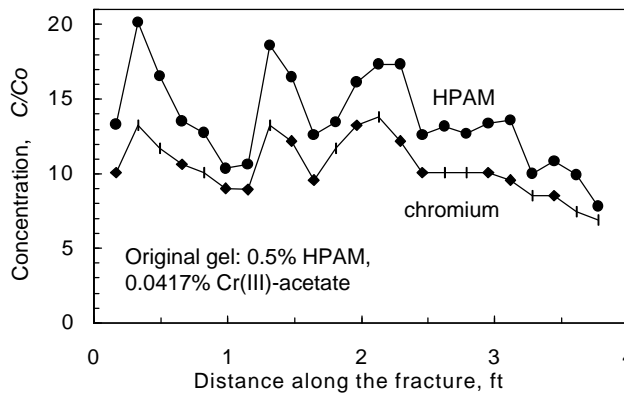


Fig. 52—Composition of gel in the fracture (2,000 cm<sup>3</sup>/hr).

### Comparison of Model Predictions

At this point, we have two models that describe gel propagation and dehydration during extrusion through fractures. The first model (Model 1) used Eqs. 1-4. In this model, Eqs. 2 and 4 were the key equations that described water leakoff from the fracture. The second model (Model 2) also used Eqs. 1 and 3, but Eq. 10 was used instead of Eqs. 2 and 4.

For Model 1, Fig. 53 compares predictions versus experimental gel propagation results at three injection velocities in 48×1.5×0.04-in. fractures. The solid symbols with solid curves show the actual data, while the open symbols with dashed curves show the predictions. For an injection velocity of 525 cm/hr (200 cm<sup>3</sup>/hr actual injection rate), the predictions very closely match the actual results. This finding is not surprising since these experimental data were originally used to empirically develop Eq. 4. For the two higher rates, the model predictions were typically 50%-70% greater than the actual values. Thus, the model needs refinement.

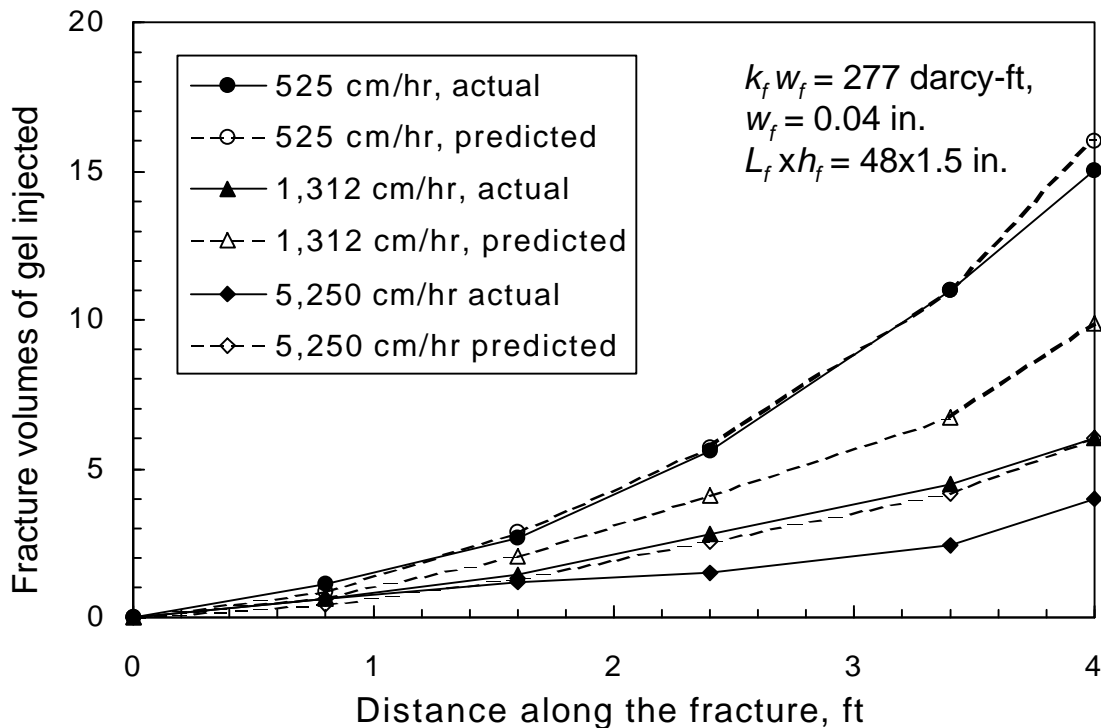


Fig. 53—Gel propagation in 48×1.5×0.04-in. fractures. Model:  $k_{gel}=0.00011+1.0(C/C_o)^{-3}$ .

For Model 2, Fig. 54 compares predictions versus experimental gel propagation results at three injection velocities in 48×1.5×0.04-in. fractures. Again, the solid symbols with solid curves show the actual data, while the open symbols with dashed curves show the predictions. For all rates, the model predictions were typically 100% greater than the actual values. Thus, Model 2 was deficient with respect to predictions before gel breakthrough. However, after gel arrival at the end of the fracture, the leakoff predictions were fairly accurate (Fig. 49).

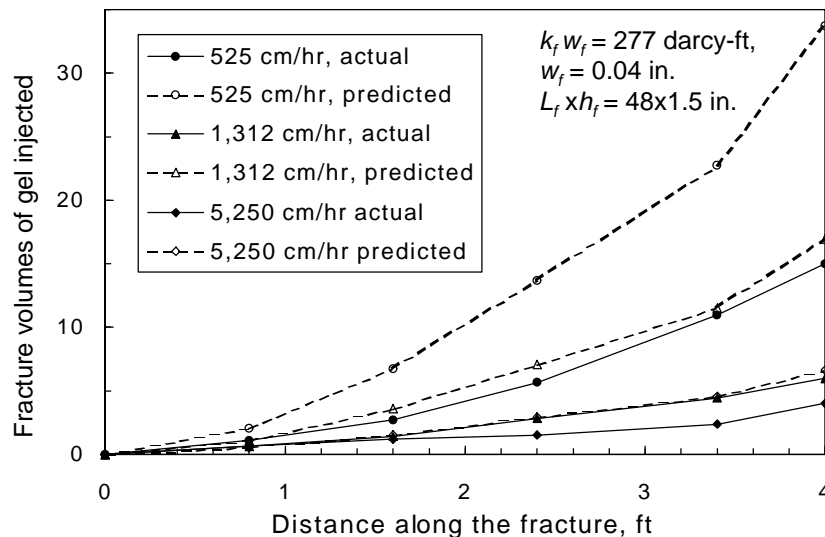


Fig. 54—Gel propagation in 48×1.5×0.04-in. fractures. Model:  $u_1 = 0.374 t^{-0.557}$ .

Additional comparisons of experimental results and predictions from Models 1 and 2 are included in Table 5. This table lists results from experiments in the 12×12×0.04-in. fractures as well as those in the 48×1.5×0.04-in. fractures. Both models over-predicted the volume of gel required to fill a fracture. However, the discrepancy was most severe for Model 2. Both models gave reasonably accurate predictions of the peak fraction of flow in the matrix. Model 2 provided the best predictions of the fraction of flow produced from the matrix at the end of the experiment. Model 1 significantly under-predicted these values except for the 200 cm<sup>3</sup>/hr experiment in the 48×1.5×0.04-in. fracture. Finally, both models over-predicted (by 25% to 175%) the final average gel composition in the fracture. Model 2 typically predicted gel compositions that were high by a factor of at least 2. In summary, both models have merit but require significant improvements to accurately describe gel propagation and dehydration in fractures.

### ***Effect of Polymer Molecular Weight***

In the work discussed to this point, the only polymer used was Alcoflood 935 HPAM. The manufacturer (Ciba) stated that this polyacrylamide had a molecular weight between 7 and 9 ×10<sup>6</sup> daltons and a 10% degree hydrolysis. For comparison, Marathon determined that this polymer had a molecular weight of 5×10<sup>6</sup> daltons and a degree of hydrolysis between 5% and 10%.

We wondered whether a gel made with a higher molecular weight polymer could be more cost-effective and/or exhibit more desirable extrusion properties in fractures. To answer this question, the HPAM polymer, Percol 338, was obtained from Ciba. Ciba stated that Percol 338 had a molecular weight between 12 and 14 ×10<sup>6</sup> daltons and a 10% degree of hydrolysis. A range of formulations was prepared to identify a gel composition that provided behavior similar to that for a gel with 0.5% Alcoflood 935 and 0.0417% Cr(III)-acetate. In all formulations, the ratio of HPAM to Cr(III)-acetate was fixed (at 12:1), the brine used for gelant preparation contained 1% NaCl and 0.1% CaCl<sub>2</sub>, and the gel was aged for 24 hours at 41°C. Similarity of behavior was

judged by tonguing from a bottle. The most similar gel contained 0.2% Percol 338 HPAM and 0.0167% Cr(III)-acetate. This composition was then used in the following extrusion tests.

Table 5—Experimental results versus predictions from Models 1 and 2.

Fracture dimensions ( $L_f \times h_f \times w_f$ )	48×1.5×0.04-in.			12×12×0.04-in.	
Injection rate, cm <sup>3</sup> /hr	200	500	2,000	500	1,600
Estimated velocity in the fracture, cm/hr	525	1,312	5,250	164	525
Total fracture volumes of gel injected	80	80	80	30	61
Gel arrival at core end, fracture volumes					
Actual	15	6.0	4.0	6.0	2.6
Predicted by Model 1 ( $k_{gel}=0.00011+1.0(C/C_o)^{-3}$ )	16	9.9	6.0	7.7	5.2
Predicted by Model 2 ( $u_1 = 0.374 t^{-0.557}$ )	33.7	17.0	6.6	28.4	12.1
Peak fraction of matrix flow, %					
Actual	100	93	75	97	91
Predicted by Model 1 ( $k_{gel}=0.00011+1.0(C/C_o)^{-3}$ )	96	94	90	92	88
Predicted by Model 2 ( $u_1 = 0.374 t^{-0.557}$ )	97	95	89	97	94
Fraction of flow produced from end of matrix, %					
Actual	35	26	16	55	17
Predicted by Model 1 ( $k_{gel}=0.00011+1.0(C/C_o)^{-3}$ )	35	13	6	16	10
Predicted by Model 2 ( $u_1 = 0.374 t^{-0.557}$ )	38	24	13	79	35
Average $C/C_o$ in fracture at end of experiment					
Actual	27	17	11	12	3.6
Predicted by Model 1 ( $k_{gel}=0.00011+1.0(C/C_o)^{-3}$ )	41	28	17	15	11
Predicted by Model 2 ( $u_1 = 0.374 t^{-0.557}$ )	59	40	23	33	21

The selected Percol 338 gel (0.2% HPAM, 0.0167% Cr(III)-acetate, 1% NaCl, 0.1% CaCl<sub>2</sub> aged for 24 hours at 41°C) was forced through a 4-ft-long fractured Berea sandstone core. The average fracture width was 0.04 in. (0.1 cm), and 39 fracture volumes of gel were injected at a fixed rate of 400 cm<sup>3</sup>/hr.

The pressure gradients in each of the five sections of the fracture are shown in Fig. 55 during gel injection. Near the end of gel injection, the pressure gradient in the fracture averaged 4.1 psi/ft, ranging from 2.7 (in Section 3) to 5.6 psi/ft (in Section 1). These values were about seven times lower than the average pressure gradients observed during injection of the Alcoflood 935 gel (with 0.5% HPAM) into a similar fractured core (see Figs. 5 and 6). This result suggests that gels made from polymers with higher molecular weights may be more likely to extrude deep into a fracture system without exceeding wellbore pressure constraints.

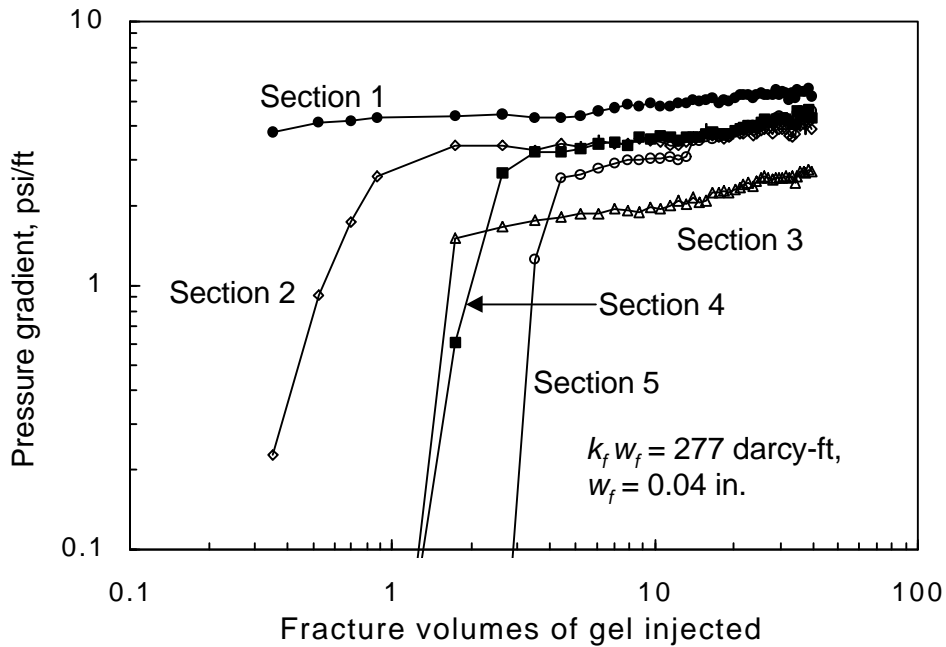


Fig. 55—Pressure behavior in the fracture taps during Percol 338 gel injection.

The chromium and HPAM concentrations in the effluent from the fracture and the matrix are shown in Fig. 56. The concentrations were expressed relative to those in the injected gel (i.e., 0.2% HPAM and 0.0167% Cr(III) acetate). Consistent with our earlier observations (see Fig. 9) no significant chromium or HPAM was produced from the porous rock during this experiment. For effluent from the fracture, chromium and HPAM were first detected after injecting 4 fracture volumes of gel. However, the chromium and HPAM concentrations did not approach the injected concentration until about 13 fracture volumes of gel. Thus, some ambiguity exists about the time at which gel arrived at the end of the fracture. After 13 fracture volumes of gel injection, the chromium and HPAM concentrations in the effluent were similar to those for the injected gel.

At the core outlet, the fraction of the fluid produced from the fracture versus from the matrix is shown in Fig. 57. This figure reveals that no significant fluid was produced from the matrix until after 13 fracture volumes of gel were injected. By analogy with the analysis associated with Fig. 8, Fig. 57 suggests that gel breakthrough occurred at 13 fracture volumes rather than at 4 fracture volumes. Interestingly, the fraction of flow in the matrix in Fig. 57 peaked at 78% of the total, compared with 100% in Fig. 8 (200 cm<sup>3</sup>/hr) and 93% in Fig. 47 (500 cm<sup>3</sup>/hr). Near the end of gel injection, 59% of the flow was produced from the fracture, while 41% was produced from the porous rock. For comparison, in previous experiments with the Alcoflood 935 gel, after injecting ~40 fracture volumes of gel, 46% and 30% of the flow was produced from the porous rock for injection rates of 200 and 500 cm<sup>3</sup>/hr, respectively. Since the average rate of water leakoff from the gel was similar for the two gels at this point of comparison, the two gels appeared to dehydrate or concentrate at roughly the same rate.

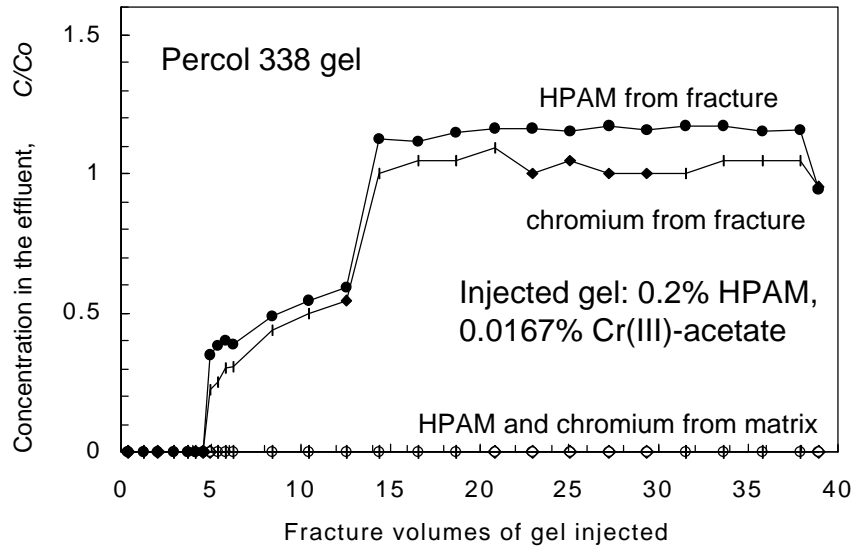


Fig. 56—Chromium and HPAM concentrations in the effluent (0.2% Percol 338 gel).

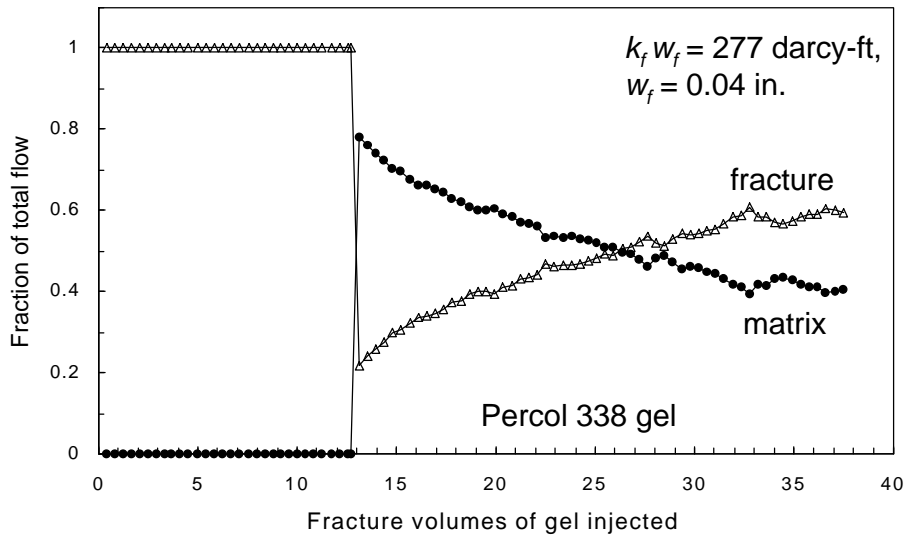


Fig. 57—Fraction of total flow measured at the core outlet (0.2% Percol 338 gel).

At the end of the experiment, the fracture was opened, and the gel in the fracture was analyzed. Figure 58 shows the chromium and HPAM compositions (relative to those for the injected gel) as a function of distance along the fracture. The chromium and HPAM concentrations for gel in the fracture averaged 10 and 20 times, respectively, the values in the original gel. The difference between the chromium and HPAM concentrations was surprising. We wonder whether an experimental error may have caused the difference (e.g., an incorrect dilution factor may have been used during the analysis of one of the chemicals). This issue will be resolved in future experiments.

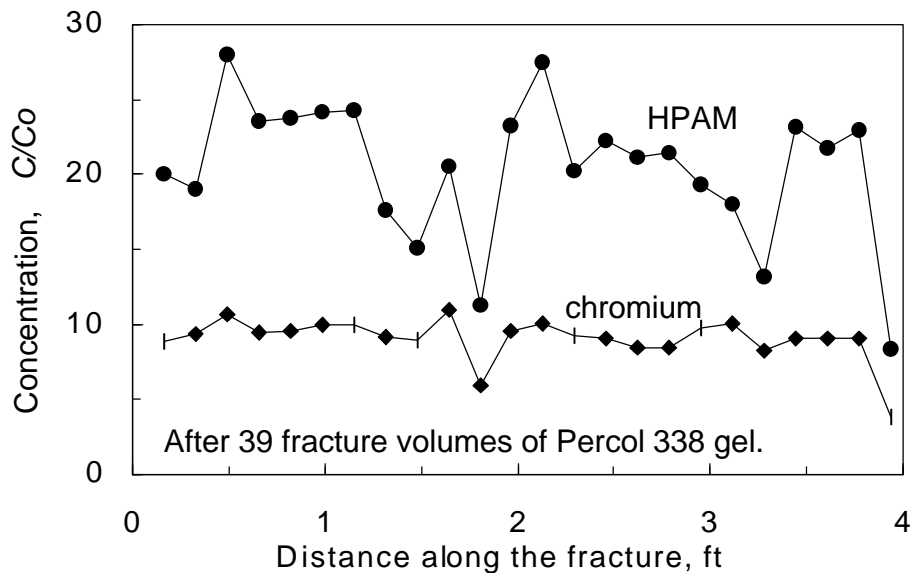


Fig. 58—Composition of gel in the fracture (0.2% Percol 338 gel).

For comparison, in previous experiments with the Alcoflood 935 gel, the gel in the fracture after injecting ~40 fracture volumes was from 10 to 20 times more concentrated than the injected gel. This similarity in degree of concentration for the Alcoflood 935 and Percol 338 gels also suggests that the two gels dehydrate or concentrate at roughly the same rate.

A summary comparison of the Percol 338 gel and the Alcoflood 935 gel are shown in Table 6. As mentioned previously, the pressure gradient needed to extrude the Percol 338 gel through the fracture was about seven times lower than that for Alcoflood 935 gel. Thus, gels made from polymers with higher molecular weights may be more likely to extrude deep into a fracture system without exceeding wellbore pressure constraints.

Table 6—Properties of two gels during extrusion through a 48×1.5×0.04-in. fracture.

	Polymer:	Alcoflood 935	Percol 338
Molecular weight, daltons*		7-9 × 10 <sup>6</sup>	12-14 × 10 <sup>6</sup>
Degree of hydrolysis, %*		10	10
HPAM concentration, %		0.5	0.2
Chromium concentration, %		0.0417	0.0167
Pressure gradient required for gel extrusion, psi/ft		28-29	4
Gel breakthrough, fracture volumes		6-15	4? 13?
Average gel C/C <sub>0</sub> in fracture after ~40 fracture volumes of gel injection		10-20	10-20
Average fraction of flow from matrix after ~40 fracture volumes of gel injection, %		30-46	41

\*Values provided by the polymer manufacturer (Ciba).

The last three data rows in Table 6 indicate that the two gels propagated and dehydrated at roughly the same rates when extruding through fractures. Interestingly, for the Percol 338 gel, the average pressure drop between the fracture and the adjacent porous rock was much lower than that for the Alcoflood 935 gel (because of the much lower pressure gradient during Percol 338 extrusion). This fact, coupled with the equivalent rates of gel dehydration, suggest that the permeability to water for the Percol 338 gel was much greater than that for the Alcoflood 935 gel. This finding was expected, since the original Percol 338 gel was 2.5 times less concentrated than the original Alcoflood 935 gel.

In summary, Table 6 reveals that the extrusion, propagation, and dehydration behaviors of the Percol 338 gel were similar to, or better than, those for the Alcoflood 935 gel. Ciba stated that the Percol 338 HPAM costs about the same as the Alcoflood 935 HPAM. Since the Percol 338 gel required 2.5 times less polymer and chromium than the Alcoflood 935 gel, a significant economic advantage may be realized by preparing gels with polymers having the highest available molecular weight.

***Preliminary Predictions for Behavior in Long Fractures***

A key motivation for undertaking this work is a need to quantify how gels propagate through fractures in field applications. Of course, these fractures are much longer and higher than those examined experimentally in this study. To accurately predict behavior in field applications, a satisfactory model is required for gel propagation and dehydration during extrusion. Clearly, more work is needed before a satisfactory model will become available.

Nevertheless, based on our experimental results to date, we made some preliminary analyses to estimate gel propagation rates in long fractures. One key observation during extrusion was that for a given fracture width, a minimum pressure gradient must be exceeded before gel will flow in a fracture.<sup>6-9</sup> For our standard 1X Cr(III)-acetate-HPAM gel, that relation was given by Eq. 1.

$$dp/dl = 0.02/w_f^2 \dots\dots\dots (1)$$

Another reality is that in order for the gel front to progress in a fracture, the total injection rate must exceed the rate of water loss from the gel (i.e., rate of water leakoff through the fracture faces). In a two-wing fracture, a minimum injection rate,  $q_{min}$ , can be calculated that exactly matches the rate of water leakoff.

$$q_{min} = [8 h_f / (\mu w_f)] \int \Delta p k_{gel} dL \dots\dots\dots(12)$$

Two terms in Eq. 12 vary with distance along the fracture— $\Delta p$  and  $k_{gel}$ . The term,  $\Delta p$ , is given by Eq. 13.

$$\Delta p = (L_f - L) 0.02 / (w_f)^2 \dots\dots\dots(13)$$

In Eq. 13, the units are psi for  $\Delta p$ , feet for  $L_f$  and  $L$ , and inches for  $w_f$ .

Given Eq. 13, Eq. 12 could be evaluated if  $k_{gel}$  was known as a function of position in the fracture. Of course, this determination is the subject of our continuing research. However, for now, uncertainty exists about this relationship. So, as an approximation, we now simply assume that  $k_{gel}$  has a constant value that is independent of fracture length. With this assumption Eq. 12 reduces to Eq. 14.

$$q_{min}/h_f = 1.078 k_{gel} (L_f)^2 / [\mu (w_f)^3] \dots\dots\dots(14)$$

In Eq. 14, the units are BPD/ft for  $q_{min}/h_f$ , darcys for  $k_{gel}$ , feet for  $L_f$ , cp for  $\mu$ , and inches for  $w_f$ . This equation suggests that the maximum distance of gel penetration into a fracture should be inversely proportional to the square root of gel permeability and directly proportional to the 1.5 power of fracture width. The maximum distance of gel penetration should also be proportional to the square root of injection rate. Therefore, penetration along a fracture should be maximized by injecting gel as fast as possible.

What values of  $k_{gel}$  should be used? Figure 50 indicated that average gel permeability typically ranged from 0.1 to 3  $\mu$ D in 0.04-in.-wide fractures. In wider fractures, gels should be dehydrated to a lesser extent (see Fig. 2), so gel concentrations should be lower and gel permeability to water should be greater. In the case of no dehydration (expected for very wide fractures), Eq. 7 suggests that  $k_{gel}=1,000 \mu$ D.

Equation 14 was used to generate Fig. 59. The figure shows minimum injection rates (per ft of fracture height) required for a given distance of gel penetration in a fracture as a function of fracture width and gel permeability. The practical range of injection rates extends from 1 to 1,000 BPD/ft. For example, if gel is injected at 1 BPM into a 100-ft-high fracture, the equivalent injection rate on the y-axis is 14.4 BPD/ft. Fracture widths less than 0.04 in. were not considered because high pressure gradients would probably create injectivity problems during gel extrusion (see Fig. 1). Figure 59 provides a means to estimate how far our 1X Cr(III)-acetate-HPAM gel might penetrate into a fracture. However, we emphasize that this figure is based on a preliminary model that applies only to a two-wing fracture. More work is needed to increase confidence in the predictions and to extend the predictions to naturally fractured systems with multiple fractures.

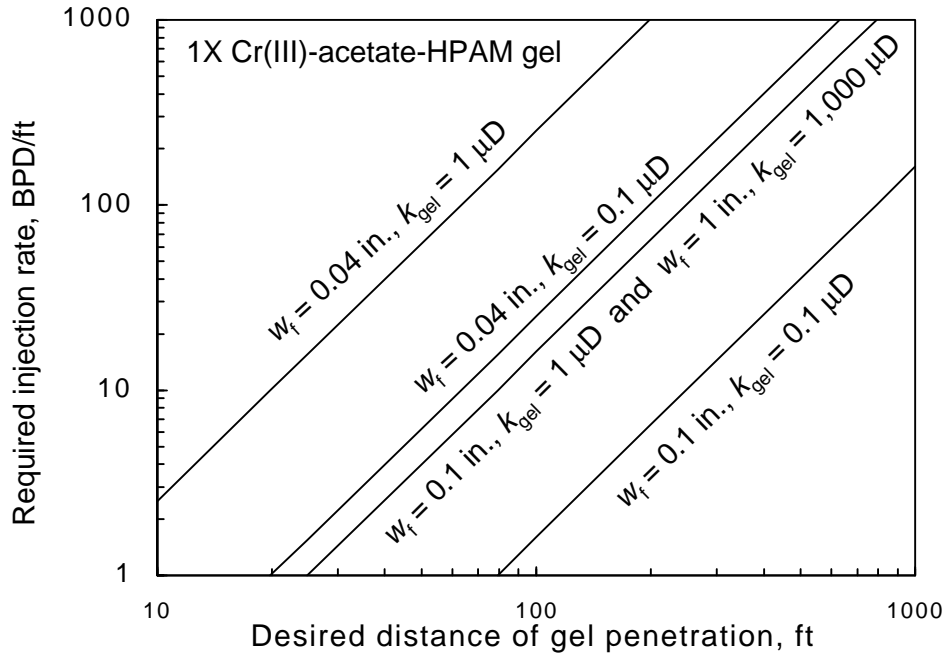


Fig. 59—Minimum injection rates required in a two-wing fracture.

### Conclusions

The following conclusions apply to a 1-day-old Cr(III)-acetate-HPAM gel at 41°C:

1. During injection of 80 fracture volumes of the gel, progressive plugging (i.e., continuously increasing pressure gradients) was not observed in any part of 48×1.5×0.04-in. fractures.
2. Effluent from the fracture had the same appearance and a similar composition as those for the injected gel, even though a concentrated, immobile gel formed in the fractures.
3. The concentrated gel formed when water leaked off from the gel along the length of the fracture. The driving force for gel dehydration (and water leakoff) was the pressure difference between the fracture and the adjacent porous rock.
4. During gel extrusion through a fracture of a given width, the pressure gradients and dehydration factors were the same for fractures in 650-mD sandstone as in 50-mD sandstone and 1.5-mD limestone.
5. A simple model was developed that accounted for many of the experimental observations. However, refinements are needed in the model, especially to account for behavior in narrow fractures and over a range of fracture heights and injection rates.
6. Gel permeability varied with polymer concentration raised to a power between -2.5 and -3.0. The initial permeability of our 1X Cr(III)-acetate-HPAM gel was around 1 mD.
7. We examined the properties of a gel made from an HPAM (Percol 338) with roughly twice the molecular weight of our standard HPAM (Alcoflood 935). Extrusion, propagation, and dehydration behaviors of the Percol 338 gel were similar to, or better than, those for an Alcoflood 935 gel. Since the Percol 338 gel required 2.5 times less polymer and chromium than the Alcoflood 935 gel, a significant economic advantage may be realized by preparing gels with polymers having the highest available molecular weight.

8. Preliminary analyses indicated that dehydration will limit the distance of gel penetration into a fracture and that the maximum distance of gel penetration should increase with the square root of injection rate.

### ***Future Work***

In future work, additional experiments will be performed to refine our model for gel extrusion and dehydration. Also, using our model and experimental findings, analyses will be performed to predict conditions, gel compositions, and gel volumes that provide the optimum gel placement in fractured reservoirs. More specifically, some of the questions that we plan to address in the near future include:

1. How does gel permeability to water ( $k_{gel}$ ) or leakoff rate ( $u_1$ ) vary with fracture length, width, and height?
2. Why does the pressure gradient for gel extrusion vary inversely with the square of fracture width?
3. Will gels made from higher molecular weight polymers show substantial technical and economic advantages?
4. Is there a practical upper limit to gel injection rate?
5. Can dehydration be reduced using fluid-loss agents?
6. How do gels and foamed gels compare for dehydration and extrusion?
7. How should gel treatments be sized in naturally fractured reservoirs?

### 3. GELANT TREATMENTS IN HYDRAULICALLY FRACTURED WELLS

One-third of all newly drilled wells are intentionally fractured. Often, when hydraulic fracturing stimulates production wells, the fracture unintentionally extends through shale or calcite barriers into water zones, causing substantially increased water production. Gelant treatments have frequently been applied in an attempt to correct this problem. However, the design of the gelant volumes for these applications has been strictly empirical, and consequently, the success rates for these treatments have been erratic. We developed a sound engineering basis and a simple 11-step procedure for sizing gelant treatments in hydraulically fractured production wells. This procedure was incorporated in user-friendly graphical-user-interface software. Details can be found in Ref. 11. From our web site at <http://baervan.nmt.edu/ResSweepEffic/reservoir.htm>, the software can be downloaded. We hope that our method will increase confidence in and applications of gel technology for reducing water production in hydraulically fractured production wells.

For recent field applications of the software, we noted several cases where engineers overestimated the static reservoir pressure (used as input for the program). This situation occurred because the engineers either used the original reservoir pressure or an outdated or inappropriate estimate of the reservoir pressure (e.g., a pre-fracture measurement or a measurement from a different part of the field). Consequently, the pressure drawdown used as input for our software was too high, and the program identified the wells (possibly incorrectly) as bad candidates for a gelant treatment. This experience emphasizes the need for recent, accurate pressure data for the target well, if our program is to be used.

We updated the software to Version 1.07. After a candidate well was determined to be inappropriate for a gel treatment, the previous version (1.05) required the user to return to the beginning of the program if the user wished to examine a new case. In contrast, Version 1.07 allows the user to continue and modify previous data entries without re-entering all reservoir and fluid properties.

In Version 1.07, improvements also were made in the routines to back-calculate in-situ water and oil residual resistance factors from previous field applications of gelant treatments.

#### 4. RHEOLOGICAL PROPERTIES OF GELS USED FOR CONFORMANCE CONTROL

Chapter 2 described an extensive investigation of extrusion of Cr(III)-acetate-HPAM gels through fractures. These experiments were both time-consuming and expensive. Can the extrusion properties of gels in fractures be deduced from or correlated with results from simpler, more cost-effective tests—such as rheological measurements? In this chapter, we begin to address this question. (This chapter is a summary of the most important results from the MS thesis of Jin Liu, which can be found in Ref. 12.)

##### *Introductory Concepts*

The Cr(III)-acetate-HPAM gels that we use are viscoelastic—meaning that their properties are intermediate between those of elastic solids and viscous liquids. For an elastic solid, application of a shear stress,  $\tau_s$ , causes the solid to deform by a “strain” or distance,  $\gamma$ . If the stress is not too great, the elastic solid will return to its original shape after the stress is removed. If the solid follows Hooke’s law, the relationship between applied stress and strain is linear.<sup>13</sup> The ratio of stress to strain is called the shear modulus,  $G$ .

If the solid is deformed too much, the deformation may become plastic rather than elastic—meaning that the solid does not completely return to its original shape after the stress is released.<sup>13</sup> For common solids, the point (stress) at which plastic behavior begins is labeled the yield point (or yield stress).

For viscous fluids, no elastic deformation occurs when a shear stress is applied. Instead, the fluid flows, dispersing the applied force and energy as heat.<sup>14</sup> The viscosity,  $\mu$ , is defined as the shear stress divided by the shear rate,  $\dot{\gamma}$ .

$$\mu = \tau_s / \dot{\gamma} \dots\dots\dots(15)$$

For Newtonian fluids, the viscosity is independent of shear rate.

For a viscoelastic material, elements of both elastic and viscous character are exhibited.<sup>14</sup> Depending on the time scale over which the stress is applied, either the elastic or the viscous nature may dominate performance. (Usually, the elastic nature dominates over short time scales, while the viscous nature becomes more evident over longer time scales.)

A common method to assess the viscoelastic nature of materials uses measurement of stresses during application of a sinusoidally oscillating shear strain. The applied strain,  $\gamma$ , is described using Eq. 16.

$$\gamma = \gamma_0 \sin (\omega t) \dots\dots\dots(16)$$

Here,  $\gamma_0$  is the maximum strain applied and  $\omega$  is the frequency of the strain wave. The top curve in Fig. 60 illustrates this strain wave.<sup>14</sup>

In a plate-plate viscometer, movement of one plate and deformation of the material between the plates generates a stress wave,  $\tau$ , that is measured at the second plate.

$$\tau = \tau_o \sin (\omega t + \delta) \dots\dots\dots(17)$$

If the material is an elastic solid, then the phase angle,  $\delta$ , in Eq. 17 is zero. In contrast, if the material is a normal liquid, the phase angle is  $90^\circ$ . If the tested material is viscoelastic, the stress wave will be shifted by an intermediate phase angle, as illustrated by the middle solid curve of Fig. 60. For analysis, the stress wave is generally separated into two waves with the same frequency (dashed curves in Fig. 60). One wave ( $\tau'$  in Fig. 60) is in phase with the strain wave, while the other wave ( $\tau''$  in Fig. 60) is  $90^\circ$  out of phase with the strain wave. In this way, the stress wave is separated into an elastic component and a viscous component.

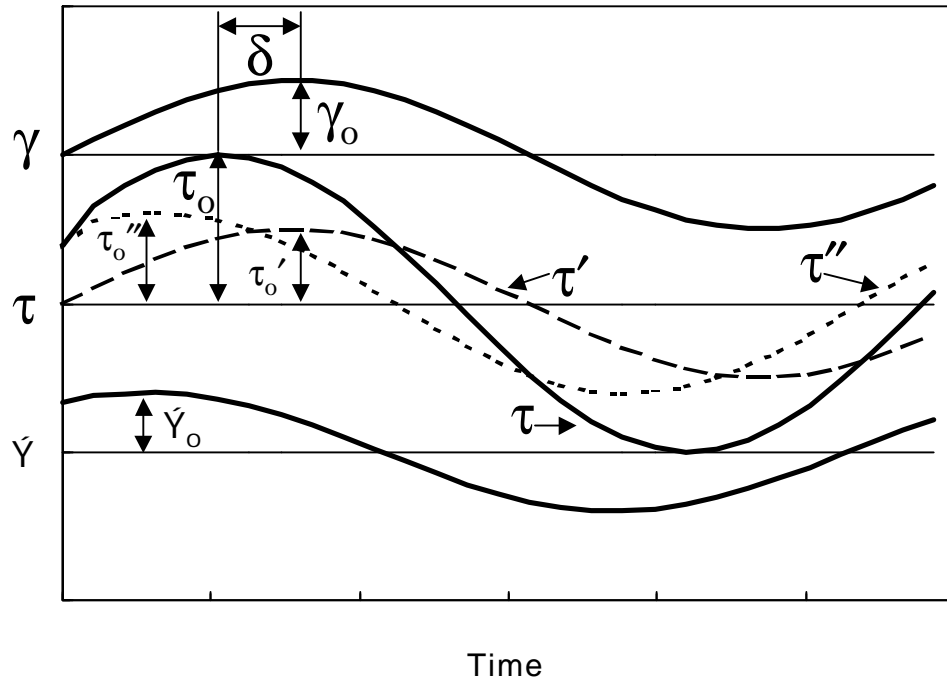


Fig. 60—Oscillating shear strain produces a sinusoidal stress.

Using the terms illustrated in Fig. 60, the elastic modulus or storage modulus,  $G'$ , is defined by Eq. 18.

$$G' = \tau_o' / \gamma_o \dots\dots\dots(18)$$

Similarly, the viscous modulus or loss modulus,  $G''$ , is defined by Eq. 19.

$$G'' = \tau_o'' / \gamma_o \dots\dots\dots(19)$$

The phase angle or loss angle,  $\delta$ , is related to  $G'$  and  $G''$  through Eq. 20.

$$\tan \delta = G''/G' \dots\dots\dots(20)$$

The bottom curve in Fig. 60 shows shear rate versus time. Shear rate,  $\dot{\gamma}$ , is defined by Eq. 21.

$$\dot{\gamma} = d\gamma/dt \dots\dots\dots(21)$$

As indicated in Fig. 60, the  $\tau'$  wave is in phase with the strain ( $\gamma$ ) wave, while the  $\tau''$  wave is in phase with the shear rate ( $\dot{\gamma}$ ) wave.

The complex viscosity,  $|\eta^*|$ , is defined by Eq. 22.

$$|\eta^*| = \tau_o''/\dot{\gamma}_o + \tau_o'/\dot{\gamma}_o = [(\eta')^2 + (\eta'')^2]^{0.5} = [(G''/\omega)^2 + (G'/\omega)^2]^{0.5} \dots\dots\dots(22)$$

The complex modulus,  $|G^*|$  is defined by Eq. 23.

$$|G^*| = [(G'')^2 + (G')^2]^{0.5} = \tau_o / \gamma_o = |\eta^*| \omega \dots\dots\dots(23)$$

The importance of the above definitions and relations is that they allow us to distinguish and quantify the elastic and viscous character of a material. In concept, this distinction could be important with regard to extruding a gel through a fracture. The extrusion properties should be quite different depending on whether the gel's behavior is dominated by its viscous character or its elastic character.

***Gels Studied***

Two gels were investigated in this work. Most work was performed using a Cr(III)-acetate-HPAM gel that contained 0.5% Allied Colloids Alcoflood 935 HPAM, 0.0417% Cr(III) acetate, 1% NaCl, and 0.1% CaCl<sub>2</sub> at pH=6. The second gel examined was a Al(III)-sulfate-HPAM gel that contained 0.5% Allied Colloids Alcoflood 935 HPAM, 0.01% Al(III) sulfate, 1% NaCl, and 0.1% CaCl<sub>2</sub>. Unless stated otherwise, the formulations were prepared at room temperature and aged for 24 hours at 41°C. Subsequently, rheological measurements were performed at 20°C using a Paar-Physica UDS 200 Universal Dynamic Spectrometer with a MP31 (50-mm diameter) plate and 1 Hz oscillation frequency.

***Elastic and Viscous Moduli versus Strain***

When a gel is extruded through a fracture, several important questions, arise:

1. How far can the gel be stretched or deformed before it breaks?
2. Does the gel's elastic character dominate over its viscous nature?
3. How does the extrusion properties of one gel compare to those of another gel?

We begin to answer these questions in Fig. 61, which plots the elastic ( $G'$ ) and viscous ( $G''$ ) moduli versus strain for the 24-hr-old Cr(III)-acetate-HPAM and Al(III)-sulfate-HPAM gels. The solid circles show  $G'$  for the Cr(III)-acetate-HPAM gel. At low strain values, the elastic modulus

was near 10 Pa. As strain increased to 200%,  $G'$  gradually decreased to 6 Pa. However, the elastic modulus was reasonably constant over this range. Thus, the gel showed near Hookean behavior over a significant range of stretching.

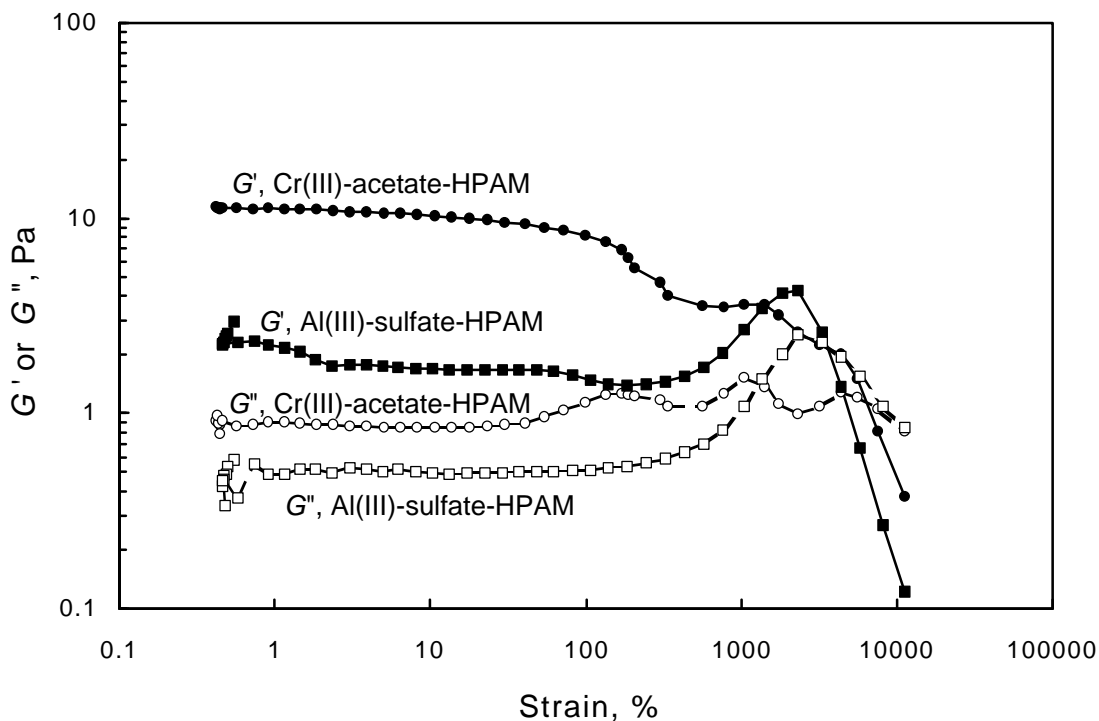


Fig. 61—Elastic ( $G'$ ) and viscous ( $G''$ ) modulus versus strain.

For strains between 200% and 3,000%,  $G'$  decreased from 6 Pa to about 2 Pa. Although the elastic component was not linear over this range, the result emphasizes this gel's tremendous ability to stretch—up to 3,000%! Thus, the utility of this gel during extrusion through fractures is not surprising.

For strains above 3,000%,  $G'$  rapidly decreased for the Cr(III)-acetate-HPAM gel—indicating irreversible breakage of the gel.

The open circles in Fig. 61 show the viscous modulus ( $G''$ ) versus strain for the Cr(III)-acetate-HPAM gel. Over the entire range of strain values,  $G''$  was about 1 Pa. Especially for the lower strain values,  $G''$  was about one-tenth  $G'$ . Thus, the elastic nature of the gel dominated over its viscous nature.

For the 24-hr-old Al(III)-sulfate-HPAM gel (solid squares in Fig. 61), the elastic modulus had a value around 2 Pa for strains up to 200%—exhibiting Hookean behavior over the same range as that for the Cr(III)-acetate-HPAM gel. However,  $G'$  for the Al(III)-sulfate-HPAM gel was 20% that of the Cr(III)-acetate-HPAM gel. Does this result indicate that the Al(III)-sulfate-HPAM gel

requires a lower pressure gradient to extrude through a fracture? Future extrusion experiments will be required to answer this question.

For strains between 200% and 3,000%,  $G'$  for the Al(III)-sulfate-HPAM gel increased with increased strain. In contrast,  $G'$  for the Cr(III)-acetate-HPAM gel decreased over this range. At present, an explanation for this difference is not available. For strains above 3,000%, the elastic modulus for the Al(III)-sulfate-HPAM gel decreased rapidly—indicating gel breakdown at the same point noted for the Cr(III)-acetate-HPAM gel.

For strains up to 200%, the viscous modulus ( $G''$ ) was about 25% of  $G'$  for the Al(III)-sulfate-HPAM gel. So, as with the Cr(III)-acetate-HPAM gel, the elastic nature dominated over the viscous nature. Interestingly, for strains between 200% and 3,000%,  $G''$  increased for the Al(III)-sulfate-HPAM gel. We have no explanation for this behavior.

### Strain versus Time

As mentioned earlier, the time scale for a deformation affects whether a material's elastic nature dominates over its viscous nature. For the experiments described in Fig. 61, the time scale for the deformation was 1 second (because 1 Hz oscillation was used). If a fixed stress is applied to a sample, how rapidly will the gel's strain response occur? For the Cr(III)-acetate-HPAM gel, this question is answered in Fig. 62. Various stress values (ranging from 2 Pa to 20 Pa) were applied instantaneously to the gel sample, and the strain was noted versus time. For stresses of 10 Pa and below, the strain response appeared complete within 1 second of the stress application.

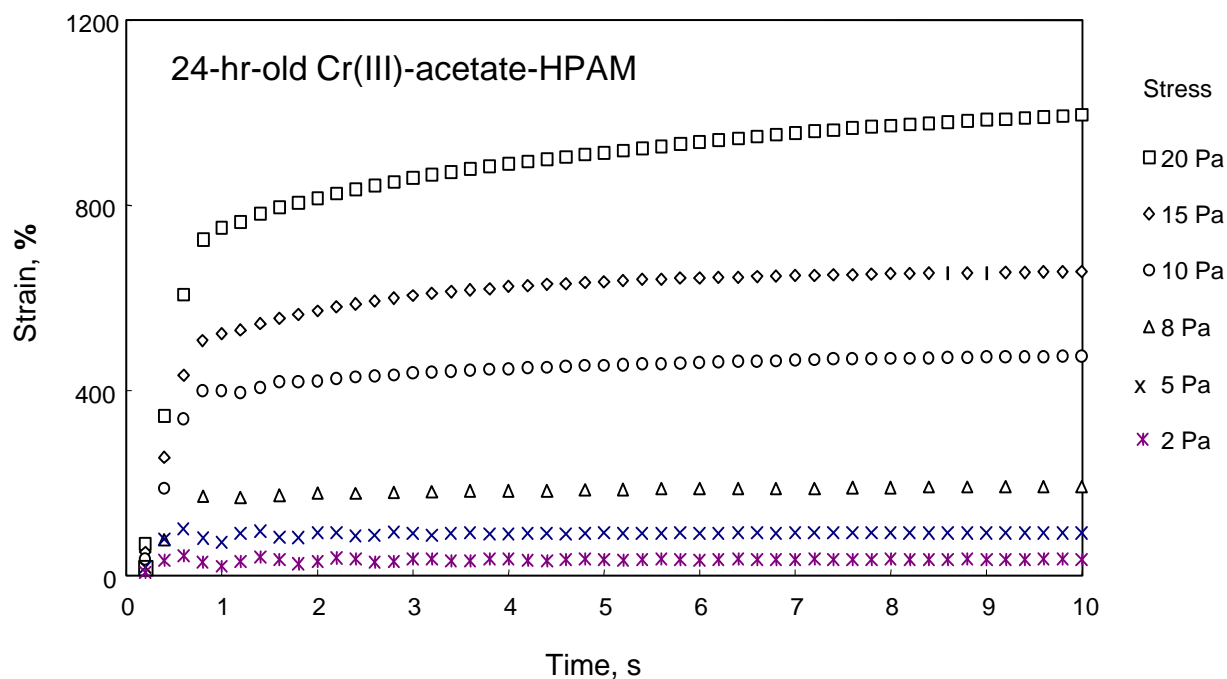


Fig. 62—Strain versus time for a Cr(III)-acetate-HPAM gel.

What time scale is expected for gel deformation during extrusion through fractures? In Table 5 (page 44), we listed Cr(III)-acetate-HPAM gel velocities between 164 and 5,250 cm/hr (0.046 and 1.46 cm/s) in fractures with widths of 0.1 cm. In the analysis of Fig. 61, we suggested that this gel could deform in a Hookean fashion up to 200% and deform up to 3,000% before breaking. Thus, in a 0.1-cm-wide fracture, an element of gel may stretch between 0.3 and 30 cm before breaking. Perhaps elements of gel propagates through the fracture in jumps between 0.3 and 30 cm. If so, an element of gel propagating with a velocity of 5,250 cm/hr would experience cycles of deformation (i.e., jumps) every 0.2 to 20 seconds. Work is needed to determine if  $G'$  and  $G''$  measurements at different time scales (frequencies of strain application) correlate with extrusion measurements in fractures at different velocities.

***Elastic and Viscous Moduli versus Polymer and Crosslinker Concentration***

The measurements to this point involved a Cr(III)-acetate-HPAM gel that contained 0.5% HPAM and 0.0417% Cr(III) acetate. How do  $G'$  and  $G''$  vary with gel composition? This question is answered in Fig. 63 for HPAM concentrations ranging from 0.3% to 1.7%. In all cases, the ratio of HPAM concentration to Cr(III)-acetate (weight/weight) was 12 to 1. The brine content was fixed (1% NaCl, 0.1% CaCl<sub>2</sub>), the gels were aged at 41°C for 24 hours before testing, and the measurements were made at 20°C. The applied strain was 40%.

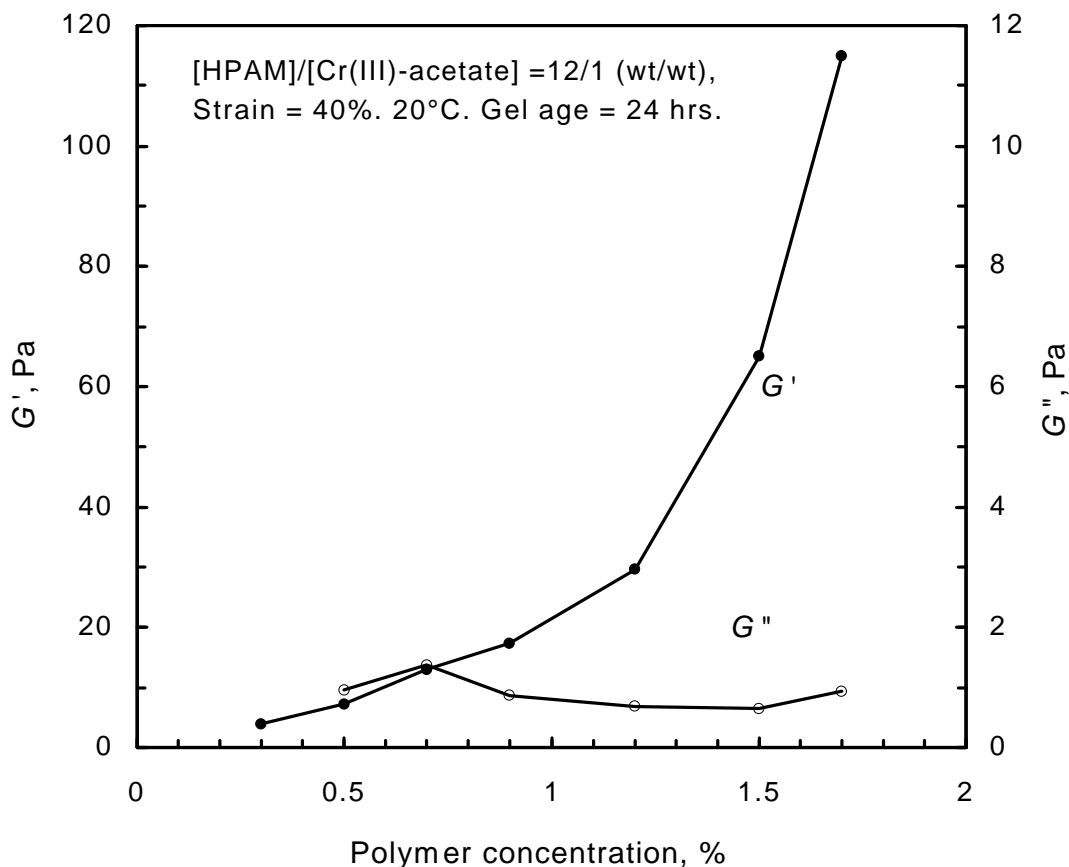


Fig. 63— $G'$  and  $G''$  versus polymer concentration for Cr(III)-acetate-HPAM gels.

As the polymer concentration in the gel increased from 0.3% to 1.7%, the elastic modulus ( $G'$ ) increased from 4 to 115 Pa. In contrast, the viscous modulus ( $G''$ ) remained near 1 Pa. Thus, as expected, the elastic component became increasingly dominant (over the viscous component) as the polymer concentration increased.

As mentioned, the polymer to crosslinker ratio was fixed for the experiments shown in Fig. 63. Fig. 64 shows the effect of crosslinker concentration on  $G'$  for a Cr(III)-acetate-HPAM gel that contained 0.5% HPAM.  $G'$  exhibited a broad maximum at ~7-8 Pa for Cr(III)-acetate concentrations between 0.02% and 0.05%. As mentioned earlier, our most-studied gel contained 0.0417% Cr(III)-acetate and 0.5% HPAM.

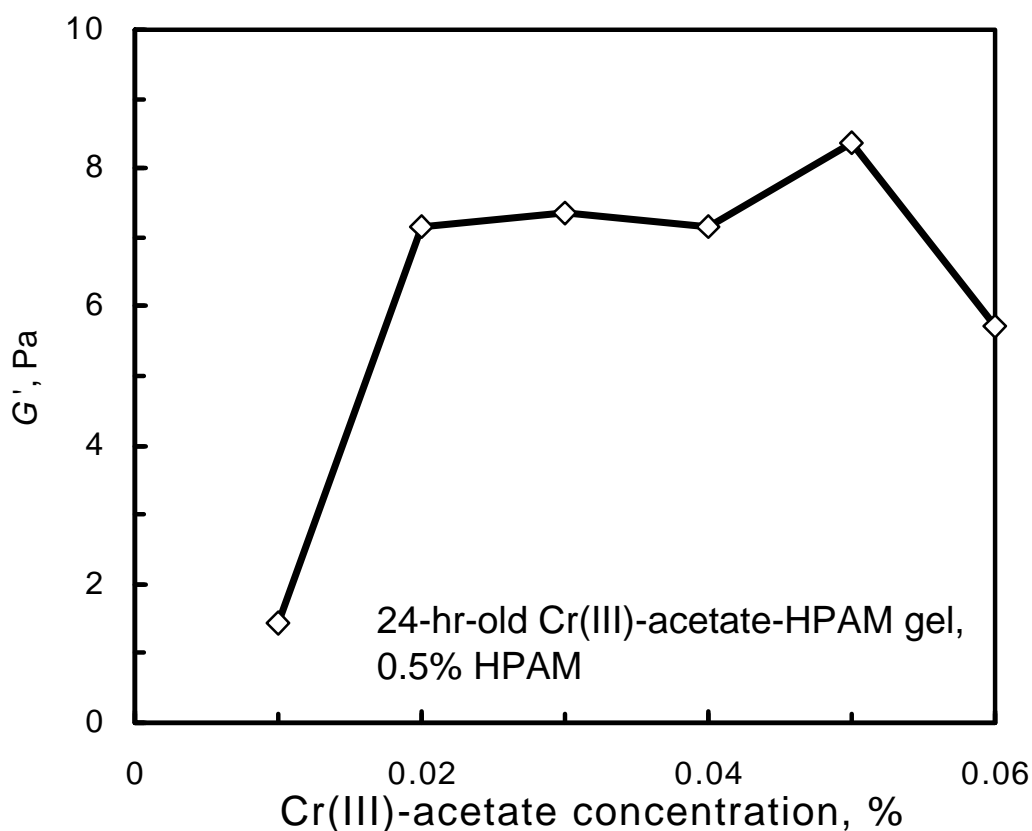


Fig. 64— $G'$  versus Cr(III)-acetate concentration.

### ***Effect of Temperature***

For the work described in Chapter 2, all experiments were performed at 41°C. In contrast, in this chapter, the measurements to this point were performed at 20°C, even though the gels were aged at 41°C. How does  $G'$  depend on temperature? This question is addressed in Fig. 65 for our standard Cr(III)-acetate-HPAM gel. The range of temperatures investigated was 15°C to 40°C. The applied strain was 40% during the measurements.

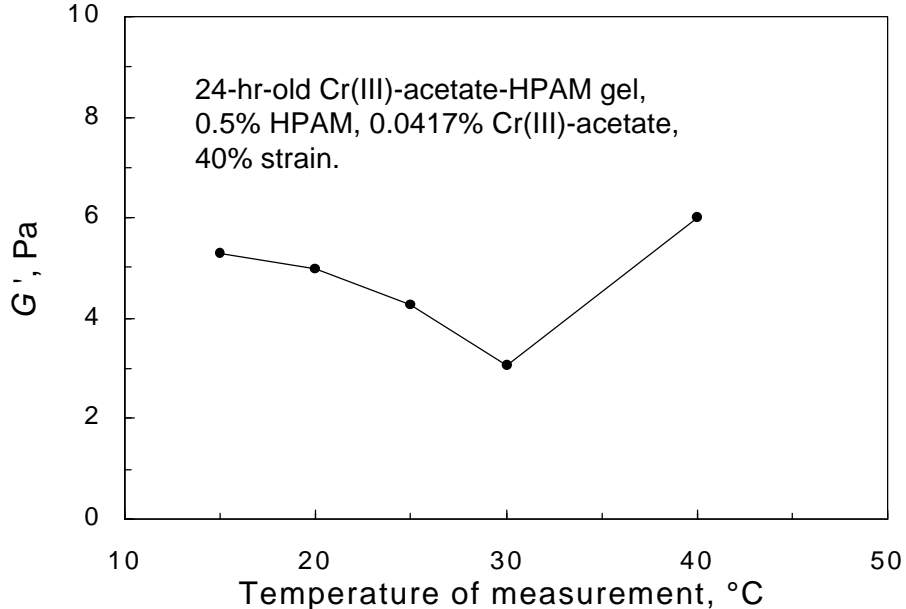


Fig. 65— $G'$  versus temperature for a Cr(III)-acetate-HPAM gel.

In this figure,  $G'$  ranged from 3 to 6 Pa.  $G'$  appeared to experience a shallow minimum at 30°C. However, we note from Fig. 61 that  $G'$  was expected to be about 10 Pa rather than 5 Pa. Clearly, some experimental error is present here. Therefore, this experiment should be repeated.

### *Effect of Gel Aging*

In field applications where large volumes of gel were injected, the times required to inject the gel were typically one week, but were up to one month in some cases.<sup>2-4</sup> Do the rheological properties of the gel change with time?

Figure 66 plots  $G'$  versus HPAM concentration for Cr(III)-acetate-HPAM gels that were aged at 41°C for one day, four days, and nine days. (Rheological measurements were made at 40% strain and at 20°C.) HPAM concentrations in these gels ranged from 0.5% to 1.5%. The ratio of polymer to crosslinker was fixed. As noted in Fig. 63, for a given gel at a given time,  $G'$  increased with increased HPAM concentration.  $G'$  also increased with increased aging time at 41°C. We speculate that this increase may have been caused by “curing” or more complete inter-molecular crosslinking reactions with increased time.

Figure 67 plots  $G'$  versus strain for Al(III)-sulfate-HPAM gels that were aged at 41°C for one day, seven days, and twelve days. (Rheological measurements were made at 20°C.) For all three curves, the gel required strains in excess of 3,000% before serious gel breakdown became evident. As noted earlier for the one-day-old gel (Fig. 61),  $G'$  increased with increased strain between 200% and 3,000%. This “hump” was not observed for the seven- and twelve-day-old gels. More work is needed to understand the origin of this “hump.”

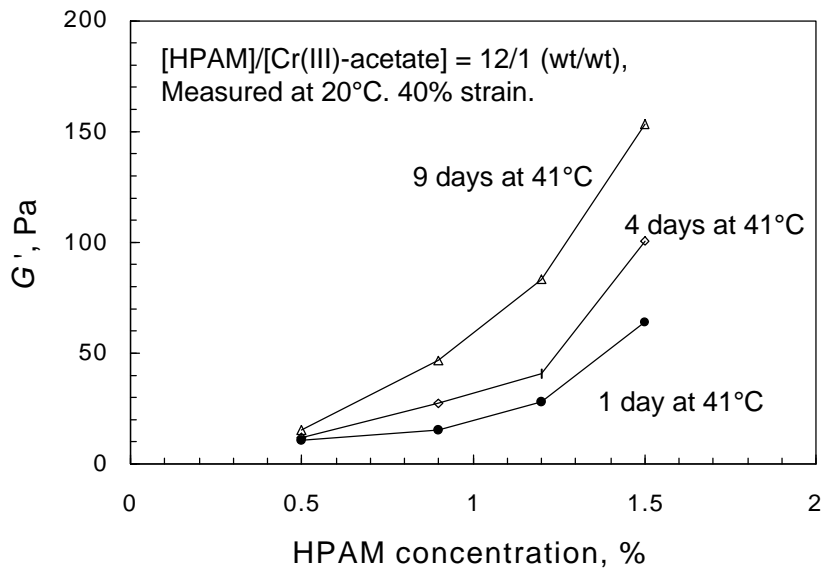


Fig. 66— $G'$  versus HPAM concentration and storage time for Cr(III)-acetate-HPAM.

Interestingly,  $G'$  for the gel aged for seven days was about five times greater than those for the gels aged for either one or twelve days. The increase in  $G'$  between one and seven days may have been caused by “curing” or more complete inter-molecular crosslinking reactions with increased time. The decrease in  $G'$  between seven and twelve days may have been caused by “syneresis” or a shift from inter-polymer crosslinks to intra-polymer crosslinks. More work is needed to test these hypotheses. These experiments should be performed using the Cr(III)-acetate-HPAM gels, as well.

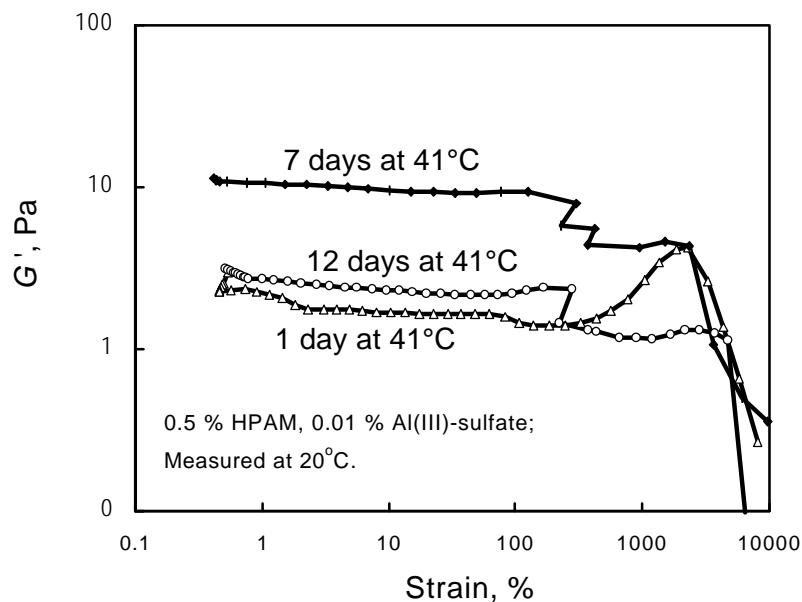


Fig. 67— $G'$  versus strain and gel age for a Al(III)-sulfate-HPAM gel.

### *Yield Stress and Stresses During Flow*

During gel extrusion through fractures, we noted that a minimum pressure gradient must be applied for the gel to flow.<sup>6-8</sup> This observation suggests that the gel has a characteristic yield stress. Can the yield behavior noted during extrusion through fractures be correlated with stress measurements in a viscometer?

Figure 68 plots shear stress versus strain for a Cr(III)-acetate-HPAM gel that was aged for 3.5 hrs at 41°C. As the strain increased from 0% to 200%, stress increased linearly. However, as strain increased further, the stress-strain relation exhibited significant curvature. The two tangents drawn to the curve in Fig. 68 show an attempt to define a yield stress for this gel. The intersection of the two tangents suggests that the yield stress was about 3.3 Pa, and that the strain value at the yield point was about 400%. However, the choice of the two tangent lines—especially the upper tangent line—was somewhat arbitrary. With other choices for the tangents, the yield stress could be anywhere from 2 to 7 Pa, and the strain associated with the yield point could be anywhere from 200% to 2,000%. Thus, some uncertainty exists about the choice of a yield point. This issue is also evident from consideration of Fig. 61. For the Cr(III)-acetate-HPAM gel, should the yield point be chosen at a strain value of 200%, where  $G'$  begins its first significant decrease? Or should the yield point be chosen at a strain of 3,000%, where  $G'$  begins a dramatic decline?

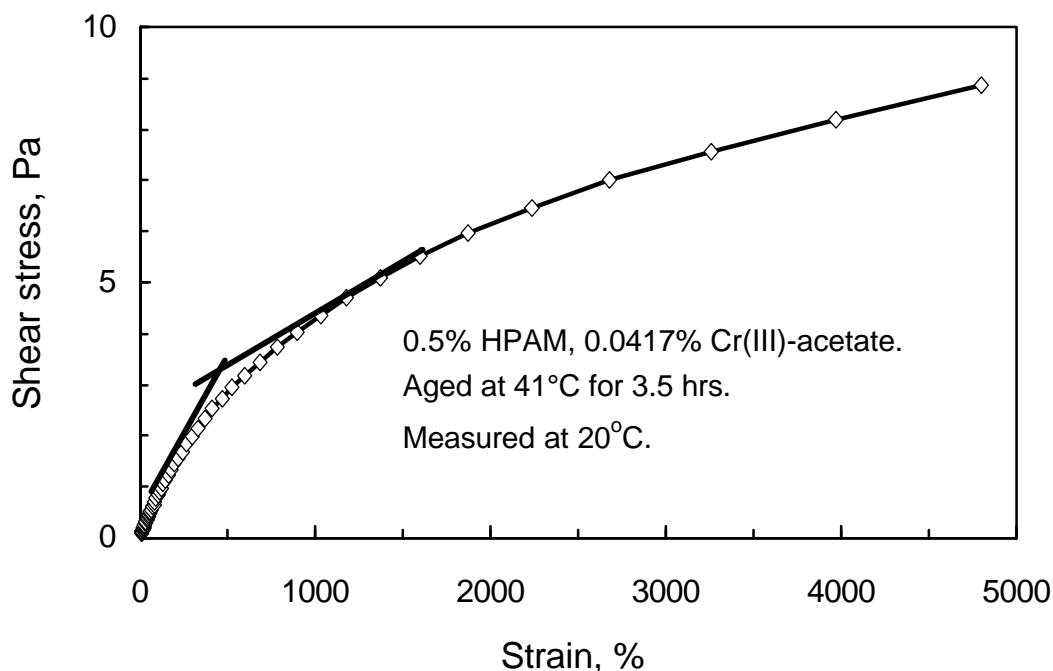


Fig. 68—Yield stress determination.

Another important issue when measuring the stresses is the rate at which the strain or deformation was applied. For a 24-hr-old Cr(III)-acetate-HPAM gel, Fig. 69 plots shear stress and complex viscosity (defined by Eq. 22) versus shear rate. The slope of the viscosity-versus-shear-rate curve is about  $-0.8$ . This value compares with slopes between  $-0.83$  and  $-0.95$  for the resistance factor

versus velocity curves during gel extrusion through tubes and fractures (Fig. 70, taken from Ref. 8).

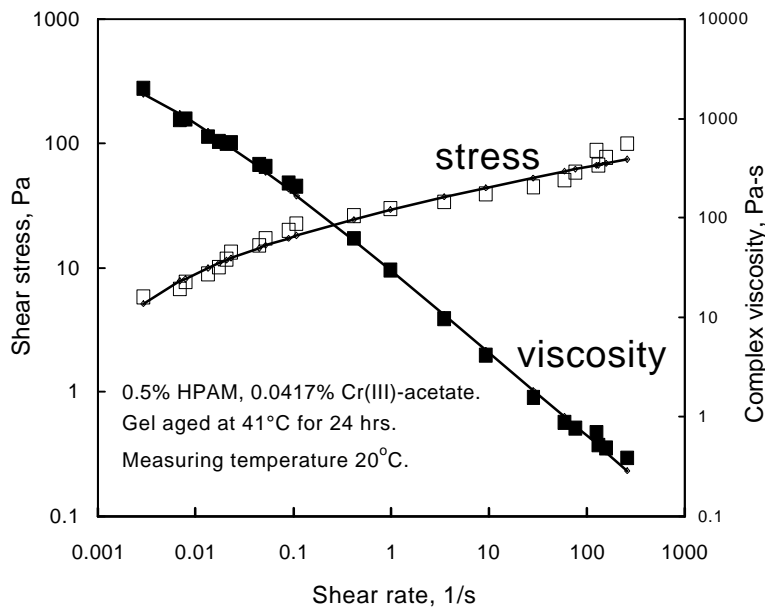


Fig. 69—Shear stress and complex viscosity versus shear rate.

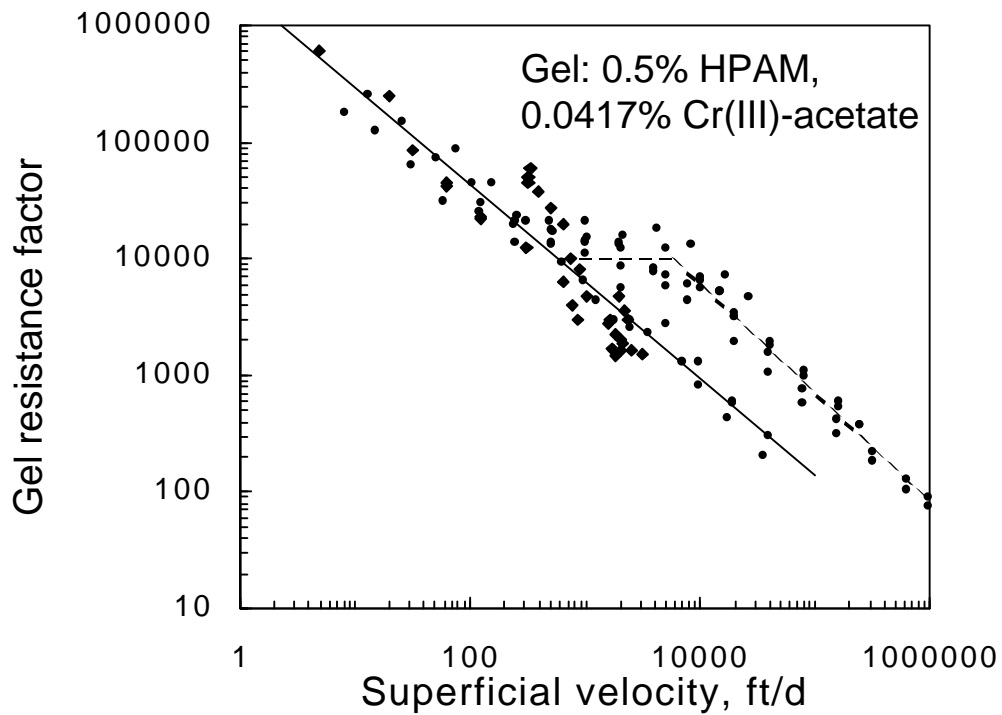


Fig. 70—Resistance factor versus velocity during gel extrusion.

Note in Fig. 69 that shear stress was fairly insensitive to shear rate. When shear rate was increased by a factor of 100,000, shear stress only increased by a factor of 10. This result was consistent with our earlier observations that the pressure gradient required to extrude a gel through a fracture was fairly insensitive to injection velocity.<sup>6-8</sup>

These similarities between behavior in fractures versus in a viscometer give us hope that a useful correlation can be found. However, additional work is needed to establish that correlation.

Earlier, the pressure gradient required for gel extrusion was shown to be inversely proportional to the square of fracture width (Fig. 1 and Eq. 1).

$$dp/dl=0.02/(w_f)^2 \dots\dots\dots (1)$$

Was this behavior expected? For a material with a yield stress,  $\tau_y$ , a simple force balance predicts that the pressure gradient required for extrusion should be given by Eq. 24.

$$dp/dl=2\tau_y /w_o \dots\dots\dots (24)$$

In this equation,  $w_o$  was the effective opening size during extrusion. For our standard one-day-old Cr(III)-acetate-HPAM gel at 41°C, the yield stress was about 10 Pa. For an opening size of 0.04 in. (0.1 cm), Eq. 24 predicted a pressure gradient of about 1 psi/ft. In contrast, the experimentally measured values ranged from 28 to 50 psi/ft when the fracture width was 0.04 in. This discrepancy needs to be resolved.

Perhaps the resolution lies in the effective shear rate or deformation rate that occurred in the fracture. If the deformation rate (or the effective shear rate) during gel extrusion through a fracture was greater than 100 s<sup>-1</sup>, the stress values from the right side of Fig. 69 might provide a more appropriate correlation with the pressure gradients observed during gel extrusion. Additional work will be performed to understand the relation between stress, fracture width, and the pressure gradient for gel extrusion.

***Properties of Gel from a Fracture***

In Chapter 2, we reported that gels concentrate or dehydrate during gel extrusion through fractures. Are the properties of these dehydrated gels similar to those expected for a gel of the same composition that was prepared by standard mixing procedures (i.e., not extruded through a fracture)?

We are still in the early stages of this investigation. In our first experiment, our standard Cr(III)-acetate-HPAM gel (containing 0.5% HPAM) was concentrated, on average, by a factor of 20 during extrusion through a fracture. The elastic modulus,  $G'$ , for this concentrated gel averaged about 20,000 Pa. Unfortunately, we have not yet been able to prepare a gel this concentrated using standard mixing methods. To date, we have only been able to prepare (by mixing) a gel that was six times more concentrated than the injected gel. For this gel,  $G'$  was 225 Pa. In the future, we plan to perform extrusion experiments in wider fractures to generate gels of intermediate concentrations.

### **Conclusions**

1. For 24-hr-old Cr(III)-acetate-HPAM and Al(III)-sulfate-HPAM gels, the elastic modulus ( $G'$ ) was fairly constant for strain values up to 200%. The elastic nature of these gels was evident even at strain values over 1,000%. This finding is consistent with observations concerning the ease with which these gels extrude through fractures.
2. For 24-hr-old Cr(III)-acetate-HPAM gels, as the polymer concentration in the gel increased from 0.3% to 1.7%, the elastic modulus increased from 4 to 115 Pa. In contrast, the viscous modulus ( $G''$ ) remained near 1 Pa. Thus, as expected, the elastic component became increasingly dominant (over the viscous component) as the polymer concentration increased.
3. For 24-hr-old Cr(III)-acetate-HPAM gels that contained 0.5% HPAM,  $G'$  exhibited a broad maximum at ~7-8 Pa for Cr(III)-acetate concentrations between 0.02% and 0.05%.
4. For Cr(III)-acetate-HPAM gels with various compositions,  $G'$  increased with increased aging time at 41°C (up to nine days). We speculate that this increase may have been caused by “curing” or more complete inter-molecular crosslinking reactions with increased time.
5. In contrast, for Al(III)-sulfate-HPAM gels,  $G'$  increased with increased aging time at 41°C up to seven days, and then declined between seven and twelve days. We speculate that  $G'$  may have decreased because of “syneresis” or a shift from inter-polymer crosslinks to intra-polymer crosslinks. More work is needed to test these hypotheses.
6. For a Cr(III)-acetate-HPAM gel, shear stress was fairly insensitive to shear rate. When shear rate was increased by a factor of 100,000, shear stress only increased by a factor of 10. This result was consistent with our earlier observations that the pressure gradient required to extrude a gel through a fracture was fairly insensitive to injection velocity.
7. For a Cr(III)-acetate-HPAM gel, a log-log plot of complex viscosity versus shear rate gave a slope of  $-0.8$ . This value was very similar to that for a log-log plot of resistance factor versus injection velocity that was noted earlier during gel extrusion through fractures.

### **Future Work**

As part of our quest to establish a correlation between gel rheology in a viscometer versus gel extrusion properties in fractures, the following are some of the issues that we hope to address in the future:

1. What stress measurement correlates with the pressure gradient required to extrude a gel through a fracture?
2. Why is the pressure gradient required to extrude a gel inversely proportional to the square of fracture width?
3. How do gels of different composition (e.g., polymer type, polymer molecular weight, crosslinker type) compare with respect to rheological behavior in a viscometer and in fractures?
4. How does gel rheology vary with the rate of the applied deformation?
5. How does gel rheology vary with temperature?

6. Are the properties of these dehydrated gels similar to those expected for a gel of the same composition that was prepared by standard mixing procedures (i.e., not extruded through fractures)?

## 5. WATER SHUTOFF IN UNFRACTURED PRODUCTION WELLS

The purpose of water shutoff treatments in production wells is to reduce water production without damaging the oil productivity. Among different blocking agents, polymers and gels are used most commonly in water shutoff in production wells. Many polymers and gels can reduce the permeability to water more than that to oil or gas.<sup>15</sup> This property can be very useful in treating production wells where vertical fractures cut through both water and hydrocarbon zones.<sup>16</sup> However, in production wells that do not contain fractures, polymers or gels penetrate a significant degree into all open zones.<sup>16,17</sup> Unless the polymers or gels can reduce the permeability to water with little or no damage to the permeability to oil or gas, the hydrocarbon productivity can be severely reduced after treatment.<sup>16,17</sup> In a previous study,<sup>18</sup> we compared different blocking agents with polymers and gels. The study concluded that most of the commercially available blocking agents suffered the same limitations that polymers and gels experience. Unless the hydrocarbon zones can be protected during placement, most of the blocking agents can cause severe damage to the oil productivity.

The objective of this study is to identify ideas and phenomena from the published literature that might be useful in future development of blocking agents that can consistently reduce water production from unfractured wells without damaging oil productivity. In addition to polymers and gels, the materials and approaches that we investigated in this study included: (1) oil-soluble particulates, (2) foams and gelled foams, (3) chemical reactions that rely on partitioning between oil and water, (4) mobility-matched postflushes, (4) thermally triggered diverting agents, and (5) dilution of gel banks in hydrocarbon zones by diffusion and dispersion.

### *Polymers and Gels*

During unrestricted injection, gels and polymers can penetrate to some extent into all open zones—not just those zones with high water saturations.<sup>16</sup> (Gelant is the liquid formulation before gelation.) Depending on the performance of the polymers or gels in the low-permeability hydrocarbon zones, hydrocarbon production can either be enhanced or impeded.

Results from the literature and our own studies showed that many polymers and gels can reduce the permeability to water more than that to oil or gas.<sup>15</sup> This property can be very useful in treating production wells where vertical fractures cut through both water and hydrocarbon zones.<sup>16</sup> However, in unfractured production wells, hydrocarbon productivity can be severely damaged unless the polymers or gels reduce the permeability to water with little or no damage to hydrocarbon permeability.<sup>16,17</sup> Typically, the residual resistance factor for oil or gas must be less than 2 to prevent damage to the oil productivity. Unfortunately, most of the polymers and gels that exhibit strong disproportionate permeability reduction also reduce the permeability to oil or gas by more than a factor of 2.<sup>15</sup> Although reports exist of gels that provide oil residual resistance factors near unity, reproducibility has been poor for many of these experiments.

**Polymers Reduce  $k_w$  Without Affecting  $k_o$ .** Zaitoun *et al.*<sup>19</sup> reported that adsorbed polyacrylamide and polysaccharide polymers in Vosges-sandstone cores reduced the water relative permeability significantly at any given water saturation. In contrast, the adsorbed polymer layer had little or no effect on the oil relative-permeability curve. In one case, they observed an

increase in oil relative permeability at a given water saturation. However, in all cases, the adsorbed polymer layer caused an increase in irreducible water saturation. A careful examination of the data revealed that the increase in irreducible water saturation lowered the endpoint relative permeability to oil. Therefore, for all practical purposes in zones with high oil saturations, the polymer treatment still reduced the effective permeability to oil. However, in these cases, the residual resistance factors for oil ( $F_{ro}$ ) were low, ranging from 1.2 for a polyacrylamide polymer to 1.4 for a polysaccharide. This result is desirable for treating production wells that contain no fractures. However, a potential drawback is that the residual resistance factors for water were also low ( $F_{rw} < 6$ ).

To increase  $F_{rw}$  values, Zaitoun *et al.*<sup>20</sup> proposed using anionic acrylamide/acrylate copolymers that shrink in a high-salinity environment and swell when the salinity is reduced. Specifically, they proposed injecting the anionic polymers in brines having a higher salinity than the reservoir brine. When the well is returned to production, the reservoir brine with lower salinity displaces the high-salinity injected brine and causes the polymer molecules to swell, thereby increasing the resistance to water flow after treatment. Results from a sandpack experiment show that following this procedure, the polymer provided a  $F_{rw}$  value of 28 and a  $F_{ro}$  value of 1.6. Zaitoun *et al.*<sup>20</sup> also proposed using in-situ hydrolysis of a nonionic polyacrylamide polymer to increase  $F_{rw}$ . During placement, a potassium carbonate solution is injected into the formation following polymer injection. Potassium carbonate induces moderate alkaline hydrolysis and swelling of the nonionic polyacrylamide polymer. Following this procedure, a nonionic polyacrylamide polymer provided a  $F_{rw}$  value of 36 and a  $F_{ro}$  value of 2.6 in a sandpack.

**Polymers Reduce  $k_w$  Without Affecting  $k_{gas}$ .** Several researchers<sup>19,21,22</sup> reported that some polymers can reduce the permeability to water with little or no effect on the permeability to gas. Zaitoun *et al.*<sup>19,22</sup> observed an increase in the effective permeability to gas after treatment in a Voltzia-sandstone core using a polyacrylamide polymer. As in the water/oil cases, the adsorbed polymer increased the irreducible water saturation. Surprisingly, the adsorbed polymer actually increased the effective permeability to gas. This phenomenon could be very useful in water shutoff in gas wells that contain no fractures. However, the mechanism that is responsible for this phenomenon is unclear. In a similar experiment using a sandpack, the adsorbed polymer lowered the endpoint permeability to gas. More work is needed to study this phenomenon—especially to determine when it can occur reliably.

### **Particulates**

In a previous study,<sup>18</sup> we performed a literature survey to examine the feasibility of using particulates as blocking agents in production wells that contain no fractures. Most of the literature made unsubstantiated claims that particulates selectively plug high-permeability water zones without damaging less-permeable oil zones. Critical analyses of these claims revealed that particulates small enough to penetrate into the formation can cause significant damage to the formation permeability. The degree of permeability reduction increases with decreasing formation permeability. This behavior is opposite to the performance desired for a blocking agent.

**Oil-Soluble Particulate Resins.** One possible way to minimize damage in the oil zones is to use oil-soluble particulate resins. Oil-soluble resins are commonly used as diverting agents in matrix

acidizing to avoid formation damage after treatment.<sup>23,24</sup> (Oil-soluble particulate resins are soluble in oil but not soluble in water.) Basically, oil-soluble particulate resins have the same placement characteristics as ordinary particulates.<sup>18</sup> For this concept to work, two requirements must be met. First, the size of the resin particles must be small enough to penetrate freely into the high-permeability water zones. Second, the particles must be sized so that they become trapped by deep-bed filtration. In this way, when the well is returned to production, the particles could significantly reduce the permeability of watered-out zones. In contrast, in zones with high fractional oil flows, the particles quickly dissolve, thus minimizing the damage to the oil-productive zones.

However, deep-bed filtration is a very complicated process.<sup>25</sup> Laboratory screening studies would be required to identify the proper particle size to achieve both the in-depth penetration and the desired permeability reduction in the water zones.

**Oil-Soluble Wax-Polymer Particulates.** Blends of oil-soluble wax-polymer materials have also been used extensively in matrix acidizing as diverting agents.<sup>26,27</sup> The wax-polymer diverting agents are soluble in oil but not in water. They also have the same placement characteristics as ordinary particulates.<sup>18</sup> Therefore, for the wax-polymer materials to be effective in reducing water production without damaging the oil productivity, they must meet the same requirements for the oil-soluble particulate resins. In particular, the particles must be sized such that they penetrate freely into the high-permeability water zones and become trapped by deep-bed filtration. However, the wax-polymer materials have one advantage over the oil-soluble resins; that is, the wax-polymer particles are deformable. During placement, high-pressure gradients could force the deformable particles through pore throats that are smaller than the particles. When the well is returned to production, the particles could be caught in the porous rock. In this way, the particles may more effectively reduce the permeability of watered-out zones. In contrast, in zones with high fractional oil flows, the particles may quickly dissolve, thus minimizing damage to the oil-productive zones. Laboratory screening studies are required to identify the right particle size to achieve both the in-depth penetration and the desired permeability reduction in the water zones.

### ***Foams***

Foams have been used successfully as mobility-control agents during steam and high-pressure gas floods.<sup>28</sup> To improve sweep efficiency, a mobility-control agent should penetrate as much into the less-permeable zones as possible so that oil can be displaced from poorly swept zones. Consistent with this goal, low-mobility foams injected during field applications shifted flow into less-permeable zones, thereby improving the injection profile. However, when gas or water injection was resumed after foam injection, the profiles quickly reverted to become the same or worse than those observed before foam injection. This behavior is opposite to the performance desired for a blocking agent.

**Selective Placement.** In a previous study,<sup>28</sup> we identified two phenomena, the limiting capillary pressure and the minimum pressure gradient for foam generation, that could allow low-mobility foams to form in high-permeability zones but not in low-permeability zones. Exploiting these phenomena during foam placement requires that (1) under given reservoir conditions, a gas/liquid composition must be identified that will foam in high-permeability zones, but not in low-

permeability zones, (2) the foam must not easily collapse or wash out from the high-permeability zones, and (3) the aqueous phase must not contain a gelant or other reactive blocking agent. Extensive laboratory screening is required to identify a foam system that satisfies the requirements under a given set of reservoir conditions.

One possible way to reduce foam washout from the water zones is to incorporate a polymer or gel into the foam. However, if a gelant is used, it must be produced from the oil zones before gelation occurs; otherwise, the oil zones could be damaged.

**Foams Collapse in the Presence of Oil.** In many cases, foam stability is significantly reduced in the presence of oil.<sup>29,30</sup> In theory, this phenomenon could be exploited to optimize placement of a foam blocking agent in oil production wells. During foam injection, the foam penetrates a substantial distance into all open zones. When the well is returned to production, the foam could provide a large resistance to water flow, thereby restricting production from zones with high water saturations. Initially, the foam block would also restrict flow from zones with high oil saturations. However, produced oil could collapse the foam much more rapidly than the produced water. Therefore, the foam may collapse or wash out from oil-productive zones much more rapidly than from zones with high water saturations. This concept is most likely to be exploitable if the water zones contain no residual oil. Residual oil in the water zones could also collapse the foam, thereby rendering the treatment ineffective.

**Disproportionate Permeability Reduction by Gelled Foams.** A previous study showed that gelled foams can provide a significant disproportionate permeability reduction.<sup>31</sup> Unfortunately, while providing a significant permeability reduction to water, the gelled foams also reduced the permeability to oil by more than a factor of 2. Thus, in production wells that contain no fractures, the gelled foam in its present form could damage oil productivity unless it was produced from the oil zones before gelation. More work should be directed at improving the disproportionate permeability reduction by the gelled foam so that damage to oil zones can be minimized.

### ***Reactive Water-Blocking Agents***

Thompson and Fogler<sup>32</sup> investigated the use of “reactive water-blocking agents” to plug water zones in preference to oil zones in production wells. These chemicals are dissolved in oil and then injected. They react upon contact with water to form a precipitate or solid barrier. Ideally, watered-out zones will be restricted by blocking agents formed at the front between the displaced water bank and the injected bank of reactive chemicals, while no blocking agent should form in zones with high oil saturations. To maximize formation of blocking agents in water zones, Thompson and Fogler proposed using relatively viscous oil as a carrier fluid for the reactive chemicals. When the well is returned to production after injecting the reactive chemicals, water should finger through the chemical bank, thereby promoting mixing and formation of the blocking agent. One of the main challenges in using these materials is that reaction with residual water in the oil-bearing zones could damage oil productivity. More work is needed to assess the potential of reactive water-blocking agents, especially their effects on oil productivity.

### ***Mobility-Matched Postflush***

In theory, a mobility-matched postflush following gelant injection could provide a desirable gel placement where crossflow can occur.<sup>33,34</sup> As illustrated in Fig. 71, a water-like gelant is injected

into a production well that contains no fractures. Because of the low viscosity, gelant penetration into less-permeable zones is minimized. Next, water is injected to displace the water-like gelant away from the wellbore. Enough water must be injected so that the rear of the gelant bank in the most-permeable zone outruns the front of the gelant bank in an adjacent less-permeable zone. Then, the well is shut in to allow gelation to occur. Finally, the well is returned to production. Hopefully, a pathway will be available for oil to crossflow from the low-permeability zone into the high-permeability zone and then be quickly produced into the production well.

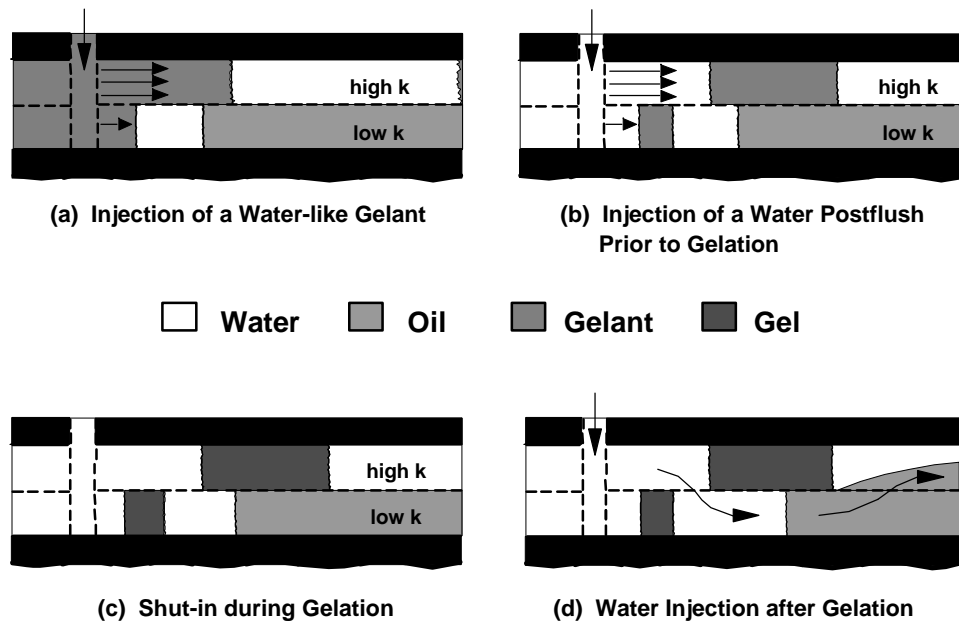


Fig. 71—Placement of a water-like gelant with crossflow.

There are several limitations for applying this process to production wells that contain no fractures. First, the amount of incremental oil recovered by this process is limited by the size of the gel bank in the high-permeability water zones. Figure 71 shows that after treatment, water in the high-permeability zones will flow around the gel banks and be diverted into the low-permeability oil zones. However, once it flows beyond the gel bank, the water will quickly crossflow back into the high-permeability zones. Therefore, the amount of incremental oil recovered is limited by the size of the gel bank in the water zone. Gelation time is an important factor that limits the amount of gelant that can be injected into the formation. Until recently, gelation times for common oilfield gelants were relatively short (0 to 10 days, typically) under reservoir conditions. To maximize the amount of incremental oil recovered, long gelation times are needed. In recent years, substantial progress has been made toward developing gelants with long gelation times, especially for use at elevated temperatures.<sup>35-38</sup>

Another important limitation is that the viscosity and resistance factor for the gelant should not exceed that of water. Viscous gelants will penetrate to a greater degree into the less-permeable zones.<sup>17,34</sup> Furthermore, before gelation, viscous gelants will crossflow continuously from the

high-permeability channel into the adjacent less-permeable zones.<sup>34</sup> This creates a barrier of viscous gelant in the less-permeable zones all along the interface with the high-permeability channel. When a water postflush is injected, the barrier hinders crossflow of water from the high-permeability channel into the less-permeable zones. Thus, viscous fingers from a water postflush will break through the viscous gelant bank in the high-permeability channel before breakthrough in less-permeable zones. This will render the process ineffective. (Incidentally, Kvanvik *et al.*<sup>39</sup> have suggested a scheme where viscous gelants could be used, so long as mobility-matched banks were used throughout the process.)

In addition, the viscosity and resistance factor of the gelant should not increase during injection of either the gelant or the water postflush. Any increase in gelant resistance factor during this time will drive additional gelant into the less-permeable zones,<sup>17,34</sup> and thereby, jeopardize the process.

### ***Thermally Triggered Diverting Agent***

Fletcher *et al.*<sup>40</sup> proposed the use of a gel where the gelation reaction is temperature-triggered to achieve in-depth fluid diversion without damaging the low-permeability oil zones. The proposed gel consisted of a medium-low molecular weight polyacrylamide with aluminum citrate as crosslinker. The gelant reportedly propagated through a long slim tube at 25°C without developing any significant resistance to flow. However, the resistance to flow increased dramatically as soon as the temperature was raised to 70°C. For injection wells, Fig. 72 shows that the temperature in the near-wellbore region is usually lower than the formation temperature due to the continuous injection of colder water. However, the cold front moves more slowly and more uniformly than the injection front. During placement, Fletcher proposed injecting a slug of low-concentration gelant into the formation, followed by water injection. Depending on the permeability contrast, most of the gelant enters the high-permeability thief zones while some of the gelant still penetrates into the low-permeability oil zones. As shown in Fig. 72, the gelant in the high-permeability thief zones quickly catches up with the cold front and develops high resistance to flow in the hot zone. In contrast, the gelant in the low-permeability oil zones remains behind the cold front and therefore causes no increase in the resistance to flow. Fletcher *et al.*<sup>40</sup> speculated that the gelant in the low-permeability oil zones might be lost due to adsorption and dispersion before reaching the hot zone.

A limiting factor for this concept is the crossflow between layers. As illustrated in Fig. 72, after treatment, the subsequently injected water will first be diverted into the low-permeability zones. However, the water will quickly crossflow back into the high-permeability zone once it flows beyond the gel bank. In other words, the treatment will not improve sweep efficiency beyond the greatest depth of gelant penetration in the formation. Also, to achieve in-depth placement, the mobility ratio of the displacing water and the gelant must remain favorable. Otherwise, viscous fingering could render the treatment ineffective. In addition, as soon as the leading edge of a gelant bank in a high-permeability zone reaches the hot zone, the elevated formation temperature triggers the gelation reaction. Figure 73 shows that the resulting increase in viscosity for the gelant in the hot zone will force the gelant still in the cold zone to crossflow into the adjacent low-permeability oil zones. Since the gelant that crossflows into the low-permeability zones is already very close to the hot zone, it could quickly reach the hot zone. The resulting gelation reaction could cause significant damage to the oil zones and render the process ineffective.

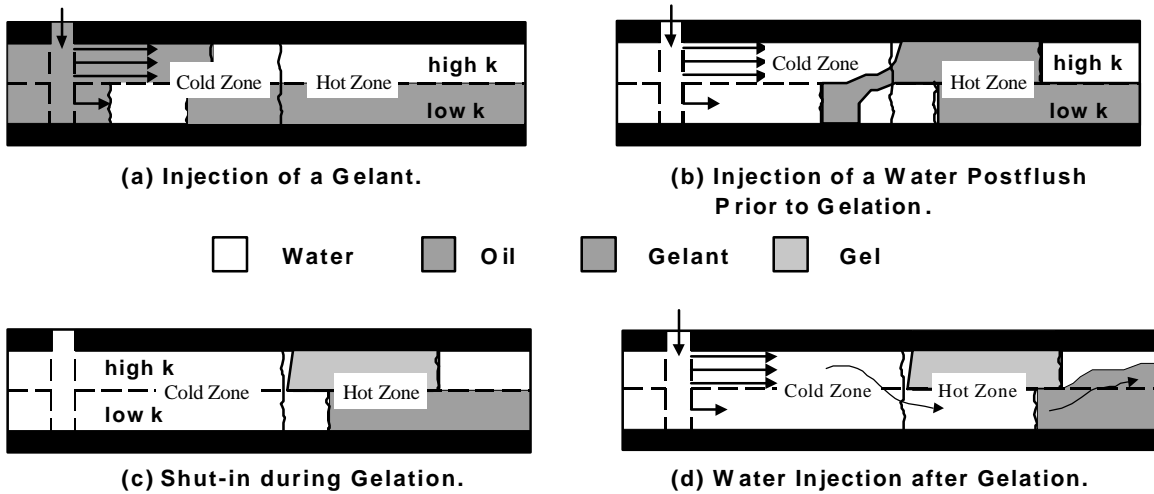


Fig. 72—Placement of a thermally triggered gelant with crossflow.

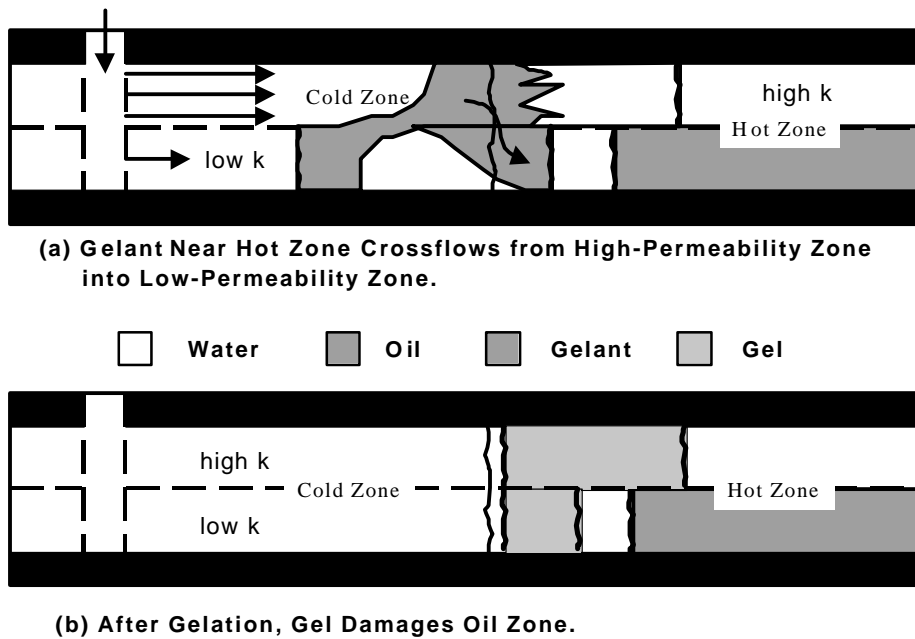


Fig. 73—Gelant crossflow near the hot zone.

The thermally triggered gel could also be used in production-well treatments. Basically, the same limitations for injection-well treatments also apply for production-well treatments. However, to use this gel in production wells, cold water must be injected before treatment to cool down the near-wellbore region. Gelant crossflowing from high-permeability layers near the hot zone into the low-permeability oil layers could damage the oil productivity and render the process ineffective. Also, the amount of incremental oil that can be recovered by this process is limited by the size of the gel bank in the high-permeability water zones.

### ***Dilution by Diffusion and Dispersion***

In concept, diffusion and dispersion could dilute gelants enough to prevent gelation in less-permeable hydrocarbon zones while allowing a gel plug to form in high-permeability water zones. Whether or not a chemical bank can be diluted enough by diffusion to prevent gelation depends on at least four factors: (1) the size of the chemical bank, (2) the diffusion coefficient, (3) the gelation time, and (4) the extent of dilution required to prevent gelation. A previous study<sup>41</sup> demonstrated that even with relatively large diffusion coefficients ( $10^{-5}$  cm<sup>2</sup>/s), diffusion will only reduce the gel-bank size by about 0.2 ft after ten days. In typical field applications in production wells that contain no fractures, gelants penetrate a significant distance into the low-permeability hydrocarbon zones (> 2 ft). Also, gelation times range from a few minutes to several days for most formulations that have been considered for near-wellbore gel treatments. Therefore, in production wells that contain no fractures, diffusion alone is not enough to prevent gelation in low-permeability hydrocarbon zones.

During injection of a gelant to miscibly displace water, both diffusion and dispersion will occur. In flow through reservoirs, dispersion usually is much more important than diffusion. A previous study<sup>41</sup> also illustrated that very high near-wellbore dispersivity values (~1 ft) are required to prevent gelation during typical field gel treatments in production wells that do not contain fractures. However, the same analysis also revealed that dispersion would dilute gelant banks in high-permeability zones by approximately the same factor as in low-permeability zones. Therefore, dispersion is unlikely to be helpful in preventing gelation in less-permeable hydrocarbon zones while allowing a gel plug to form in high-permeability water zones.

### ***Summary of Potentially Useful Ideas and Phenomena***

A review of the literature has identified some ideas and phenomena that might be useful in future development of blocking agents that can consistently reduce water production without damaging the oil productivity in production wells that contains no fractures.

**Polymers Reduce  $k_w$  Without Affecting  $k_o$  or  $k_{gas}$ .** Some polymers can provide low hydrocarbon residual resistance factors simultaneously with significant water residual resistance factors. However, the mechanism that is responsible for this phenomenon is unclear. More work is needed to understand why this phenomenon occurs. A better understanding of the mechanism may lead to improved reproducibility for this phenomenon under different conditions.

**Oil-Soluble Particulates.** Under certain circumstances, oil-soluble particulates could be useful in controlling water production without damaging the oil productivity in unfractured production wells. For this concept to work, the particles must be small enough to penetrate freely into high-permeability water zones, and the particles must become trapped by deep-bed filtration. However, deep-bed filtration is a very complicated process. Laboratory screening studies are required to identify the right particle size to achieve both the in-depth penetration and the desired permeability reduction in the water zones. Using deformable oil-soluble particulates may improve the effectiveness of reducing the permeability of water zones.

**Selective Placement of Foams in Water Zones but not in Hydrocarbon Zones.** By exploiting the concepts of the limiting capillary pressure and the minimum pressure gradient for foam generation, a foam can be designed that forms in high-permeability water zones but not in low-permeability hydrocarbon zones. The foam must not easily collapse or wash out from the high-permeability zones. Foam washout could be reduced by incorporating a polymer or gel into the foam. However, if a gelant is used, it must be produced from the oil zones before gelation occurs; otherwise, oil zones could be damaged.

**Foams Collapse in the Presence of Oil.** In many cases, foam stability is significantly reduced in the presence of oil. This concept is most likely to be exploitable if the water zones contain no residual oil. Residual oil in the water zones could collapse the foam, thereby rendering the treatment ineffective.

**Gelled Foams.** Gelled foams can provide a significant disproportionate permeability reduction. Unfortunately, the gelled foam in its present form can also cause severe damage to hydrocarbon productivity. More work should be directed at improving the disproportionate permeability reduction by the gelled foams so that damage to the oil zones can be minimized.

**Reactive Water-Blocking Agents.** Reactive water-blocking agents form precipitates upon contact with water but not with oil. These chemicals are dissolved in oil and then injected. However, the reaction between the chemicals and the residual water in the oil zones could damage the oil productivity. More work is needed to assess the potential of reactive water-blocking agents, especially their effects on oil productivity.

**Mobility-Matched Postflush.** Under limited circumstances, a mobility-matched postflush could result in a desirable gel placement in production wells that contain no fractures. However, the amount of incremental oil that can be recovered by this process is limited by the size of the gel bank in the high-permeability water zones. Gelation time is an important factor that limits the amount of gelant that can be injected into the formation. To maximize the amount of incremental oil recovered, long gelation times are needed.

**Thermally Triggered Diverting Agent.** Under limited circumstances where crossflow can occur, thermally triggered diverting agents could be placed selectively into high-permeability water zones without damaging the oil productivity in production wells that contain no fractures. The amount of incremental oil that can be recovered by this process is limited by the size of gel bank in the high-permeability water zones.

## 6. DISPROPORTIONATE PERMEABILITY REDUCTION

The purpose of water-shutoff treatments in production wells is to reduce water production without damaging the oil productivity. Among different blocking agents, polymers and gels are used most commonly for water shutoff in production wells. Many polymers and gels can reduce the permeability to water more than that to oil or gas.<sup>15</sup> This property is critical to the success of water-shutoff treatments in production wells if hydrocarbon-productive zones cannot be protected during placement.<sup>16,17</sup> However, the magnitude of the effect has been unpredictable from one application to the next. Presumably, the effect would be more predictable and controllable if we understood why the phenomenon occurs. In this study, we first briefly review the validity of several possible explanations for this disproportionate permeability reduction. Then, we describe experiments that test the validity of the most promising mechanism—a combined “wall-effect” and “gel-droplet” model. In this study, we also describe experiments designed to identify parameters that maximize the disproportionate permeability reduction. The parameters examined include the effects of residual oil saturation, pressure drawdown, and absolute permeability.

### *Review of Previous Findings*

Our previous studies showed that this effect was not caused by simple hysteresis of relative permeabilities or by gel breakdown during successive injection of oil and water banks.<sup>15,16</sup> This phenomenon was observed in core experiments using constant-pressure and constant-rate drive. Also, the disproportionate permeability reduction did not vary with core length.<sup>42</sup> Finally, this phenomenon was observed not only with polymers or weak polymer-based gels, but also with a resorcinol-formaldehyde gel and strong polymer-based gels.<sup>15</sup> Thus, the effect does not appear to be an experimental artifact.

In our previous studies, we extensively examined several possible mechanisms for this disproportionate permeability reduction.<sup>1,15,42-44</sup> We ruled out gravity and lubrication effects as possible mechanisms. Also, gel shrinking and swelling were unlikely to be responsible for this phenomenon. We examined whether the disproportionate permeability reduction was caused by a balance between capillary forces and gel elasticity. Our experimental results suggested that this mechanism was valid only in micromodels and small glass tubes, not in porous rock. Results from our previous studies also showed that water and oil following segregated pathways on a microscopic scale cannot explain this phenomenon. Our experimental results indicated that wettability may play a role; however its effect is unclear. Also, neither the wall-effect model proposed by Zaitoun *et al.*<sup>45</sup> nor the gel-droplet model proposed by Nilsson *et al.*<sup>46</sup> could satisfactorily explain all aspects of the disproportionate permeability reduction. However, our analyses demonstrated that a combined wall-effect and gel-droplet model could explain why this phenomenon occurs. Nonetheless, this combined model is still highly idealized. Some issues remain unresolved, so more work is needed to test this model.

### *Effect of Pressure Drawdown*

Our previous study showed that the disproportionate permeability reduction was observed using constant-pressure displacement.<sup>42</sup> Can controlling the pressure drawdown maximize the disproportionate permeability reduction? To answer this question, we performed oil/water experiments using different pressure gradients. For each pressure gradient, two similar oil-water

experiments were performed: one with oil injected immediately after shut-in to measure oil residual resistance factor,  $F_{\text{ro}}$ , and the other with brine injected immediately after shut-in to measure water residual resistance factor,  $F_{\text{rw}}$ . In total, we performed eight oil/water experiments using eight different Berea cores of similar permeability. (Detailed mobility and saturation values for all the cores used in this study are listed in Tables A1 through A14.) The gel contained 0.5% HPAM, 0.0313% Cr(III)-acetate, 0.0121%  $\text{CrCl}_3$ , 1% NaCl, and 0.1%  $\text{CaCl}_2$ . Unless otherwise mentioned, this composition is the standard Cr(III)-acetate-HPAM gel throughout this chapter. Soltrol 130 was the oil phase. The residual resistance factors listed in Table 7 were measured immediately after shut-in. (Detailed residual-resistance-factor data are listed in Tables A15 through A22.)

In this study, we used the ratio of  $F_{\text{rw}}$  to  $F_{\text{ro}}$  to quantify disproportionate permeability reduction. Higher  $F_{\text{rw}}/F_{\text{ro}}$  ratios indicate more pronounced disproportionate permeability reduction. Table 7 shows that  $F_{\text{rw}}/F_{\text{ro}}$  increased with increased pressure gradient from 45 psi/ft to 180 psi/ft. This increase in pressure gradient resulted in a 50% reduction in  $F_{\text{ro}}$  while the  $F_{\text{rw}}$  remained relatively unchanged. The ratio of  $F_{\text{rw}}$  to  $F_{\text{ro}}$  increased from 233 at 45 psi/ft to 409 at 180 psi/ft. However, at 225 psi/ft, a dramatic decrease in  $F_{\text{rw}}$  occurred and the disproportionate permeability reduction disappeared ( $F_{\text{rw}}/F_{\text{ro}} = 1$ ). This implies a washout of the gel by brine from the porous medium at 225 psi/ft. These findings suggest that to a certain extent, an increase in pressure drawdown after treatment might reduce the productivity damage to oil without affecting the ability of the gel to reduce water production. More work is underway to examine the effect of pressure drawdown in less-permeable rock.

Table 7—Effect of pressure drawdown on disproportionate permeability reduction.  
Gel: 0.5% HPAM, 0.0313% Cr(III)-acetate, 0.0121%  $\text{CrCl}_3$ , 1% NaCl, 0.1%  $\text{CaCl}_2$   
Cores: High-permeability Berea sandstone

Pressure Gradient, psi/ft	$F_{\text{rw}}$	$F_{\text{ro}}$	$F_{\text{rw}}/F_{\text{ro}}$
45	47,000	202	233
90	30,000	127	236
180	42,200	103	409
225	73	107	~1

### ***Effect of Rock Permeability***

During water-shutoff treatments in production wells, we want a blocking agent that can provide more pronounced disproportionate permeability reduction in low-permeability hydrocarbon zones than in high-permeability water zones. However, results from our previous studies showed that for a water-based Cr(III)-acetate-HPAM gel, the disproportionate permeability reduction decreased with decreased absolute permeability in both water- and oil-wet cores.<sup>1</sup> In this study, we performed additional oil/water experiments using an oil-based gel in strongly water-wet Berea cores. The oil-based gel consisted of 18% 12-hydroxystearic acid in Soltrol 130. Our previous study showed that the oil-based gel reduced the permeability to oil more than that to water.<sup>28</sup> (This is opposite of what we observed for water-based gels.) Table 8 shows that the  $F_{\text{ro}}/F_{\text{rw}}$  increased from 5 to 14 as the absolute permeability decreased from 1,800 md to 170 md.

(Detailed residual-resistance-factor data are listed in Table 27 of Ref. 28 and Tables A23 and A24.) In other words, the reverse disproportionate permeability reduction increased with decreased absolute permeability in strongly water-wet Berea cores. More work is underway using the oil-based gel in oil-wet cores. The objective is to understand the implications of this phenomenon on the mechanism of the disproportionate permeability reduction.

Table 8—Effect of rock permeability on disproportionate permeability reduction.  
Gel: 18% 12-hydroxystearic acid in Soltrol 130  
Cores: Strongly water-wet Berea sandstone

$k_w$ , md	$F_{rw}$	$F_{ro}$	$F_{ro}/F_{rw}$
1,800	184	860	5
600	34	300	9
170	25	350	14

### ***Combined “Wall-Effect” and “Gel-Droplet” Model***

Our analyses in a previous study demonstrated that a combined wall-effect and gel-droplet model could explain why the disproportionate permeability reduction occurs.<sup>1</sup> However, this combined model is still highly idealized and some issues remain unresolved. In this study, we performed additional oil/water experiments to further test this model.

**“Wall-Effect” Model.** Zaitoun *et al.*<sup>45</sup> attributed the disproportionate permeability reduction to wall effects resulting from an adsorbed polymer layer on the pore walls. Figure 74 shows that in a strongly water-wet system, the presence of residual oil droplets at the center of the pores can significantly reduce the effective width of the water channels during waterflooding. In contrast, this restriction may not exist during oilflooding. Therefore, for a given thickness of an adsorbed polymer layer, the permeability reduction for water during waterflooding is greater than that for oil during oilflooding. In an oil-wet system, they proposed that the polymer could still cover most of the rock surface by anchoring on the small part of the rock surface that remains water-wet. The layer of polymer covering the oil-wet surface would shift the wettability toward water-wet. In this way, the polymer could reduce the permeability to water more than that to oil in an oil-wet core. Zaitoun *et al.*<sup>45</sup> reported that the capillary pressure of a silane-treated oil-wet sandstone core shifted from negative before treatment to positive after treatment. Also, the polymer reduced the permeability to water more than that to oil in the oil-wet core. Based on these findings, they concluded that the adsorbed polymer layer was responsible for the disproportionate permeability reduction in both the oil- and water-wet cores.

If this theory is correct, the disproportionate permeability reduction should vanish in strongly oil-wet polyethylene cores where there is no water-wet surface on which the polymer molecules can anchor. However, results from our earlier work shows that a water-based gel reduced the permeability to water much more than that to oil in an oil-wet polyethylene core. This finding does not support the wall-effect theory. Also, the wall-effect model can not explain why an oil-based gel reduced the permeability to oil more than that to water in a strongly water-wet system.<sup>1</sup> (It is unlikely that the oil-based gel would adsorb onto the strongly water-wet pore walls.) As will

be demonstrated in the next section, the gel-droplet model proposed by Nilsson *et al.*<sup>46</sup> could explain the observations that could not be explained by the wall-effect model.

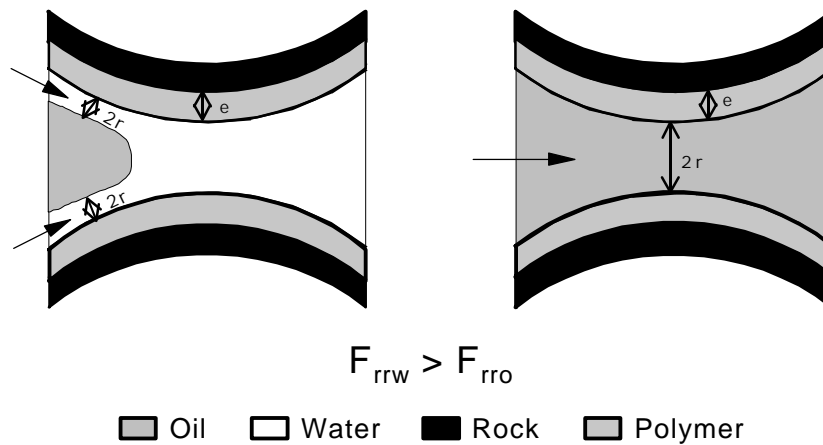


Fig. 74—Wall-effect model proposed by Zaitoun *et al.*<sup>45</sup>

**“Gel-Droplet” Model.** Nilsson *et al.*<sup>46</sup> proposed that the mechanism for the disproportionate permeability reduction is that water and oil flow more easily in some channels than in others.

Fig. 75 shows that when water flows through an oil-wet pore, the only restriction to the water flow is a thin film of oil on the pore wall. In contrast, when oil flows through the same pore, a residual water droplet in the pore restricts the oil flow. (This explains why the endpoint permeability of the wetting phase is always lower than that of the non-wetting phase.) During placement, a water-based gelant flows through the center of the oil-wet core. After gelation, a gel droplet forms at the center of the pore replacing the residual water droplet. Fig. 75 shows that if the size of the gel droplet is the same as that of the residual water droplet, the volume fraction of the pore available to oil flow remains the same as before treatment. However, Fig. 75 also shows that the presence of the gel droplet significantly reduces the volume fraction of the pore available to water flow. (Recall that the only restriction to water flow before treatment was the thin film of oil on the pore wall.) Thus, the gel could reduce the permeability to water without affecting the permeability to oil. Of course, if the gel droplet is larger than the residual water droplet, the permeability to oil will be reduced. Also, the disproportionate permeability reduction diminishes when the size of the gel droplet falls below that of the residual water droplet. Following similar logic, Fig. 76 illustrates that an oil-based gel should reduce the permeability to oil more than that to water in a strongly water-wet system. In support of this theory, results from our previous study showed that an oil-based gel reduced the permeability to oil more than that to water in a strongly water-wet system.<sup>1</sup>

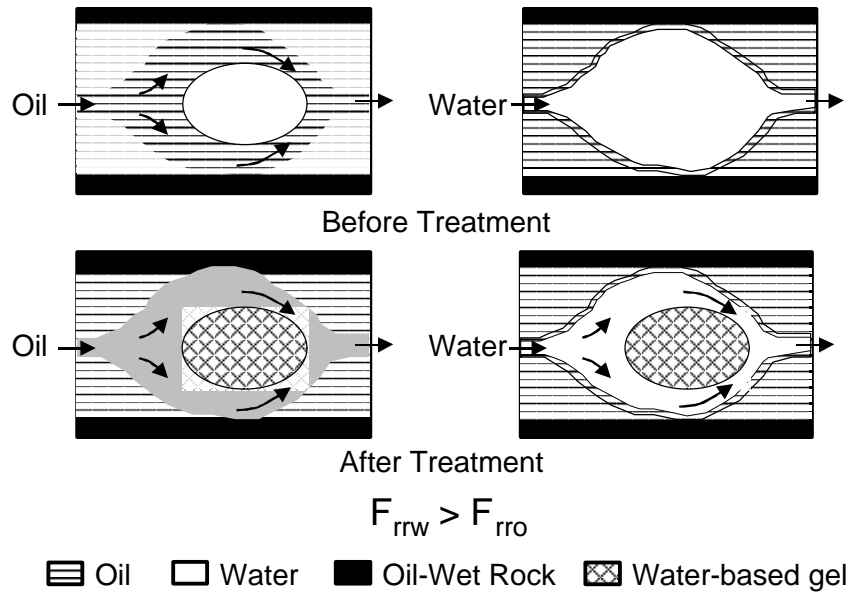


Fig. 75—Gel-droplet model proposed by Nilsson *et al.*<sup>46</sup>

In a strongly water-wet system, the model predicts that a strong water-based gel could block the pores completely by encapsulating the residual oil droplets. Even with syneresis, the authors argued that the gel droplet could still occupy a significant volume fraction of the pore, thereby causing significant permeability reduction to both water and oil. However, this gel-droplet model could not explain why a water-based gel reduced the permeability to water much more than that to oil in a strongly water-wet system.<sup>1</sup> Also, this model cannot explain why an oil-based gel reduced the permeability to oil more than that to water in an oil-wet system.<sup>1</sup>

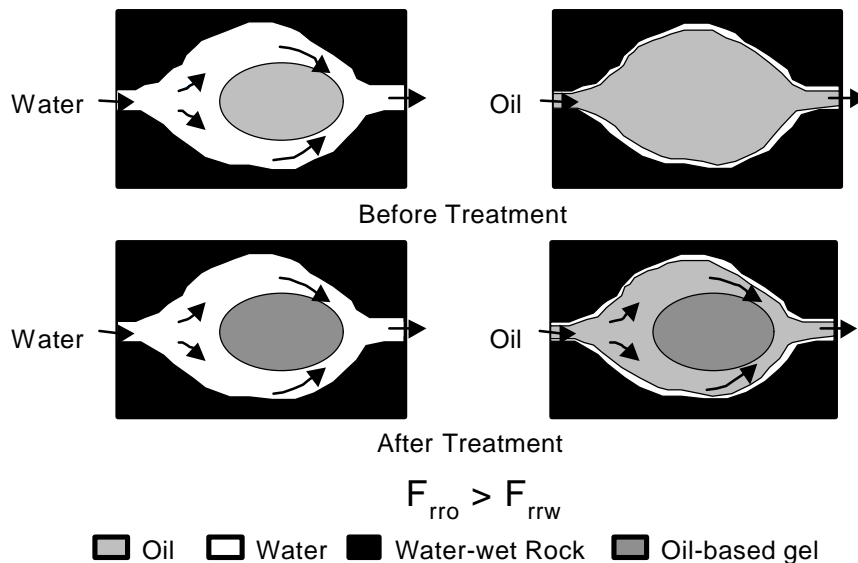


Fig. 76—Gel-droplet model proposed by Nilsson *et al.*<sup>46</sup>

**Modified “Wall-Effect” Model.** However, with minor modifications, the wall-effect model proposed by Zaitoun *et al.*<sup>45</sup> could provide satisfactory explanations for these observations. In a modified wall-effect model, we assume that in a strongly water-wet system, the adsorbed layer on the pore walls after treatment can either be a polymer or a water-based gel (Figs. 74 and 77). As discussed in the previous section, the presence of residual oil droplets at the center of the pores in a strongly water-wet system can significantly reduce the effective radius of the water channels during waterflooding. However, this restriction may not exist during oilflooding. Therefore, for a given thickness of an adsorbed polymer or gel layer, the permeability reduction for water during waterflooding is greater than that for oil during oilflooding.

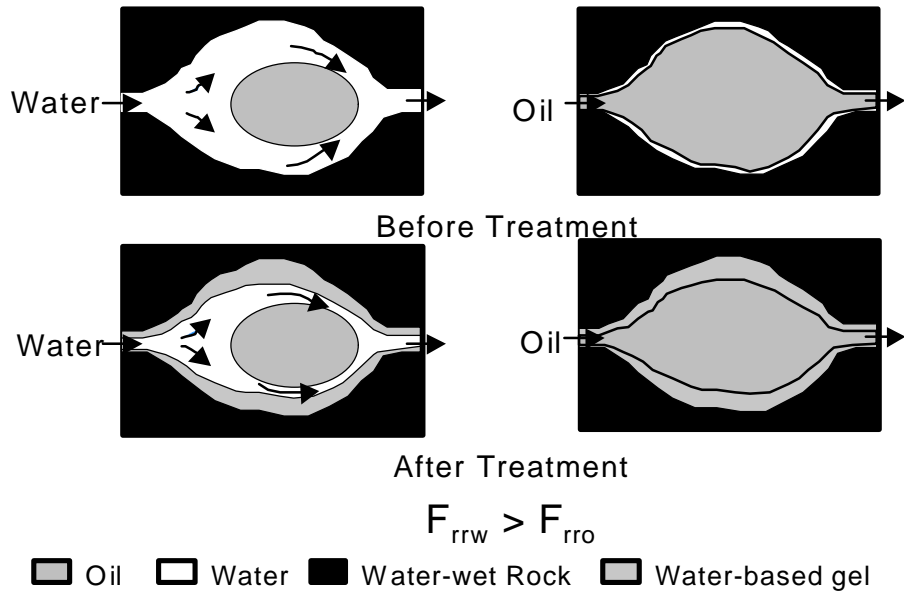


Fig. 77—Modified wall-effect model.

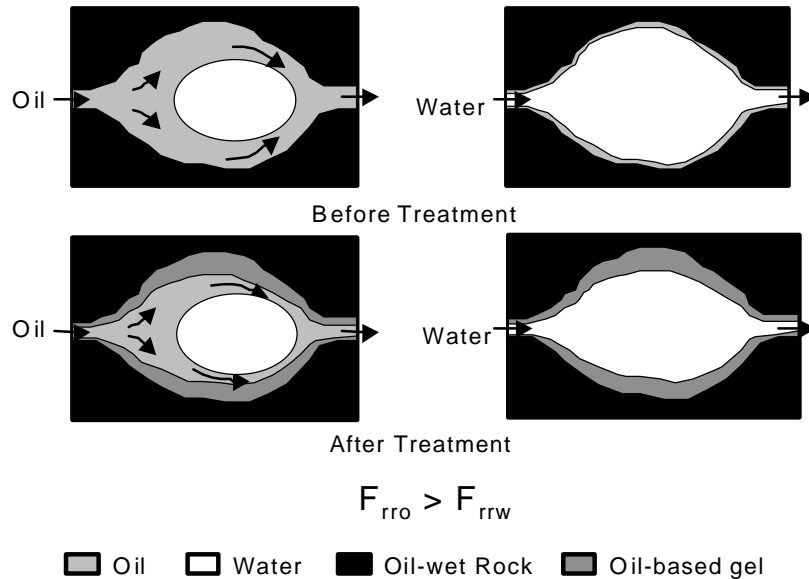


Fig. 78—Modified wall-effect model.

Following similar logic, Fig. 78 illustrates that an oil-based gel could form a gel layer on the pore walls of a strongly oil-wet system. In this case, the presence of residual water droplets at the center of the pores could significantly reduce the effective width of the oil channels during oilflooding. However, this restriction may not exist during waterflooding. Therefore, for a given thickness of an adsorbed layer of the oil-based gel, the permeability reduction for oil during oilflooding is greater than that for water during waterflooding. This explains why an oil-based gel reduced the permeability to oil more than that to water in an oil-wet system.<sup>1</sup>

**The Combined Model.** Our analyses suggest that if a gelant is the wetting phase, a modified wall-effect model proposed by Zaitoun *et al.*<sup>45</sup> could explain why the disproportionate permeability reduction occurs. In contrast, when the gelant is the non-wetting phase, the gel-droplet model proposed by Nilsson *et al.*<sup>46</sup> could be used to explain the disproportionate permeability reduction.

### ***Effect of Residual Oil Saturation***

According to the combined wall-effect and gel-droplet model, residual non-wetting-phase droplets play an important role in the disproportionate permeability reduction. Usually, the residual non-wetting-phase droplets are trapped in the larger pores as globules in a porous medium.<sup>47</sup> The combined model predicts that the disproportionate permeability reduction should increase when the total number of pores occupied by the residual non-wetting-phase droplet increases. In other words, the disproportionate permeability reduction should increase with increasing residual non-wetting-phase saturation.

One possible way to test this theory is to perform oil/water experiments in cores of different residual non-wetting phase saturation. Under a specific range of conditions, lowering the capillary number,  $N_{ca}$ , causes the residual non-wetting-phase saturation to increase.<sup>47</sup> In this study, we performed oil/water experiments in strongly water-wet Berea cores using our standard Cr(III)-acetate-HPAM gel. We varied the residual oil saturation by using different capillary numbers during waterflooding before treatment. During gelant injection, we stayed below the capillary number used during waterflooding before treatment to avoid mobilizing the residual oil in the core. After shut-in, the residual resistance factors were measured below this capillary number as well. For each capillary number, two similar oil-water experiments were performed: one with oil injected immediately after shut-in to measure oil residual resistance factor,  $F_{ro}$ , and the other with brine injected immediately after shut-in to measure water residual resistance factor,  $F_{rw}$ . Table 9 shows that lowering the capillary number from  $10^{-4}$  to  $10^{-5}$  increased the residual oil saturation from 0.21 to 0.35. The increase in residual oil saturation resulted in a 4.5X increase in the disproportionate permeability reduction. ( $F_{rw}/F_{ro}$  shown in Table 9 increased from 50 to 223.) This finding supports the combined wall-effect and gel-droplet model. (Detailed residual-resistance-factor data are listed in Tables A25 through A28.)

In field applications, the water zones are often completely watered out with very low residual oil saturation while the oil zones contain higher residual oil saturation. This can be very helpful in maximizing the disproportionate permeability reduction. As illustrated in Table 10, for our standard Cr(III)-acetate-HPAM gel, increasing the residual oil saturation in the oil zone from 0.21 to 0.35 without changing that in the water zone would result in a 22X increase in the

disproportionate permeability reduction. ( $F_{\text{rw}}/F_{\text{ro}}$  increased from 50 to 1,100.) Table 10 also shows that the increase in the disproportionate permeability reduction is a result of a significant decrease in  $F_{\text{ro}}$ . These findings suggest that maintaining a higher residual oil saturation in the treated region of an oil zone could significantly reduce the damage to oil productivity after treatment.

Table 9—Effect of  $S_{\text{or}}$  on disproportionate permeability reduction.  
Gel: 0.5% HPAM, 0.0313% Cr(III)-acetate, 0.0121% CrCl<sub>3</sub>, 1% NaCl, 0.1% CaCl<sub>2</sub>  
Cores: High-permeability Berea sandstone

$S_{\text{or}}$	$N_{\text{ca}}$	$F_{\text{rw}}$	$F_{\text{ro}}$	$F_{\text{rw}}/F_{\text{ro}}$
0.21	$10^{-4}$	26,400	525	50
0.35	$10^{-5}$	5,360	24	223

Table 10—Effect of  $S_{\text{or}}$  on disproportionate permeability reduction.  
Gel: 0.5% HPAM, 0.0313% Cr(III)-acetate, 0.0121% CrCl<sub>3</sub>, 1% NaCl, 0.1% CaCl<sub>2</sub>  
Cores: High-permeability Berea sandstone

$S_{\text{or}}$ (Water zone)	$S_{\text{or}}$ (Oil zone)	$F_{\text{rw}}$	$F_{\text{ro}}$	$F_{\text{rw}}/F_{\text{ro}}$
0.21	0.21	26,400	525	50
0.21	0.34	26,400	24	1,100

### ***Imaging Experiments Using Synchrotron X-Ray Microtomography***

In a previous study, we performed NMR imaging experiments to observe disproportionate permeability reduction on a microscopic scale.<sup>31</sup> Results from the NMR imaging experiments revealed that the imaging technique had many limitations, which prevented us from obtaining reliable pore-level images. Most importantly, the spatial resolution was on the order of hundreds of micrometers, which was too poor to clearly distinguish fluid pathways on the pore level. Recent advancements in computed microtomography (CMT) technology using synchrotron X-ray sources provide the ability to obtain three-dimensional pore-level images of rock samples with a spatial resolution on the order of micrometers.<sup>48</sup> This technology has been available at the National Synchrotron Light Source (NSLS) at Brookhaven National Laboratory for many years. Recent improvements in data acquisition, transmission, and reconstruction have reduced the time requirement to produce 3-D pore-level images to a few hours, which is a fraction of the time required in previous first generation scanning methods.

Imaging experiments are currently underway using the high-resolution CMT technology to compare the oil and water pathways as well as the fluid distribution before and after gel treatment. The objective is to study the disproportionate permeability reduction on a microscopic scale. In these experiments, we use high-permeability Berea sandstone as the porous medium. The gel is our standard Cr(III)-acetate-HPAM. Hexadecane is the oil phase. To increase the image contrast between the brine and the oil phases, hexadecane was doped with 10% w/w iodo-hexadecane. We will report the results from these experiments as soon as they become available.

### ***Conclusions***

1. Our analyses suggest that if a gelant is the wetting phase, a modified wall-effect model proposed by Zaitoun *et al.*<sup>45</sup> could explain why the disproportionate permeability reduction occurs. In contrast, when the gelant is the non-wetting phase, the gel-droplet model proposed by Nilsson *et al.*<sup>46</sup> could be used to explain the disproportionate permeability reduction.
2. In strongly water-wet Berea cores, the disproportionate permeability reduction increased with increased residual oil saturation. This finding is consistent with predictions from the combined model.
3. Results from our oil/water experiments suggest that maintaining a higher residual oil saturation in the treated region of an oil zone could significantly reduce the damage to oil productivity after treatment.
4. Results from our oil/water experiments indicated that the disproportionate permeability reduction increased with increased pressure drawdown (between 45 psi/ft to 180 psi/ft). This finding suggests that to a certain extent, an increase in pressure drawdown after treatment might reduce the productivity damage to oil without affecting the ability of the gel to reduce water production.
5. An oil-based gel reduced the permeability to oil more than that to water. This is opposite of what we observed for a water-based gel. For the oil-based gel, the reverse disproportionate permeability reduction increased with increased rock permeability. More work is under way to understand the implication of this phenomenon on the mechanism of disproportionate permeability reduction.

## NOMENCLATURE

- $A$  = area, m<sup>2</sup>  
 $C$  = produced concentration, g/m<sup>3</sup>  
 $C_o$  = injected concentration, g/m<sup>3</sup>  
 $e$  = thickness of adsorbed polymer or gel layer, ft [m]  
 $F_{rg}$  = gas residual resistance factor (gas mobility before gel divided by that after gel)  
 $F_{ro}$  = oil residual resistance factor (oil mobility before gel divided by that after gel)  
 $F_{rw}$  = water residual resistance factor (water mobility before gel divided by that after gel)  
 $G$  = shear modulus, Pa  
 $G'$  = elastic or storage modulus, Pa  
 $G''$  = viscous or loss modulus, Pa  
 $h_f$  = fracture height, inches [cm]  
 $k_f$  = fracture permeability, darcys [ $\mu\text{m}^2$ ]  
 $k_{\text{gas}}$  = relative permeability to gas, darcys [ $\mu\text{m}^2$ ]  
 $k_{\text{gel}}$  = gel permeability to water, darcys [ $\mu\text{m}^2$ ]  
 $k_o$  = relative permeability to oil, darcys [ $\mu\text{m}^2$ ]  
 $k_w$  = relative permeability to water, darcys [ $\mu\text{m}^2$ ]  
 $L$  = filter cake thickness, cm  
 $L_f$  = fracture length, inches [cm]  
 $N_{ca}$  = capillary number based on darcy velocity  
 $Dp$  = pressure drop, psi [Pa]  
 $dp/dl$  = pressure gradient, psi/ft [Pa/m]  
 $q$  = flow rate, cm<sup>3</sup>/hr  
 $q_{\text{min}}$  = minimum injection rate to match water leakoff from gel dehydration, cm<sup>3</sup>/hr  
 $r$  = correlation coefficient or radius of flow pathways, ft [m]  
 $S_{or}$  = residual oil saturation  
 $S_w$  = water saturation  
 $S_{wr}$  = residual water saturation  
 $u_l$  = water leakoff rate, ft/min [cm/s]  
 $t$  = time, s  
 $w_f$  = fracture width, in. [cm]  
 $w_o$  = opening size during extrusion, in. [cm]  
 $\delta$  = phase shift or loss angle, °  
 $\gamma$  = shear strain, %  
 $\gamma_o$  = maximum strain, %  
 $\dot{\gamma}$  = shear rate, s<sup>-1</sup>  
 $\dot{\gamma}_o$  = maximum shear rate, s<sup>-1</sup>  
 $\eta'$  = dynamic viscosity, Pa-s  
 $\eta''$  = elastic component of complex viscosity, Pa-s  
 $\eta^*$  = complex viscosity, Pa-s  
 $\mu$  = viscosity, cp [Pa-s]  
 $\mu_o$  = oil viscosity, cp [mPa-s]  
 $\mu_w$  = water viscosity, cp [mPa-s]  
 $\tau$  = stress, psi [Pa]

$\tau'$  = elastic component of stress, psi [Pa]  
 $\tau''$  = viscous component of stress, psi [Pa]  
 $\tau_o$  = maximum component of stress, psi [Pa]  
 $\tau_o'$  = maximum component of elastic stress, psi [Pa]  
 $\tau_o''$  = maximum component of viscous stress, psi [Pa]  
 $\tau_s$  = shear stress, psi [Pa]  
 $\tau_y$  = yield stress, psi [Pa]  
 $\omega$  = frequency, s<sup>-1</sup>

## REFERENCES

1. Seright, R.S.: "Improved Methods for Water Shutoff," Final Technical Progress Report (U.S. DOE Report DOE/PC/91008-14), U.S. DOE Contract DE-AC22-94PC91008, BDM-Oklahoma Subcontract G4S60330 (Oct. 1998) 21-54, 59-69.
2. Sydansk, R.D. and Moore, P.E.: "Gel Conformance Treatments Increase Oil Production in Wyoming," *Oil & Gas J.* (Jan. 20, 1992) 40-45.
3. Borling, D.C.: "Injection Conformance Control Case Histories Using Gels at the Wertz Field CO<sub>2</sub> Tertiary Flood in Wyoming, USA," paper SPE 27825 presented at the 1994 SPE/DOE Symposium on Improved Oil Recovery, April 17-20.
4. Hild, G.P. and Wackowski, R.K.: "Reservoir Polymer Gel Treatments To Improve Miscible CO<sub>2</sub> Flood," *SPEE* (April. 1999) 196-204.
5. Lane, R.H. and Sanders, G.S.: "Water Shutoff Through Fullbore Placement of Polymer Gel in Faulted and in Hydraulically Fractured Producers of the Prudhoe Bay Field," paper SPE 29475 presented at the 1995 SPE Production Operations Symposium, Oklahoma City, April 2-4.
6. Seright, R.S.: "Gel Dehydration During Extrusion Through Fractures," *SPEPF* (May 1999) 110-116.
7. Seright, R.S.: "Gel Placement in Fractured Systems," *SPEPF* (Nov. 1995), 241-248.
8. Seright, R.S.: "Use of Preformed Gels for Conformance Control in Fractured Systems," *SPEPF* (Feb. 1997) 59-65.
9. Seright, R.S.: "Mechanism for Gel Propagation Through Fractures," paper SPE 55628 presented at the 1999 SPE Rocky Mountain Regional Meeting, Gillette, May 15-19.
10. Seright, R.S.: "Effect of Rock Permeability on Gel Performance in Fluid-Diversion Applications," *In Situ* (1993) **17**, No. 4, 363-386.
11. Seright, R.S., Liang, J., and Seldal, M.: "Sizing Gelant Treatments in Hydraulically Fractured Production Wells," *SPEPF* (Nov. 1998) 223-229.
12. Liu, Jin: "Rheological Properties of Gels Used for Conformance Control," MS thesis, New Mexico Institute of Mining and Technology (Sept. 1999).
13. Callister, Jr., W.D.: *Materials Science and Engineering, An Introduction, 4<sup>th</sup> ed.*, John Wiley, New York (1997) 108-140.
14. Macosko, C.W.: *Rheology Principles, Measurements, and Applications*, Wiley-Vch, New York (1994) 108-140.
15. Liang, J., Sun, H., Seright, R.S.: "Reduction of Oil and Water Permeabilities Using Gels," paper SPE 24195 presented at the 1992 SPE/DOE Symposium on Enhanced Oil Recovery, Tulsa, April 22-24.
16. Seright, R.S., Liang, J., and Sun, H.: "Gel Treatments in Production Wells with Water Coning Problems," *In Situ* (1993) **17**, No. 3, 243-272.
17. Liang, J., Lee, R.L., and Seright, R.S.: "Placement of Gels in Production Wells," *SPE Production & Facilities* (Nov. 1993) 276-284; *Transactions AIME* **295**.
18. Seright, R.S. and Liang, J.: "A Comparison of Different Types of Blocking Agents," paper SPE 30120 presented at the 1995 European Formation Damage Conference, The Hague, The Netherlands, May 15-16.
19. Zaitoun, A. and Kohler, N.: "Modification of Water/Oil and Water/Gas Relative Permeabilities after Polymer Treatment of Oil or Gas Wells," *In Situ* (1989) **13**, No.1&2, 55-77.

20. Zaitoun, A., Kohler, N., and Guerrini, Y.: "Improved Polyacrylamide Treatments for Water Control in Producing Wells," *JPT* (July 1991) 862-867.
21. Ranjbar, M., Czolbe, P., and Kohler, N.: "Comparative Laboratory Selection and Field Testing of Polymers for Selective Control of Water Production in Gas Wells," paper SPE 28984 presented at the 1995 SPE International Symposium on Oil Field Chemistry, San Antonio, Feb. 14-17.
22. Zaitoun, A., Kohler, N., and Marrast, J.: "On the Use of Polymers to Reduce Water Production from Gas Wells," *In Situ* (1990) **14**, No. 2, 133-146.
23. Crowe, C.W.: "Evaluation of Oil Soluble Resin Mixtures as Diverting Agents for Matrix Acidizing," paper SPE 3505 presented at the 1971 SPE Annual Technical Conference and Exhibition, New Orleans, Oct. 3-6.
24. Houchin, L.R., Dunlap, D.D., Hudson, L.M., and Begnaud, P.C.: "Evaluation of Oil Soluble Resin as Acid-Diverting Agent," paper SPE 15574 presented at the 1986 SPE Annual Technical Conference and Exhibition, New Orleans, Oct. 5-8.
25. Tien, C. and Payatakes, A.C.: "Advances in Deep Bed Filtration," *AIChE J.* (1979) **25**, No. 5, 737-759.
26. Gallus, J.P. and Pye, D.S.: "Deformable Diverting Agent for Improved Well Stimulation," *JPT* (April 1969) 497-504.
27. Gallus, J.P. and Pye, D.S.: "Fluid Diversion to Improve Well Stimulation," paper 3811 presented at the 1972 MIMM-MMIJ Meeting, Tokyo, May 25-27.
28. Seright, R.S.: "Improved Techniques for Fluid Diversion in Oil Recovery Processes," Second Annual Report, DOE/BC/14480-10, U.S. DOE (Feb. 1995) 1-50, 147-158.
29. Bernard, G.G. and Holm, L.W.: "Effect of Foam on Permeability of Porous Media to Gas," *SPEJ* (Sept., 1964) 267-274.
30. Bernard, G.G., Holm, L.W., and Jacobs, W.L.: "Effect of Foam on Trapped Gas Saturation and on Permeability of Porous Media to Water," *SPEJ* (Dec. 1965) 295-300.
31. Seright, R.S.: "Improved Techniques for Fluid Diversion in Oil Recovery Processes," Final Report, DOE/BC/14480-15, U.S. DOE (Jan. 1996) 62-89.
32. Thompson, K.E. and Fogler, H.S.: "A Study of Diversion Mechanisms by Reactive Water-Diverting Agents," paper SPE 25222 presented at the 1993 SPE International Symposium on Oil Field Chemistry, New Orleans, March 2-5.
33. Seright, R.S. and Martin, F.D.: "Fluid Diversion and Sweep Improvement with Chemical Gels in Oil Recovery Processes," Second Annual Report, DOE/BC/14447-10, U.S. DOE (Nov. 1991) 73-110.
34. Sorbie, K.S. and Seright, R.S.: "Gel Placement in Heterogeneous Systems with Crossflow," paper SPE 24192 presented at the 1992 SPE/DOE Symposium on Enhanced Oil Recovery, Tulsa, April 22-24.
35. Kolnes, J. and Nilsson, S.: "Effect of the Core Material on Gelation of a HPAM/Chromium System at High Temperature," paper SPE/DOE 35377 presented at the 1996 SPE/DOE Symposium on Improved Oil Recovery, Tulsa, April 21-24.
36. Lockhart, T.P. and Albonico, P.: "New Chemistry for the Placement of Chromium(III)/Polymer Gels in High-Temperature Reservoirs," *SPEPF* (Nov. 1994) 273-279.
37. Moradi-Araghi, A.: "Thermally Stable Gels for Near-Wellbore Permeability Contrast Corrections," *SPE Advanced Technology Series* (June 1993) **1**, No. 1, 140-145.

38. Whitney, D.D, Montgomery, D.W., and Hutchins, R.D.: "Water Shutoff in the North Sea: Testing a New Polymer Gel System in the Heather Field, UKCS Block 2/5," *SPEPF* (May 1996) 108-112.
39. Kvanvik, B.A. *et al.*: "An Evaluation of Stable Gel Systems for Deep Injector Treatments and High-Temperature Producer Treatments," presented at the 8<sup>th</sup> European IOR Symposium, Vienna, Austria, May 15-17, 1995.
40. Fletcher, A.J.P. *et al.*: "Deep Diverting Gels for Very Cost-Effective Waterflood Control," *J. Polym. Sci. & Eng.* (April 1992) 7 (1-2) 33-43.
41. Seright, R.S. and Martin, F.D.: "Fluid Diversion and Sweep Improvement with Chemical Gels in Oil Recovery Processes," First Annual Report, DOE/BC/14447-8, U.S. DOE (June. 1991) 56-79.
42. Seright, R.S.: "Improved Methods for Water Shutoff," Annual Technical Progress Report (U.S. DOE Report DOE/PC/91008-4), U.S. DOE Contract DE-AC22-94PC91008, BDM-Oklahoma Subcontract G4S60330 (Nov. 1997).
43. Liang, J. and Seright, R.S.: "Further Investigations of Why Gels Reduce  $k_w$  More Than  $k_o$ ," *SPEPF* (Nov. 1997).
44. Liang, J., Sun, H., Seright, R.S.: "Why Do Gels Reduce Water Permeability More Than Oil Permeability?" *SPEPF* (Nov. 1995) 282-286.
45. Zaitoun, A., Bertin, H., and Lasseux, D.: "Two-Phase Flow Property Modifications by Polymer Adsorption," paper SPE 39631 presented at the 1998 SPE/DOE Improved Oil Recovery Symposium, Tulsa, April 19-22.
46. Nilsson, S., Stavland, A. and Jonsbraten, H. C.: "Mechanistic Study of Disproportionate Permeability Reduction," paper SPE 39635 presented at the 1998 SPE/DOE Improved Oil Recovery Symposium, Tulsa, April 19-22.
47. Lake, L.W.: *Enhanced Oil Recovery*, Prentice Hall, Englewood Cliffs, New Jersey (1989) 62-77.
48. Coles, M.E., Hazlett, R.D., Muegge, E.L., Jones K.W., Andrews, B., Dowd, B., Siddons, P., Peskin, A., Spanne, P., and Soll, W.E.: "Developments in Synchrotron X-Ray Microtomography with Applications to Flow in Porous Media," paper SPE 36531 presented at the 1998 Annual Technical Conference and Exhibition, Denver, Oct. 6-9.

## APPENDIX A: Data Supplement to Chapter 6

Table A1—Summary of Water and Oil Mobilities Before Gel Treatment  
(Core SSH-204, High-permeability Berea sandstone, 41°C)

$(k/\mu)_w$ , md/cp @ $S_w=1.0$	$(k/\mu)_o$ , md/cp @ $S_{wr}=0.31$	$(k/\mu)_w$ , md/cp @ $S_{or}=0.22$
1,180	660	372

Table A2—Summary of Water and Oil Mobilities Before Gel Treatment  
(Core SSH-217, High-permeability Berea sandstone, 41°C)

$(k/\mu)_w$ , md/cp @ $S_w=1.0$	$(k/\mu)_o$ , md/cp @ $S_{wr}=0.30$	$(k/\mu)_w$ , md/cp @ $S_{or}=0.25$	$(k/\mu)_w$ , md/cp @ $S_{ow}=0.26$
1,211	684	359	423

Table A3—Summary of Water and Oil Mobilities Before Gel Treatment  
(Core SSL-218, Low-permeability Berea sandstone, 41°C)

$(k/\mu)_w$ , md/cp @ $S_w=1.0$	$(k/\mu)_o$ , md/cp @ $S_{wr}=0.36$	$(k/\mu)_w$ , md/cp @ $S_{or}=0.37$	$(k/\mu)_w$ , md/cp @ $S_{ow}=0.34$
115	60	15	67

Table A4—Summary of Water and Oil Mobilities Before Gel Treatment  
(Core SSH-222, High-permeability Berea sandstone, 41°C)

$(k/\mu)_w$ , md/cp @ $S_w=1.0$	$(k/\mu)_o$ , md/cp @ $S_{wr}=0.31$	$(k/\mu)_w$ , md/cp @ $S_{or}=0.21$
1,242	678	511

Table A5—Summary of Water and Oil Mobilities Before Gel Treatment  
(Core SSH-224, High-permeability Berea sandstone, 41°C)

$(k/\mu)_w$ , md/cp @ $S_w=1.0$	$(k/\mu)_o$ , md/cp @ $S_{wr}=0.29$	$(k/\mu)_w$ , md/cp @ $S_{or}=0.24$
1,092	630	359

Table A6—Summary of Water and Oil Mobilities Before Gel Treatment  
(Core SSH-228, High-permeability Berea sandstone, 41°C)

$(k/\mu)_w$ , md/cp @ $S_w=1.0$	$(k/\mu)_o$ , md/cp @ $S_{wr}=0.34$	$(k/\mu)_w$ , md/cp @ $S_{or}=0.17$
1,211	667	404

Table A7—Summary of Water and Oil Mobilities Before Gel Treatment  
(Core SSH-232, High-permeability Berea sandstone, 41°C)

$(k/\mu)_w$ , md/cp @ $S_w=1.0$	$(k/\mu)_o$ , md/cp @ $S_{wr}=0.32$	$(k/\mu)_w$ , md/cp @ $S_{or}=0.23$
1,128	628	329

Table A8—Summary of Water and Oil Mobilities Before Gel Treatment  
(Core SSH-235, High-permeability Berea sandstone, 41°C)

$(k/\mu)_w$ , md/cp @ $S_w=1.0$	$(k/\mu)_o$ , md/cp @ $S_{wi}=0.32$	$(k/\mu)_w$ , md/cp @ $S_{or}=0.22$
1,024	532	311

Table A9—Summary of Water and Oil Mobilities Before Gel Treatment  
(Core SSH-237, High-permeability Berea sandstone, 41°C)

$(k/\mu)_w$ , md/cp @ $S_w=1.0$	$(k/\mu)_o$ , md/cp @ $S_{wi}=0.32$	$(k/\mu)_w$ , md/cp @ $S_{or}=0.21$
980	532	269

Table A10—Summary of Water and Oil Mobilities Before Gel Treatment  
(Core SSH-238, High-permeability Berea sandstone, 41°C)

$(k/\mu)_w$ , md/cp @ $S_w=1.0$	$(k/\mu)_o$ , md/cp @ $S_{wi}=0.31$	$(k/\mu)_w$ , md/cp @ $S_{or}=0.34$
978	576	185

Table A11—Summary of Water and Oil Mobilities Before Gel Treatment  
(Core SSH-244, High-permeability Berea sandstone, 41°C)

$(k/\mu)_w$ , md/cp @ $S_w=1.0$	$(k/\mu)_o$ , md/cp @ $S_{wi}=0.30$	$(k/\mu)_w$ , md/cp @ $S_{or}=0.21$
1,036	608	407

Table A12—Summary of Water and Oil Mobilities Before Gel Treatment  
(Core SSH-245, High-permeability Berea sandstone, 41°C)

$(k/\mu)_w$ , md/cp @ $S_w=1.0$	$(k/\mu)_o$ , md/cp @ $S_{wi}=0.29$	$(k/\mu)_w$ , md/cp @ $S_{or}=0.36$
1,020	599	177

Table A13—Summary of Water and Oil Mobilities Before Gel Treatment  
(Core SSH-247, High-permeability Berea sandstone, 41°C)

$(k/\mu)_w$ , md/cp @ $S_w=1.0$	$(k/\mu)_o$ , md/cp @ $S_{wi}=0.28$	$(k/\mu)_w$ , md/cp @ $S_{or}=0.23$
1,002	565	347

Table A14—Summary of Water and Oil Mobilities Before Gel Treatment  
(Core SSH-253, High-permeability Berea sandstone, 41°C)

$(k/\mu)_w$ , md/cp @ $S_w=1.0$	$(k/\mu)_o$ , md/cp @ $S_{wi}=0.28$	$(k/\mu)_w$ , md/cp @ $S_{or}=0.22$
1,153	620	424

Table A15—Summary of Residual Resistance Factors—Core SSH-222

Core: High-permeability Berea sandstone

Gel: 0.5% HPAM, 0.0313% Cr(III)-acetate, 0.0121% CrCl<sub>3</sub>, 1% NaCl, 0.1% CaCl<sub>2</sub>

1 <sup>st</sup> Waterflood		
Pressure Drop, psi/ft	$F_{rrw}$ (1 <sup>st</sup> short core segment)	$F_{rrw}$ (center core segment)
45	18,000	47,000
1 <sup>st</sup> Oilflood		
Pressure Drop, psi/ft	$F_{rro}$ (1 <sup>st</sup> short core segment)	$F_{rro}$ (center core segment)
45	42	140
2 <sup>nd</sup> Waterflood		
Pressure Drop, psi/ft	$F_{rrw}$ (1 <sup>st</sup> short core segment)	$F_{rrw}$ (center core segment)
45	6,000	31,500

Table A16—Summary of Residual Resistance Factors—Core SSH-224

Core: High-permeability Berea sandstone

Gel: 0.5% HPAM, 0.0313% Cr(III)-acetate, 0.0121% CrCl<sub>3</sub>, 1% NaCl, 0.1% CaCl<sub>2</sub>

1 <sup>st</sup> Oilflood		
Pressure Drop, psi/ft	$F_{rro}$ (1 <sup>st</sup> short core segment)	$F_{rro}$ (center core segment)
45	43	202
1 <sup>st</sup> Waterflood		
Pressure Drop, psi/ft	$F_{rrw}$ (1 <sup>st</sup> short core segment)	$F_{rrw}$ (center core segment)
45	4,000	10,400
2 <sup>nd</sup> Oilflood		
Pressure Drop, psi/ft	$F_{rro}$ (1 <sup>st</sup> short core segment)	$F_{rro}$ (center core segment)
45	23	103

Table A17—Summary of Residual Resistance Factors—Core SSH-228  
 Core: High-permeability Berea sandstone  
 Gel: 0.5% HPAM, 0.0313% Cr(III)-acetate, 0.0121% CrCl<sub>3</sub>, 1% NaCl, 0.1% CaCl<sub>2</sub>

1 <sup>st</sup> Waterflood		
Pressure Drop, psi/ft	$F_{irw}$ (1 <sup>st</sup> short core segment)	$F_{irw}$ (center core segment)
90	9,225	30,000
67.5	11,400	31,100
45	15,000	32,700
1 <sup>st</sup> Oilflood		
Pressure Drop, psi/ft	$F_{iro}$ (1 <sup>st</sup> short core segment)	$F_{iro}$ (center core segment)
90	53	215
2 <sup>nd</sup> Waterflood		
Pressure Drop, psi/ft	$F_{irw}$ (1 <sup>st</sup> short core segment)	$F_{irw}$ (center core segment)
90	707	5,365

Table A18—Summary of Residual Resistance Factors—Core SSH-232  
 Core: High-permeability Berea sandstone  
 Gel: 0.5% HPAM, 0.0313% Cr(III)-acetate, 0.0121% CrCl<sub>3</sub>, 1% NaCl, 0.1% CaCl<sub>2</sub>

1 <sup>st</sup> Oilflood		
Pressure Drop, psi/ft	$F_{iro}$ (1 <sup>st</sup> short core segment)	$F_{iro}$ (center core segment)
90	34	127
45	31	120
1 <sup>st</sup> Waterflood		
Pressure Drop, psi/ft	$F_{irw}$ (1 <sup>st</sup> short core segment)	$F_{irw}$ (center core segment)
90	1,900	11,600
2 <sup>nd</sup> Oilflood		
Pressure Drop, psi/ft	$F_{iro}$ (1 <sup>st</sup> short core segment)	$F_{iro}$ (center core segment)
90	32	98

Table A19—Summary of Residual Resistance Factors—Core SSH-235

Core: High-permeability Berea sandstone

Gel: 0.5% HPAM, 0.0313% Cr(III)-acetate, 0.0121% CrCl<sub>3</sub>, 1% NaCl, 0.1% CaCl<sub>2</sub>

1 <sup>st</sup> Waterflood		
Pressure Drop, psi/ft	$F_{rrw}$ (1 <sup>st</sup> short core segment)	$F_{rrw}$ (center core segment)
180	24,600	42,200
1 <sup>st</sup> Oilflood		
Pressure Drop, psi/ft	$F_{rro}$ (1 <sup>st</sup> short core segment)	$F_{rro}$ (center core segment)
180	43	142
2 <sup>nd</sup> Waterflood		
Pressure Drop, psi/ft	$F_{rrw}$ (1 <sup>st</sup> short core segment)	$F_{rrw}$ (center core segment)
180	2,500	10,250

Table A20—Summary of Residual Resistance Factors—Core SSH-237

Core: High-permeability Berea sandstone

Gel: 0.5% HPAM, 0.0313% Cr(III)-acetate, 0.0121% CrCl<sub>3</sub>, 1% NaCl, 0.1% CaCl<sub>2</sub>

1 <sup>st</sup> Oilflood		
Pressure Drop, psi/ft	$F_{rro}$ (1 <sup>st</sup> short core segment)	$F_{rro}$ (center core segment)
180	42	103
1 <sup>st</sup> Waterflood		
Pressure Drop, psi/ft	$F_{rrw}$ (1 <sup>st</sup> short core segment)	$F_{rrw}$ (center core segment)
180	640	2,016
2 <sup>nd</sup> Oilflood		
Pressure Drop, psi/ft	$F_{rro}$ (1 <sup>st</sup> short core segment)	$F_{rro}$ (center core segment)
180	11	31

Table A21—Summary of Residual Resistance Factors—Core SSH-253

Core: High-permeability Berea sandstone

Gel: 0.5% HPAM, 0.0313% Cr(III)-acetate, 0.0121% CrCl<sub>3</sub>, 1% NaCl, 0.1% CaCl<sub>2</sub>

1 <sup>st</sup> Waterflood		
Pressure Drop, psi/ft	$F_{rrw}$ (1 <sup>st</sup> short core segment)	$F_{rrw}$ (center core segment)
225	56	73
1 <sup>st</sup> Oilflood		
Pressure Drop, psi/ft	$F_{rro}$ (1 <sup>st</sup> short core segment)	$F_{rro}$ (center core segment)
225	12	22
2 <sup>nd</sup> Waterflood		
Pressure Drop, psi/ft	$F_{rrw}$ (1 <sup>st</sup> short core segment)	$F_{rrw}$ (center core segment)
225	18	29

Table A22—Summary of Residual Resistance Factors—Core SSH-247

Core: High-permeability Berea sandstone

Gel: 0.5% HPAM, 0.0313% Cr(III)-acetate, 0.0121% CrCl<sub>3</sub>, 1% NaCl, 0.1% CaCl<sub>2</sub>

1 <sup>st</sup> Oilflood		
Pressure Drop, psi/ft	$F_{rro}$ (1 <sup>st</sup> short core segment)	$F_{rro}$ (center core segment)
225	31	107
1 <sup>st</sup> Waterflood		
Pressure Drop, psi/ft	$F_{rrw}$ (1 <sup>st</sup> short core segment)	$F_{rrw}$ (center core segment)
225	122	216
2 <sup>nd</sup> Oilflood		
Pressure Drop, psi/ft	$F_{rro}$ (1 <sup>st</sup> short core segment)	$F_{rro}$ (center core segment)
225	21	60

Table A23—Summary of Residual Resistance Factors—Core SSH-217  
 Core: High-permeability Berea sandstone  
 Gel: 18% 12-hydroxystearic acid in Soltrol-130

1 <sup>st</sup> Waterflood		
Flux, ft/d	$F_{rrw}$ (1 <sup>st</sup> short core segment)	$F_{rrw}$ (center core segment)
0.366 ( $\Delta p_{center} \approx 10$ psi)	41	184
1 <sup>st</sup> Oilflood		
Flux, ft/d	$F_{irro}$ (1 <sup>st</sup> short core segment)	$F_{irro}$ (center core segment)
0.094 ( $\Delta p_{center} \approx 10$ psi)	290	860
2 <sup>nd</sup> Waterflood		
Flux, ft/d	$F_{rrw}$ (1 <sup>st</sup> short core segment)	$F_{rrw}$ (center core segment)
0.376 ( $\Delta p_{center} \approx 10$ psi)	35	194
2 <sup>nd</sup> Oilflood		
Flux, ft/d	$F_{irro}$ (1 <sup>st</sup> short core segment)	$F_{irro}$ (center core segment)
0.784 ( $\Delta p_{center} \approx 10$ psi)	27	105

Table A24—Summary of Residual Resistance Factors—Core SSL-218  
 Core: Low-permeability Berea sandstone  
 Gel: 18% 12-hydroxystearic acid in Soltrol-130

1 <sup>st</sup> Waterflood		
Flux, ft/d	$F_{rrw}$ (1 <sup>st</sup> short core segment)	$F_{rrw}$ (center core segment)
0.120 ( $\Delta p_{center} \approx 10$ psi)	8	25
1 <sup>st</sup> Oilflood		
Flux, ft/d	$F_{irro}$ (1 <sup>st</sup> short core segment)	$F_{irro}$ (center core segment)
0.039 ( $\Delta p_{center} \approx 10$ psi)	185	350
2 <sup>nd</sup> Waterflood		
Flux, ft/d	$F_{rrw}$ (1 <sup>st</sup> short core segment)	$F_{rrw}$ (center core segment)
0.301 ( $\Delta p_{center} \approx 10$ psi)	3	10
2 <sup>nd</sup> Oilflood		
Flux, ft/d	$F_{irro}$ (1 <sup>st</sup> short core segment)	$F_{irro}$ (center core segment)
0.069 ( $\Delta p_{center} \approx 10$ psi)	69	190

Table A25—Summary of Residual Resistance Factors—Core SSH-244  
 Core: High-permeability Berea sandstone  
 Gel: 0.5% HPAM, 0.0313% Cr(III)-acetate, 0.0121% CrCl<sub>3</sub>, 1% NaCl, 0.1% CaCl<sub>2</sub>

1 <sup>st</sup> Waterflood		
Flux, ft/d	$F_{rrw}$ (1 <sup>st</sup> short core segment)	$F_{rrw}$ (center core segment)
0.012	9,700	26,400
1 <sup>st</sup> Oilflood		
Flux, ft/d	$F_{rro}$ (1 <sup>st</sup> short core segment)	$F_{rro}$ (center core segment)
0.772 ( $\Delta p_{center} \approx 10$ psi)	103	275
2 <sup>nd</sup> Waterflood		
Flux, ft/d	$F_{rrw}$ (1 <sup>st</sup> short core segment)	$F_{rrw}$ (center core segment)
0.012	350	14,500

Table A26—Summary of Residual Resistance Factors—Core SSH-204  
 Core: High-permeability Berea sandstone  
 Gel: 0.5% HPAM, 0.0313% Cr(III)-acetate, 0.0121% CrCl<sub>3</sub>, 1% NaCl, 0.1% CaCl<sub>2</sub>

1 <sup>st</sup> Oilflood		
Flux, ft/d	$F_{rro}$ (1 <sup>st</sup> short core segment)	$F_{rro}$ (center core segment)
0.348 ( $\Delta p_{center} \approx 10$ psi)	138	525
1 <sup>st</sup> Waterflood		
Flux, ft/d	$F_{rrw}$ (1 <sup>st</sup> short core segment)	$F_{rrw}$ (center core segment)
0.011	2,950	17,800
2 <sup>nd</sup> Oilflood		
Flux, ft/d	$F_{rro}$ (1 <sup>st</sup> short core segment)	$F_{rro}$ (center core segment)
0.697 ( $\Delta p_{center} \approx 10$ psi)	50	250
2 <sup>nd</sup> Waterflood		
Flux, ft/d	$F_{rrw}$ (1 <sup>st</sup> short core segment)	$F_{rrw}$ (center core segment)
0.011	1,000	14,500
3 <sup>rd</sup> Oilflood		
Flux, ft/d	$F_{rro}$ (1 <sup>st</sup> short core segment)	$F_{rro}$ (center core segment)
0.697 ( $\Delta p_{center} \approx 10$ psi)	36	203

Table A27—Summary of Residual Resistance Factors—Core SSH-245  
 Core: High-permeability Berea sandstone  
 Gel: 0.5% HPAM, 0.0313% Cr(III)-acetate, 0.0121% CrCl<sub>3</sub>, 1% NaCl, 0.1% CaCl<sub>2</sub>

1 <sup>st</sup> Waterflood		
Flux, ft/d	$F_{rrw}$ (1 <sup>st</sup> short core segment)	$F_{rrw}$ (center core segment)
0.012	834	5,360
1 <sup>st</sup> Oilflood		
Flux, ft/d	$F_{rro}$ (1 <sup>st</sup> short core segment)	$F_{rro}$ (center core segment)
3.088 ( $\Delta p_{center} \approx 10$ psi)	3	40
2 <sup>nd</sup> Waterflood		
Flux, ft/d	$F_{rrw}$ (1 <sup>st</sup> short core segment)	$F_{rrw}$ (center core segment)
0.012	90	4,400

Table A28—Summary of Residual Resistance Factors—Core SSH-238  
 Core: High-permeability Berea sandstone  
 Gel: 0.5% HPAM, 0.0313% Cr(III)-acetate, 0.0121% CrCl<sub>3</sub>, 1% NaCl, 0.1% CaCl<sub>2</sub>

1 <sup>st</sup> Oilflood		
Flux, ft/d	$F_{rro}$ (1 <sup>st</sup> short core segment)	$F_{rro}$ (center core segment)
6.176 ( $\Delta p_{center} \approx 10$ psi)	5	24
1 <sup>st</sup> Waterflood		
Flux, ft/d	$F_{rrw}$ (1 <sup>st</sup> short core segment)	$F_{rrw}$ (center core segment)
0.099 ( $\Delta p_{center} \approx 10$ psi)	45	377
2 <sup>nd</sup> Oilflood		
Flux, ft/d	$F_{rro}$ (1 <sup>st</sup> short core segment)	$F_{rro}$ (center core segment)
12.351 ( $\Delta p_{center} \approx 10$ psi)	3	12

## **APPENDIX B: Technology Transfer**

### ***Presentations***

On September 23, 1999, we presented the talk, “Disproportionate Permeability Reduction by Gels,” at the 1999 IEA Meeting in Paris, France.

On September 13, 1999, we presented the talk, “Gel Propagation Through Fractures,” at Marathon Oil in Littleton, Colorado.

On July 27 and 28, 1999, we held a project review in Socorro, NM. The review was attended by 13 people (not including New Mexico Tech personnel) representing 9 different organizations.

On June 29, 1999, we presented the talk, “Sizing Gelant Treatments in Hydraulically Fractured Production Wells,” at the 1999 DOE Oil and Gas Conference in Dallas, Texas.

On May 17, 1999, we presented SPE paper 55628, “Mechanism for Gel Propagation Through Fractures,” at the 1999 Rocky Mountain Regional Meeting in Gillette, WY.

On April 23, 1999, we presented the talk, “Gel Dehydration During Extrusion Through Fractures,” at Saga Petroleum in Stavanger, Norway.

On April 22, 1999, we presented the talk, “Gel Dehydration During Extrusion Through Fractures,” at Stavanger College in Stavanger, Norway.

On April 22, 1999, we presented the talk, “A Strategy for Attacking Excess Water Production Problems,” at Elf Norge in Stavanger, Norway.

On March 11, 1999, we presented the talk, “A Strategy for Attacking Excess Water Production Problems,” for the Midcontinent SPE Section in Tulsa, OK.

From November 16-20, 1998, we presented talks on “Improved Methods for Water Shutoff,” at Chinese Petroleum Corporation in Maioli, Taiwan.

On October 6 and 7, 1998, we held a project review in Socorro, NM. The review was attended by 26 people (not including New Mexico Tech personnel) representing 17 different organizations.

### ***Internet Postings on the Project and Software to Download***

A description of our research group can be found at the following New Mexico PRRC web site: <http://baervan.nmt.edu/ResSweepEffic/reservoir.htm>

This web site also allows downloading of software, Version 1.07 of “Gel Design,” for sizing gelant treatments in hydraulically fractured production wells.

***Papers and Publications:***

Seright, R.S. and Lee, R.: “Gel Treatments for Reducing Channeling Through Naturally Fractured Reservoirs,” *SPE Production & Facilities* (Nov. 1999).

Seright, R.S.: “Mechanism for Gel Propagation Through Fractures,” paper SPE 55628 presented at the 1999 Rocky Mountain Regional Meeting, Gillette, WY, May 15-18.

Seright, R.S.: “Polymer Gel Dehydration During Extrusion Through Fractures,” *SPE Production & Facilities* (May 1999) 110-116.

Seright, R.S., Liang, J., and Seldal, M.: “Sizing Gelant Treatments in Hydraulically Fractured Production Wells,” *SPE Production & Facilities* (Nov. 1998) 223-229.

Seright, R.S.: “Improved Methods for Water Shutoff,” Final Technical Progress Report (U.S. DOE Report DOE/PC/91008-14), U.S. DOE Contract DE-AC22-94PC91008, BDM-Oklahoma Subcontract G4S60330 (Oct. 1998).